SDAC-TR-74-15

12

DETECTION OF LONG-PERIOD S FROM EARTHQUAKES AND EXPLOSIONS AT LASA AND LRSM STATIONS WITH APPLICATION TO POSITIVE AND NEGATIVE DISCRIMINATION OF EARTHQUAKES AND UNDERGROUND EXPLOSIONS

BLANDFORD, R. AND CLARK, D.

Seismic Data Analysis Center

Teledyne Geotech, 314 Montgomery Street, Alexandria, Virginia 22314

12 December 1974

DDC

RECEIVED
AUG 14 1975

B

REPORT DOCUMENTATION PAGE

READ INSTRUCTIONS
BEFORE COMPLETING FORM

1. REPORT NUMBER	2. GOVT ACCESSION NO.	3. RECIPIENT'S CATALOG NUMBER
SDAC-TR-74-15		

4. TITLE (and Subtitle)	5. TYPE OF REPORT & PERIOD COVERED
DETECTION OF LONG-PERIOD S FROM EARTHQUAKES AND EXPLOSIONS AT LASA AND LRSM STATIONS WITH APPLICATION TO POSITIVE AND NEGATIVE DISCRIMINATION OF EARTHQUAKES AND UNDERGROUND EXPLOSIONS.	Technical rept.
	6. PERFORMING ORG. REPORT NUMBER

7. AUTHOR(s)	8. CONTRACT OR GRANT NUMBER(s)
R. Blandford D. Clark	F08606-74-C-0006, ARPA Order-1620

9. PERFORMING ORGANIZATION NAME AND ADDRESS	10. PROGRAM ELEMENT, PROJECT, TASK AREA & WORK UNIT NUMBERS
Teledyne Geotech 314 Montgomery Street Alexandria, Virginia 22314	124 p.

11. CONTROLLING OFFICE NAME AND ADDRESS	12. REPORT DATE
Defense Advanced Research Projects Agency Nuclear Monitoring Research Office 1400 Wilson Blvd., Arlington, Va. 22209	12 December 1974
	13. NUMBER OF PAGES
	114

14. MONITORING AGENCY NAME & ADDRESS(if different from Controlling Office)	15. SECURITY CLASS. (of this report)
VELA Seismological Center 312 Montgomery Street Alexandria, Virginia 22314	Unclassified
	15a. DECLASSIFICATION/DOWNGRADING SCHEDULE

16. DISTRIBUTION STATEMENT (of this Report)

APPROVED FOR PUBLIC RELEASE; DISTRIBUTION UNLIMITED.

17. DISTRIBUTION STATEMENT (of the abstract entered in Block 20, if different from Report)

18. SUPPLEMENTARY NOTES

19. KEY WORDS (Continue on reverse side if necessary and identify by block number)

Discrimination
Shear Waves
Seismic Discrimination

Detection
Seismic Detection

found to be

20. ABSTRACT (Continue on reverse side if necessary and identify by block number)

An improved distance-amplitude relation for long-period S waves is developed and applied to long-period S waves measured from megaton-range explosions. We find that the difference between magnitude determined from the maximum amplitude long-period S waves and the magnitude determined from Rayleigh waves is a good discriminant between worldwide earthquakes and explosions at NTS and Amchitka. The long-period SH/SV ratio is not a discriminant. (cont on p 1473B)

DD FORM 1473 1 JAN 73 EDITION OF 1 NOV 65 IS OBSOLETE

The 90% incremental threshold for detection of earthquake long-period S waves at LASA from Japan and the Kuril Islands is m_b = 5.2. Beamforming and program FKCOMB were found to be equal in detection capability. Strauss (1973) reported data which imply a 90% incremental threshold of m_b = 4.7 for detection of long-period S waves at ALPA from the Kuril Islands and Kamchatka. The difference between LASA and ALPA capability can be explained by the average distance-amplitude relation together with the lower noise level at ALPA.

For a possible seismic network, (Romney, 1971) the use of negative discriminants (no detection of S waves) with .01 probability of a false alarm for explosions is shown to result in an M_s threshold approximately equal to the threshold of 90% probability of detection of S waves from earthquakes by two or more stations (positive discrimination). A significant lowering of the negative threshold is possible if one station of the network has an especially low detection threshold.

DETECTION OF LONG-PERIOD S FROM EARTHQUAKES AND EXPLOSIONS AT LASA
AND LRSM STATIONS WITH APPLICATIONS TO POSITIVE AND NEGATIVE
DISCRIMINATION OF EARTHQUAKES AND UNDERGROUND EXPLOSIONS

SEISMIC DATA ANALYSIS CENTER REPORT NO.:   SDAC-TR-74-15

AFTAC Project No.:   VELA VT/4709

Project Title: Seismic Data Analysis Center

ARPA Order No.:   1620

ARPA Program Code No.:   3F10

Name of Contractor: TELEDYNE GEOTECH

Contract No.:   F08606-74-C-0006

Date of Contract: 01 July 1974

Amount of Contract: $2,152,172

Contract Expiration Date: 30 June 1975

Project Manager: Royal A. Hartenberger
                                  (703) 836-3882

P. O. Box 334, Alexandria, Virginia   22314

APPROVED FOR PUBLIC RELEASE; DISTRIBUTION UNLIMITED.

ABSTRACT

An improved distance-amplitude relation for long-period S waves is developed and applied to long-period S waves measured from megaton-range explosions. We find that the difference between magnitude determined from the maximum amplitude long-period S waves and the magnitude determined from Rayleigh waves is a good discriminant between worldwide earthquakes and explosions at NTS and Amchitka. The long-period SH/SV ratio is not a discriminant.

The 90% incremental threshold for detection of earthquake long-period S waves at LASA from Japan and the Kuril Islands is $m_b = 5.2$. Beamforming and program FKCOMB were found to be equal in detection capability. Strauss (1973) reported data which imply a 90% incremental threshold of $m_b = 4.7$ for detection of long-period S waves at ALPA from the Kuril Islands and Kamchatka. The difference between LASA and ALPA capability can be explained by the average distance-amplitude relation together with the lower noise level at ALPA.

For a possible seismic network (Romney, 1971) the use of negative discriminants (no detection of S waves) with .01 probability of a false alarm for explosions is shown to result in an M_s threshold approximately equal to the threshold of 90% probability of detection of S waves from earthquakes by two or more stations (positive discrimination). A significant lowering of the negative threshold is possible if one station of the network has an especially low detection threshold.

TABLE OF CONTENTS

Page

LIST OF TABLES

LIST OF FIGURES

LIST OF FIGURES (Continued)

LIST OF FIGURES (Continued)

LIST OF FIGURES (Continued)

INTRODUCTION

Detection

Evernden (1969) examined records from all underground explosions before 1966 and detected long-period shear waves from only two explosions at one station each. This led him to suggest that for fixed m_b the S wave amplitudes for earthquakes would be about a factor of ten greater than for explosions.

Nuttli (1969) reported 131 measurements of long-period S wave arrival time, first peak amplitude, sign, and period for HALFBEAK and GREELEY at 43 WWSSN and LRSM stations. Measurements were made on all three components when possible. He was able to establish a good distance-amplitude relation for the first peak of SH motion from GREELEY measurements alone, and established that there was a node in the SH radiation pattern of HALFBEAK and GREELEY.

Von Seggern (1972) reviewed the Seismic Data Laboratory (SDL) shot reports and Geotech earthquake bulletins for the decade 1960-1970 for the LRSM network and for the VELA observatories. From these he was able to construct histograms of the amplitude ratios for earthquakes and explosions of short-period S to short-period P, long-period S to short-period P, long-period S to long-period P, long-period S to Rayleigh wave, and Love wave to Rayleigh wave. He found only 8, 11, and 9 observations of short period S, long-period S and long-period P respectively for explosions out of the explosions studied in the SDL shot reports, a total of approximately 40 explosions.

The difference of the means of von Seggern's long-period S to short-period P ratios were in general agreement with Evernden's, although there was some overlap of individual ratios. Von Seggern also showed good discrimination using the ratio of long-period S to LR. All of von Seggern's ratios were uncorrected for distance or magnitude.

Von Seggern and Lambert (1972) reported several S wave observations from the explosion MILROW, and Johns (1971) detected and measured long-period S waves from CANNIKIN at 6 out of a possible 8 LRSM portable stations.

Strauss (1973) determined the long-period S threshold at ALPA for earth-quakes in Kamchatka and the Kuril Islands by beamforming the vertical, radial, and transverse components and measuring A/T on the trace with the largest amplitude. He plotted S waves from 43 earthquakes and four presumed explo-sions and concluded that there was a factor of ten separation between the average A/T values of the two populations when the log (A/T) values were normalized by subtracting m_b. He also made a distance correction similar to that of Evernden's (1969) which, as we shall see below, disagrees seriously with other observations. With this normalization, however, he found that the largest A/T for explosions was only a factor of 2.0 below the lowest value of A/T for earthquakes.

Distance-Amplitude Relations

Gutenberg (1954b, 1945c), and Gutenberg and Richter (1956), (see also Richter (1958) from which Figure 1 is copied), developed distance-amplitude curves for S as well as P. The data were normalized to M_s from LR as dis-cussed by Gutenberg (1945a). The data used were 1923-1939 station bulletins Gutenberg, 1945c). The instruments in use at that time were varied and it is not clear what the observed predominant period would have been (Stauder, personal communication). Thus it might be surprising if Gutenberg's curves were approximately valid for S waves recorded on modern long-period instru-mentation. However, we shall see that his curves appear to be fairly accurate for this application. Evernden (1969) proposed a distance-amplitude formula for long-period S which decays much more slowly than that of Gutenberg and Richter, i.e. A/T proportional to $\Delta^{-.7}$. Nuttli (1969) plotted amplitude data for the first motion SH from GREELEY as a function of distance; see Figure 2 for definition of the phase branches, and Figure 3 for the amplitude data. These data show the rapid fall-off with distance seen also in Figure 1 for surface focus, and are in striking disagreement with a $\Delta^{-.7}$ law, as drawn in Figure 2 and normalized at 20°. This rapid decay of S with distance has also been found for the pure S wave uncontaminated by PL by Helmberger (1974) using theoretical calculations for reasonable velocity structures in the mantle.

In this study we report a distance-amplitude relation for S waves from earthquakes which is in excellent agreement with the shape of Nuttli's GREELEY data and which disagrees with Gutenberg and Richter's only around $\Delta = 20°$, where the shape of our curve shows the sharp maximum found by Nuttli. Gutenberg and Richter's curve is about 0.5 magnitude units smaller than Nuttli's and our data around 20°.

Source of S Waves from Explosions

While SV radiation from explosions could be created by P to S conversion at the free surface and other horizontal interfaces, early workers in seismic discrimination had hopes that SH waves would not be present in explosion signals and would prove to be a powerful diagnostic.

In 1962 Wright and Carpenter suggested that common field experience with small explosives indicated that SH waves were generally observed. To help explain this they exploded small charges in soft clay and made plaster casts of the resulting holes. Figure 4 shows cross-sections of the plaster cast as drawn by Wright and Carpenter. We see in the left-hand polar diagram a substantial asymmetry about the shot point. One would expect that this would be accompanied by substantial SH motion. Wright and Carpenter tentatively explained the asymmetry as being a result of Taylor instability which occurs when a light material is accelerating a heavy one. This experiment and accompanying explanation might lead one to expect more SH motion from explosions in weak material than from explosions in strong material.

Kisslinger, Mateker, and McEvilly (1961) made careful measurements of the SH radiation from small explosions in soil. In Figure 5 we see one of their observed radiation patterns, and a perfect fit (after polarity reversal) of SH waveforms at two stations 144° apart. Kisslinger et al. reached the general conclusion that, surprisingly, "the radiation pattern seems to be tied into the geography of the test site".

The most difficult set of their experiments to understand was the finding of nearly identical SH radiation from a series of three shots in which the first 0.5 lb charge was tamped in soil at a shallow depth which

-3-

led to cratering. The hole was then dug out into a smooth hemisphere and filled with water in which another 0.5 lb charge was detonated; the hole was filled again, and an 0.5 lb charge again detonated.

This experiment would seem to rule out cracking as a possible generation mechanism, leaving only Taylor instability. The most obvious reason we can imagine for having a preferred orientation for the SH radiation resulting from Taylor instability in these experiments is a consistent asymmetry in the orientation of the actual explosive. Such an asymmetry might preferentially trigger one particular mode of Taylor instability. However, Carl Kisslinger (personal communication) says that the dynamite sticks were exploded one on top of the other, not side by side; and that the firing cap was placed in the end of one of the sticks of dynamite. A remaining possibility is that the soil is anisotropic, leading to a preferred form of Taylor instability when the water pressure wave hits the soil surface.

White and Sengbush (1963) also detected SH motion from small explosions. The data in Kisslinger et al. (1961) were all recorded at the surface, and as a result were predominantly of the Love wave type. They found "Love to Rayleigh" ratios on the order of 1:4. Geyer and Martner (1969) on the other hand used down-hole recorders and thus were able to measure SH and SV directly. They obtained SH to SV ratios as great as 5 or 10 to 1 in some cases (the apparent relative amplitudes in their Figures are accurate; S. T. Martner, personal communication) and they conclude:

"1. SH waves are commonplace. In fact, they have been identified in almost every area where we have used three-component seismometers.

2. The most striking development of the SH waves is associated with horizontal, high-contrast interfaces. (In fact, it might be suggested that this could be a way to shoot nuclear devices to generate large amounts of SH waves so that they could be disguised as earthquakes.)

3. The amplitude of SH waves increases approximately linearly as a function of charge weight.

4. Azimuthal data, though limited in these experiments, does not indicate appreciable change in the amplitude of SH waves as a function of the direction of propagation.

5. The data in this paper have not, as yet, contributed to a satisfactory theoretical explanation for the generation of SH waves from explosive sources."

Geyer and Martner's second conclusion might be understood in terms of Taylor instability if one assumed that at sharp, high-contrast interfaces the material strength is low and variable.

In all the above studies one must, of course, remember that there is a substantial difference in scale between small explosions in soil, and underground weapons tests. For example, it might have been expected that any displacement of an NTS cavity or collapse cone similar to that in Figure 4 would have been noticed.

Evidence for tectonic strain release is given by Nuttli (1969), who showed that there was a node in the S wave radiation patterns of GREELEY and HALFBEAK, as seen in Figures 6a and 6b in which the direction of first motion change with azimuth.

W. R. Perret in several publications has demonstrated the presence of substantial close-in SH radiation from nuclear explosions. Figure 7, from Perret (1972) shows the instrumental layout for the GASBUGGY gas stimulation experiment. Figures 8 through 14 give his recorded velocity, displacement and reduced displacement potential traces. Only the radial data (Figures 10, 11, and 14) were reproduced in Perret (1972); the vertical and transverse data may be found in Perret (1970). We see from these data that the vertical and transverse motion at shot level is typically 1/4 the amplitude of the radial motion.

In Figure 15 (from Perret, 1968) we see the instrumental layout for the STERLING explosion which was set off in the cavity created in a salt dome by the SALMON explosion. Figures 16 and 17 give the radial and vertical shot-level recordings and we see that at the closest distance the SV to P ratio is

about 1/3 but at greater distances the ratio is about 1/10. Analysis of a mis-oriented instrument enabled Perret to conclude that the SH to SV ratio is very small. These results are consistent with the idea that the SV radiation observed resulted from conversion due to the non-spherical cavity resulting from the recrystallized pool of molten salt from the SALMON explosion. The absence of SH radiation is open to the natural explanation that because of decoupling there could be neither strain release, Taylor instability, nor cracking.

On the other hand, Perret's (1967) data for the original SALMON shot (Figures 18, 19, 20) show SH to P amplitude ratios ranging between 0.5 and 0.1. These data are difficult to understand in view of the teleseismic observations (Teledyne Geotech, 1964) of no detectible horizontally polarized long-period radiation from SALMON. We have verified this conclusion by examination of the original LRSM film data at EU-AL and JE-LA, the two closest stations. At JE-LA, which is oriented nearly radial and transverse to SALMON, the Love to Rayleigh ratio is less than 0.1. The short-period records, dominated by 2 Hz energy, show a transverse to radial ratio of about 0.5. One might argue that EU-AL and JE-LA were near nodes in the long period Love wave radiation patterns, while more distant stations had insufficient signal to noise ratios for reliable estimation of Love waves. Perret's observations of $S/P \approx 1/3$ for explosion together with the 6-7/1 ratio expected from a simple double-couple earthquake lead one to expect about 1.3 magnitude units S-LR separation, assuming that S and P convert to LR equally efficiently at the free surface.

Toksöz and Kehrer (1972), Thomson et al. (1969), Lambert et al. (1972), Toksöz et al. (1971), Toksöz et al. (1965), Brune and Pomeroy (1963), and others have generally interpreted the Love wave radiation from underground nuclear tests as being evidence for earthquake triggering, or as evidence of release of prestress due to the bomb cavity or due to cracks controlled by the prestress. It seems clear, however, in view of the results of Kisslinger et al. (1961) and Geyer and Martner (1969) quoted above, that there are alternative explanations for the data.

For example, perhaps the most convincing evidence for strain release in Toksöz et al. (1972) is the observed reversal of phase for Rayleigh waves

between explosions with small and large F values. (Toksöz et al., and earlier workers, define F as the fraction of low-frequency displacement amplitude due to strain release.) However, as seen in Figure 5, similar phenomena were found by Kisslinger et al. for the horizontally polarized surface radiation from their explosions in soil and these reversals could not have been caused by strain release.

As a summary of this literature review on the origin of SH radiation from underground explosions we may say that while strain release is a tenable hypothesis which can explain anomalies in radiation from nuclear explosions at NTS; the existence of SH radiation from smaller explosions, which cannot be explained by this mechanism, leaves the hypothesis open to doubt.

DETECTION

Table I is a list of 56 events for which we attempted to detect long-period S and P waves at LASA. Table II gives the criteria which define the population. There were approximately 10 events which fit the criteria but which could not be examined because of unrecoverable data. Table III defines the four-dimensional "window" used for the detection study. If in one of the three 128-second overlapping detection windows surrounding the expected arrival time the program FKCOMB (Smart, 1972) printed out a detection meeting these criteria, then the event was declared detected.

The false alarm rate was evaluated by looking for detections in the other three quadrants for those time windows in which there was no detection in the quadrant from which the arrival was expected. An S or P in the FA column in Table I indicates the phase for which a false alarm was obtained. Some false alarms were detected in runs on data not presented here.

Out of 156 P time windows examined, there were 3 false alarms. Each time window had three possible quadrants; however, a false alarm in any one of three time windows constitutes a detection; therefore the P false alarm probability per event is given by (3/156) x (1/3) x 3 = 0.02. Similarly, there were 10 false alarms out of 100 S wave windows examined for a false alarm probability of 0.1, five times the P-wave value.

A full discussion of program FKCOMB may be found in Smart (1972) and Smart and Flinn (1971); however, we will give a brief discussion of the method here. The program forms the full three-dimensional f-k spectrum and searches for three-dimensional maxima. It prints these out with the appropriate estimated parameters. The program has an option to strip away the energy resulting from a large interfering signal in order to look at a smaller one; however, all our statistics are without stripping, since in running about 20 events with stripping we did not pick up any additional detections.

To conserve computation time we attempted to detect SH waves only, since we thought at the beginning of this study that SH waves would be most powerful for discrimination. An analysis of long-period SH and SV waves at NORSAR beamed for about 50 Asian earthquakes yielded a median SH to SV amplitude ratio of 0.7. This would imply that SH thresholds achieved in this report

-8-

TABLE I

Events Analyzed

Date	Origin Time	Lat(N)	Long(E)	Depth	m_b	Detection P	S	FA
2 June 1970	23:33:30.2	45.7	150.9	20	5.4	Y	Y	
10 June 1970	16:17:48.7	44.9	149.5	57	5.7	Y	Y	
12 June 1970	03:05:20.7	44.9	148.9	33	4.9	N	N	
12 June 1970	12:47:31.4	43.5	147.0	40	4.9	N	BT	
13 June 1970	11:48:46.3	44.6	148.3	50	5.0	N	<u>N</u>	
22 June 1970	21:33:32.6	43.5	147.6	33	5.6	Y	Y	
18 Dec 1970	22:28:54.1	50.2	156.7	61	5.1	Y	Y	
21 Dec 1970	10:52:54.9	43.8	151.0	38	5.1	N	Y	
27 Dec 1970	20:44:48.9	44.9	150.7	48	5.2	<u>N</u>	Y	
6 Feb 1971	10:43:05.5	47.0	154.1	60	5.6	Y	Y	
17 Feb 1971	00:43:45.5	46.8	152.8	47	4.9	N	Y	
27 Feb 1971	02:26:41.8	45.6	150.8	33	5.1	N	<u>N</u>	
18 Mar 1971	03:13:15.4	49.2	156.3	33	5.1	N	Y	
24 Mar 1971	18:25:17.9	45.0	148.9	56	5.0	N	<u>N</u>	S
11 June 1971	10:48:47.9	49.9	156.5	55	5.2	<u>Y</u>	Y	
17 June 1971	09:32:05.4	44.4	148.9	33	4.9	N	N	S
9 July 1971	06:39:47.0	43.4	147.7	49	5.1	N	<u>N</u>	S
9 July 1971	08:06:35.2	43.4	147.7	54	4.9	N	N	
9 July 1971	16:44:15.8	43.4	147.7	46	4.9	N	Y	
1 Aug 1971	02:06:06.6	50.4	156.8	20	5.6	Y	Y	
19 Aug 1971	22:15:37.7	49.3	155.4	33	6.0	Y	Y	
23 Aug 1971	21:55:17.7	45.6	151.0	34	5.7	Y	Y	P
1 Sept 1971	10:54:04.6	48.4	154.9	50	4.9	N	N	
8 Sept 1971	07:25:14.5	37.2	141.3	56	5.5	Y	Y	
9 Sept 1971	10:35:23.2	46.0	150.0	47	5.1	N	Y	
9 Sept 1971	23:01:06.8	44.4	150.9	7	6.0	Y	Y	
14 Sept 1971	06:56:31.8	42.3	144.7	39	4.9	N	N	S
15 Sept 1971	14:55:05.3	39.1	143.4	17	5.8	Y	Y	

TABLE I (Continued)

Events Analyzed

Date	Origin Time	Lat(N)	Long(E)	Depth	m_b	Detection P	S	FA
16 Sept 1971	18:51:44.1	39.0	143.5	43	5.2	<u>Y</u>	Y	
24 Sept 1971	01:10:00.4	39.4	143.2	22	5.6	Y	Y	
27 Sept 1971	15:37:23.2	49.4	155.6	33	5.3	<u>N</u>	Y	
11 Oct 1971	01:29:36.2	45.4	150.7	60	5.2	<u>N</u>	Y	S
11 Oct 1971	10:16:14.7	35.8	140.4	66	5.1	Y	Y	
26 Oct 1971	12:52:10.0	42.2	142.9	69	4.9	N	N	
29 Oct 1971	14:06:27.0	49.9	154.9	95	5.6	Y	Y	
3 Nov 1971	10:32:00.0	43.4	146.7	60	4.8	N	N	
7 Nov 1971	07:51:44.8	41.8	142.2	75	5.0	N	<u>N</u>	
11 Nov 1971	10:19:55.9	42.0	142.5	71	5.3	<u>Y</u>	Y	S
24 Nov 1971	00:58:06.1	46.7	152.6	54	5.3	<u>N</u>	Y	
28 Nov 1971	17:48:09.7	49.5	155.5	85	5.0	N	Y	
2 Dec 1971	17:18:21.8	44.8	153.3	24	6.2	Y	Y	
3 Dec 1971	19:13:07.7	47.1	153.1	33	4.8	N	N	
22 Dec 1971	11:50:26.4	44.3	147.4	65	4.8	N	N	
26 Dec 1971	14:20:46.5	43.5	147.9	27	5.2	<u>N</u>	Y	
12 Jan 1972	02:36:25.5	50.8	156.6	80	4.8	N	N	
13 Jan 1972	13:54:16.3	46.8	152.8	60	5.2	<u>N</u>	<u>N</u>	
18 Jan 1972	14:02:01.1	44.6	149.1	52	4.8	Y	N	
7 Feb 1972	05:07:53.7	39.5	143.4	38	5.0	N	Y	
19 Feb 1972	22:40:17.9	44.6	149.1	48	5.0	N	<u>N</u>	
22 Feb 1972	19:59:56.8	41.8	142.8	53	5.3	<u>N</u>	Y	
23 Feb 1972	03:07:03.8	43.7	148.3	41	4.8	N	N	
23 Feb 1972	03:42:41.1	43.9	148.2	39	4.9	N	N	
24 Feb 1972	10:19:36.6	48.8	155.7	55	5.0	Y	Y	
26 Feb 1972	02:12:57.3	49.2	156.2	33	4.9	Y	Y	
26 Feb 1972	05:58:22.1	46.8	152.6	33	4.9	N	N	
29 Feb 1972	11:07:57.3	33.5	141.0	51	5.0	N	Y	

TABLE II

Criteria for Selecting Events
from the USGS Earthquake List

$h \leq 100$ km

$m_b \geq 4.9$

June 1970   GR 221 and 222 (Kurils)

Dec 1971 - 30 March 1971

June 1971 - August 1971

$m_b \geq 4.8$

Sept 1971 - Feb 1972   GR 221, 222, 224, 228, 229
                                 (Kurils and Japan)

TABLE III

Criteria for Detection of
Long-Period P and S at
LASA from Kurils and Japan
using Program FKCOMB

Velocity

    P   17-25 km/sec

    S   7-13 km/sec

Azimuth   270° - 360°

Period   10 - 40 seconds

F statistic $\geq$ 7

would be lowered by about .15 magnitude units had FKCOMB been called upon to make the appropriate rotations for SV. Inspection of these same data shows that SV is more easily detected on the radial than on the vertical component, reflecting the fact that SV motion has a larger radial than vertical component.

The P and S columns of Table I show whether or not the P or S wave was detected. Figures 21 and 22 are computer-fitted cumulative normal curves for these data giving the probability of detecting P or S waves as a function of m_b. The 90% point for P and S waves are m_b 5.6 and 5.2 respectively. The 50% points are 5.25 and 5.0, respectively.

We attempted to evaluate the efficacy of FKCOMB as compared to beamforming by beaming P waves from all magnitude 5.2 and 5.3 events. We also beamed all the S wave FKCOMB non-detections for events with $m_b \geq 5.0$. These events are indicated by underlining in the P or S detection columns of Table I, and in every case if FKCOMB detected or did not detect the signal we reached the same conclusion upon viewing the plotted beam. In general there seems to be a close equivalence between the power of the two techniques.

We have, however, found other examples in which FKCOMB failed to detect an S wave which was apparent on the beam. Figure 23 shows the SH beam for an earthquake in Kamchatka. The time windows used in an attempt at detection by FKCOMB are indicated on the plot. No suitable detection was declared on the FKCOMB printout.

An even more interesting example of the failure of FKCOMB to detect is given in Figure 24. FKCOMB failed to detect the CANNIKIN SH wave which is quite clear on the beam. The reason for this is, as we shall see in Figure 33, that the SH component is quite different on different channels at LASA. FKCOMB detections are determined by an F statistic which is large only if the signal is nearly the same on every channel.

One interpretation of this result is that the true SH emitted from the CANNIKIN source was negligible, and that the transversely polarized signals at each LASA sensor consisted only of SV waves which had been refracted through angles which varied from site to site.

Comparison of radial and transverse components for the LR and LQ waves from CANNIKIN show that the calibrations and orientations of the individual sites were accurate. The calibrations closest in time to CANNIKIN both before and after the event were reviewed and found to be in agreement with each other to within 5%.

As discussed in the Introduction, the best previously available distance-amplitude relation was presumably that of Gutenberg and Richter (1956), and it was not clear how accurate it would be for use with modern instrumentation with different passbands.

We have therefore developed a preliminary distance-amplitude relation for long-period S from the data base developed by von Seggern (1974). The data base consisted of all long-period S waves measured at the operational Long Period Experiment (LPE) stations for all January-April 1972 events for which LR amplitudes with periods between 17 and 23 seconds were measured at 3 or more LPE stations, and for which the depth was less than 60 km. For each such event an average M_S value was calculated using the formulas:

$$M_S = \log(A/T) + 1.16 \log \Delta + .74 \quad \Delta < 15°$$

$$M_S = \log(A/T) + 1.66 \log \Delta - 0.18 \quad \Delta > 15°$$

where A is peak-to-peak amplitude in millimicrons. These formulas are due to von Seggern (1970) and to Gutenberg (1954a) respectively.

The event average M_S values as subtracted from each $\log(A/T)$ value for S from that event, and the results plotted in 2° intervals as a function of distance, as seen in Figure 25. In each 2° interval the location of the mean was determined, and a smooth curve was then drawn by hand. The tabulated values of this curve are given in Table IV. Use of this distance-amplitude formula must be guided by the realization that the seismic analysts picked the largest amplitude on either component, and that they made no attempt to exclude either late branches of the S-wave or PL-type motion.

On Figure 25 we have plotted a few B values from Gutenberg and Richter's (1965) surface focus distance-amplitude relation (see Figure 1). We see that the agreement is probably within experimental error except around 20° where Gutenberg and Richter's data seem to be too low. Also in Figure 5 we have plotted a few points from the smooth curve drawn through Nuttli's (1969) data in Figure 6. These are normalized at 20° and we see that the agreement is excellent despite the fact that Nuttli measured only the first peak and only for SH.

TABLE IV

Distance-amplitude B Factor
to be used in the Formula

$$M_{SHEAR} = \log(A/T)_{SHEAR} + B$$

Δ	B	GB	Δ	B	GB
10	2.61		54	3.50	
12	2.50		56	3.58	
14	2.48		58	3.71	
16	2.45		60	3.75	3.6
18	2.48		62	3.76	
20	2.50	3.0	64	3.77	
22	2.57		66	3.78	
24	2.75		68	3.78	
26	3.00		70	3.78	3.9
28	3.27		72	3.78	
30	3.36	3.35	74	3.78	
32	3.40		76	3.78	
34	3.43		78	3.78	
36	3.44		80	3.79	3.6
38	3.44		82	3.80	
40	3.45	3.7	84	3.81	
42	3.45		88	3.82	
44	3.45		90	3.86	3.85
46	3.45		92	3.90	
48	3.45		94	3.95	
50	3.45	3.6	96	4.00	
52	3.46		98	4.10	
			100	4.15	4.4

Jan-Apr; LPE Data; h < 60 km.
LR detected at 3 or more LPE stations.
GB is Gutenberg B factor.

As an additional check on the accuracy of our distance-amplitude curve, we have plotted in Figure 26 the points on Figure 25 for those events for which LR was measured at 7 or more of the 8 LPE stations. By thus restricting the data base to large events, we hope to detect any bias due to preferential detection of large-amplitude S waves. By comparison with the original curve, also plotted in Figure 26 we see that it does not appear to be biased with respect to the selected data.

By use of this distance-amplitude relation we may attempt to reconcile our S wave thresholds with those found by Strauss (1973). In Figure 27 we see his results, together with a fitted cumulative normal curve suggesting that the 50 and 90% points are m_b 4.2 and 4.7 respectively. The range of distances from ALPA to events in Kamchatka and the Kurils is 27°-42°, over which our B factor varies from 3.13 to 3.45, a range of 0.32 magnitude units. Let us assume an average B factor of 3.40, keeping in mind the sharp increase in the B factor right at 27° and the greater seismicity in the Kuril Islands. The range of distances from LASA to events in the Kurils and Japan is 56° to 84° with a range of B factors between 3.58 and 3.81. Over most of this range the B factor is 3.78. Let us select this as an average B factor. The difference in average B factors is 0.38 magnitude units. Since M_s is approximately proportional to the first power of m_b in Seismic Region 19 (von Seggern, 1974) this difference in long period magnitude should translate into an approximately equal difference in short-period thresholds.

From Figures 22 and 27 we see that the observed difference in 50% thresholds is 0.78 m_b units, leaving a difference of 0.4 magnitude units unexplained.

This difference may be accounted for by the differing noise levels at the two arrays. From Strauss (1973, Figures 1, 2, 3) we can estimate the rms 18-40 second median single sensor LPZ noise level to be 10 mμ. Dividing by the square root of 19 to obtain the beam rms amplitudes we obtain 2.3 mμ (from Clark et al. 1972, Table V, one may obtain the median ALPA LPZ beam rms value as 7.5 mμ, but their bandpass limits were 15-50 seconds, and the data are from 1970, when there was a severe long-period system noise problem at ALPA). The noise level at LASA may be obtained from Farnham (1968),

-17-

Table II, and Massé et al. (1970, Table III). The median rms LPZ 15-50 second value from these studies is 4.5 mμ. Thus we see that the beam noise level at ALPA is approximately 4.5/2.3 - 2.0 times lower tnan at LASA. Assuming that the horizontal noise levels are proportional to the vertical noise levels, this could account for 0.3 of the 0.4 magnitude units discrepancy. The discrepancy could be further reduced to 0.05 magnitude units by allowing for the SH/SV ratio of -0.15 magnitude units as discussed in the previous section.

MEASUREMENTS OF S FROM EXPLOSIONS, AND DISCRIMINATION
WITH RESPECT TO EARTHQUAKES

In measuring S waves from NTS explosions we decided to concentrate on those LRSM stations oriented radially and transverse to the test site in order to eliminate the possibility that inaccurate calibrations could introduce an apparent SH component which was in fact rotated SV motion. The further requirement that the stations be in operation for most of the events of interest reduced the list of stations to RKON, WH2YK, HNME, and NPNT. For MILROW and CANNIKIN in this report, we have used some rotated data, and for the CANNIKIN event several other LRSM stations were specially deployed radial and transverse to the event.

For the sake of concreteness, we have included in this report several illustrations of S waves from explosions. Figure 28 gives the rotated vertical, radial, and transverse waveforms from CANNIKIN as observed at the LASA AO subarray. A distinct SH component about 1/4 the amplitude of SV can be seen. Figures 29, 30, and 31 give a more detailed look at the vertical, radial, and transverse components of the CANNIKIN P wave. Note the very small upward first motion, which might well be attributed to the effect of pP. (It is possible that the P waveforms are distorted by non-linearities in the amplifier, which will clip at 30 mv peak-to-peak input (Gudzin and Hennen, 1967 and Gudzin, personal communication). The seismometer output is 4.5 mv/μ at 1 Hz, and the CANNIKIN short-period P at LASA is about 6μ peak-to-peak at .9 Hz, which yields 24 mv peak-to-peak.) Note that the transverse component is equal in amplitude to the radial although both are only about 0.1 times the vertical. Figures 32 and 33 give the radial and transverse components of the CANNIKIN S wave at all the LASA subarrays. Note that the amplitude for SV ranges over a factor of 2460/1504 = 1.6. A review of the instrument calibrations shows that the variation must be real. The variation is even greater for SH, on the order of 1064/341 = 3.1, and it is clear that the actual waveform varies in shape from instrument to instrument. Figures 34 and 35 show the SV and SH waves at LASA for MILROW. We see that the beam SH/SV ratio is much greater for MILROW than for CANNIKIN. Figures 36-39a show tracings of the best signal-to-noise ratio data available at RKON, WH2YK,

HNME, and NPNT. In Figures 38 and 39a for HNME and NPNT we see that following an initial motion on R and T, the motion grows larger and appears on Z. This motion may be interpreted either as PL motion (Oliver, 1961; Helmberger and Engen, 1974); or as late arrivals due to triplication of the travel-time curve (Nuttli, 1959, 1964; Nuttli and Whitmore, 1962; Haskell, 1962). Note that at HNME this late-arriving energy also shows up clearly on the transverse component, suggesting that if it is due to PL-type conversion, then it must be converted from the incoming SH motion, a possibility suggested by Oliver (1961).

For routine discrimination purposes it seems clear, considering the controversy over the nature of this energy, that we must rely on the analyst only to pick the maximum amplitude in the first few cycles of an apparent phase. This is the approach taken in the present report.

In Figure 40 we show tracings of S waves at RKON for PILEDRIVER. PILEDRIVER is of special interest because it has the highest F value reported by Toksöz and Kehrer (1972).

In selecting events to analyze we decided to restrict ourselves to explosions of about a megaton or larger in order to avoid signal-to-noise ratio problems and to ensure that we fully sampled the range of S wave amplitudes emitted from the explosions. The resulting set of events is described in Table V. FAULTLESS is included, even though the yield is listed by Springer and Kinnaman (1971) as intermediate, because it was exploded at a depth greater than 3000 feet, and because its M_s value is larger than all other events in the list except BOXCAR. The M_s values for FAULTLESS, HANDLY, and JORUM were determined by us, using LR readings at NPNT, RKON, PGBU, and HNME together with the distance formula and station corrections given by von Seggern (1973), and with a further correction as described below.

Von Seggern's formulas were derived using continental United States and Canada LRSM data for NTS explosions. His station corrections and distance-amplitude relations ensured that approximately the same M_s value would result from measurement of the maximum film amplitude at any station. The overall

TABLE V

Parameters of Selected Explosions

From Springer and Kinnaman (1971) Unless Otherwise Noted

Event Number	Name and Date (GMT)	Shot Time (GMT)	Yield (kt)	Ms	mb	F (1)	Fault Azimuth (1)	Location	Depth (ft)	Remarks
1	Benham 12/19/68	16:30	1100	5.42 (6)	6.12 (6)	.85	345°	37 13 53.3N 116 04 41.9W	4600	Pahute Mesa
2	Boxcar 4/26/68	15:00	1200	5.52 (6)	6.11 (6)	.59	346°	37 17 43.5N 116 27 20.5W	3800	Pahute Mesa
3	Faultless 1/19/68	18:15	I	5.36 (5)	6.3 (8)	.50	344°	38 38 03.4N 116 12 55.2W	3200	Hot Creek Valley
4	Greeley 12/20/66	15:30	825	5.31 (6)	6.14 (6)	1.60	355°	37 18 07.4N 116 24 29.9W	3985	Pahute Mesa
5	Handley 3/26/70	19:00	Slightly >1 Mt	5.35 (5)	6.5 (7)	NA	NA	37 18 01.7N 116 32 02.8W	3957	Pahute Mesa
6	Jorum 9/16/69	14:30	LM	5.12 (5)	6.2 (7)	NA	NA	37 18 50.9N 116 27 38.4W	3800	Pahute Mesa
7 (4)	Cannikin 11/06/71	22:00	<5 Mt (9)	5.76	7.05	.60	60°	51 28 19.0N 179 06 24.0E	5875	Amchitka
8	Milrow 10/2/69	22:06	LM (1 Mt) 3	4.84 (2)	6.42 (2)	<.6		51 25 01.6N 179 10 56.3E	4000	Amchitka
9	Piledriver 6/2/66	15:30	~56	4.05 (6)	5.37 (6)	3.20	340°	37 13 37.4N 116 03 19.9W	1518	Climax stock N. of Yucca

(1) Toksöz and Kehrer (1972)
(2) von Seggern and Lambert (1972)
(3) United States Atomic Energy Commission (1969)
(4) All Cannikin information, unless otherwise indicated, from Johns (1971). See also
(5) Willis et al. (1972) for $m_b = 7.02$, $M = 5.74$.
This study using formulas of von Seggern (1973), -0.52.
(6) von Seggern (1973) - 0.52 for M_s as determined in this study.
(7) USGS Earthquake Data Reports
(8) Clark (1968)
(9) Perret (1972).

level was set to yield the same M_s as would Gutenberg's formula at distances greater than 20°. This was accomplished by adjusting the overall magnitude level to be in agreement with that of Lambert and Alexander (1971). However, while almost all of the LRSM data even at distances of 40° in North America have maxima at the Airy phase, such pure continental data was rare in Gutenberg's original data set (Gutenberg, 1945a) and in von Seggern's (1974) data set, from which M_s values for normalization of our S wave distance-amplitude relation were taken. An example of such an Airy phase may be seen on the bottom trace in Figure 39b. Note the strikingly different waveforms for events of the same yield recorded at the same station at approximately equal distances.

The existence of this Airy phase will cause earthquakes or explosions near NTS, recorded in North America, to have too large an M_s. This effect was recognized by Marshall and Basham (1972). However, their correction factors, derived from WWSSN data, do not seem to be large enough to account for the discrepancies illustrated in Figure 39b. This may be due to the fact that because of the narrower response of the LRSM system, the Airy phase maximum occurs at a longer period than on the WWSSN system. Another explanation would be that the dispersion curves chosen by Marshall and Basham for North America are not truly typical.

We choose instead to make our own correction by measuring at a period away from the Airy phase, as did Gutenberg, and using the resulting difference in magnitude as a path correction for magnitudes computed from measurements made on the Airy phase. In reference to Figure 39b we plotted the group velocity as a function of period, and found that a period of 23 seconds is well away from the group velocity minimum ($dU/dT = 0$). We have therefore measured the amplitude in Figures 39b at 23 seconds period. The result is 0.53 units smaller than the magnitude resulting from measurements on the Airy phase maximum. The other megaton-sized NTS explosions recorded at NPNT have very similar waveforms, and measurements of the corresponding cycles yields a mean ΔM_s of 0.53.

Work by von Seggern (1974) and other authors has established that the proper worldwide distance amplitude relationship for LR in the absence of

dominant Airy phases is $\log A \sim (0.9-1.0)\log\Delta$ for $5° < \Delta < 150°$. Von Seggern's 1973 formula, with $\log A \sim 0.87 \log\Delta$ is used in this report and is consistant with the above values. Thus we may interpret von Seggern's station corrections (C_i) as being predominantly due to effects peculiar to the Airy phase, and we would expect that they would not be satisfactory corrections for measurements at other locations on the waveform. Thus, the C_i corrections (0.01 for NPNT) should not be applied directly to the NPNT measurements at 23 seconds discussed above. But we can use them with the following formulation:

$$M_{Gutenberg} = M_{Airy} + [M_{Gutenberg} - M_{Airy}]$$

$$= M_{Airy} + \{\log(A/T)_{T=23} - [\log(A/T)_{Airy} - C_i]\}$$

$$= M_{Airy} - \{[\log(A/T)_{Airy} - \log(A/T)_{T=23}] - C_i\}.$$

Thus we shall subtract $\Delta = 0.52 = 0.53 - 0.01$ magnitude units from all M_s values determined using the method of von Seggern (1973). As a check on this result, we analyzed JORUM at HNME where $C_i = -0.20$ and found $\Delta = 0.37 - (-0.20) = 0.57$. The result at NPNT is preferable, however, since the waveform there shows the clearest dispersion. Ideally, we should determine Δ for all stations used and average them; but this is not possible for the other LRSM stations because their range from NTS is too short for an adequately dispersed wave to clearly show 20 second cycles.

This result illustrates a possible general approach to the measurement of M_s and was analyzed in some detail by von Seggern (1971). We suggest that a graph of group-velocity vs period be constructed for each epicentral region-station pair. A period near 20 seconds well away from any Airy phases should be selected, and the amplitude corrected using the formula from Marshall and Basham (1972) appropriate for stationary phases: $A \sim UT^{-3/2}(dU/dT)^{-1/2}$. The difference between the corrected amplitude and the maximum amplitude on the record can be used as a path correction for measurements made at the maximum amplitude on future records. In addition, the corrected amplitudes could be plotted as a function of distance to determine an improved distance-amplitude relation.

In Table VI we give the amplitude and period measurements for S together with the M_{SV} and M_{SH} magnitudes calculated using the distance-amplitude formula in Table IV and Figure 25.

Finally, in Figure 41a we present a plot of $M_{SH} - M_s$ versus $M_{SV} - M_s$ for the data measured in this report. We expect the earthquakes to cluster 0.1 - 0.2 magnitude units diagonally below (0,0) since we defined the distance-correction terms for S-wave M_s using measurements taken from the component with the larger S amplitude.

We note that the center of gravity for the NTS explosion points lies slightly below the diagonal line near the point (-.6, -.9), showing good separation from the mean earthquake population. While GREELEY, with an F value of 1.6, is above the line for NPNT and HNME, the absolute value of the S wave is still small compared to the Rayleigh wave. The same remark is true for the single reading at RKON of an S wave from PILEDRIVER, which has an F value of 3.20.

There are several possible explanations for the separation between earthquakes and explosions other than energy variation at the source.

o   A low Q region beneath nuclear test sites absorbs the long-period S waves but is deep enough not to attenuate the surface waves.

o   Due to a low-velocity surface layer, the incidence angle (with respect to the vertical) for S-waves observed at $\Delta = 20°-40°$ is substantially less than the value of 30° given by Chandra (1972). Then if the strain release fault mechanism is vertical strike-slip, as suggested by Toksöz and Kehrer (1972), the shear radiation would be close to the downward null axis of the source mechanism.

o   The strain release fault may in fact not be vertical strike-slip, but may dip to the northeast, creating a node in the teleseismic radiation pattern for the signals at almost all of our observing stations.

We will now discuss each of these possibilities in more detail. If a low-Q layer existed, one would expect that teleseismic long-period S arriving in the Basin and Range would have lower amplitudes than waves from the same event arriving on the East Coast. However, examination of the long-period

-24-

TABLE VI

S_H and S_V Measurements

Δ°	S_H A	T	Log(A/T)	M_{SH}	S_V A	T	Log(A/T)	M_{SV}	Comments
Benham (1)									
RK	3.18+3	20	2.20	4.74	2.90+3	12	2.38	4.92	
WH	1.09+3	21	1.72	4.75	7.05+3	19	2.57	5.60	
HN	5.60+2	18	1.50	4.94	1.10+3	21	1.72	5.16	Funny pulse, possible PcS
NP	1.00+3	20	1.70	5.15	1.49+3	30	1.69	5.14	
				4.90				5.20	
Boxcar (2)									
RK	1.54+3	21	1.87	4.41	1.87+3	13	2.16	4.70	
WH	8.61+2	18	1.68	4.71	8.06+3	17	2.68	5.71	Peculiar phase
HN	2.59+2	33	.89	4.33	7.9+2	30	1.42	4.86	
NP	5.25+2	16	1.52	4.97	1.14+3	30	1.58	5.03	
				4.60				5.08	
Faultless (3)									
RK	1.27+3	13	1.99	4.53	3.64+2	18	1.30	3.84	
WH	5.0+2	22	1.36	4.39	3.02+3	19	2.20	5.23	
HN	1.38+2	20	.84	4.28	4.8+2	24	1.30	4.74	
NP	<2.15+2	20	<1.03	<4.48	1.44+3	31	1.67	5.02	
				4.40				4.70	
Greeley (4)									
RK	1.06+3	25	1.63	4.17	1.00+3	11	1.96	4.50	
HN	2.60+2	20	1.11	4.55	<1.18+2	20	< .64	<4.09	
NP	9.20+2	16	1.76	5.21	<1.23+2	20	< .79	<4.24	
				4.64				~4.50	

TABLE VI (Continued)

S_H and S_V Measurements

Δ°		S_H A	T	Log(A/T)	$\dot{M}_{SH}$	S_V A	T	Log(A/T)	M_{SV}	Comments
Handley (5)										
RK	21.1	1.27+3	15	1.93	4.47	1.31+3	15	1.94	4.48	
HN	36.7	<1.85+2	18	<1.01	<4.45	6.0 +2	26	1.36	4.80	
NP	39.0	2.81+2	20	1.15	4.60	1.0 +3	28	1.55	5.0	PcS
					4.51				4.76	
Jorum (6)										
RK	21.1	6.85+2	18	1.58	4.12	1.05+3	15	1.85	4.39	
WH	26.1	4.27+2	20	1.27	4.30	2.72+3	19	2.16	5.19	
HN	36.6	1.68+2	20	.92	4.36	6.30+2	26	1.38	4.82	
NP	39.0	1.73+2	20	.93	4.38	1.12+3	29	1.59	5.04	
					4.29				4.86	
Cannikin (7)										
WH	26.5	<4.00+2	15	<1.43	<4.49	5.80+3	15	2.59	5.65	
PG	34.6	4.92+2	24	1.31	4.74	2.25+3	19	2.07	5.40	
LAO	47.2	2.31+2	24	.98	4.43	1.72+3	27	1.80	5.25	
KN	49.2	3.16+2	16	1.30	4.75	1.60+3	19	1.92	5.37	
RK	51.6	<3.70+2	24	<1.18	<4.64	1.68+3	24	1.85	5.31	
SJ	64.5	1.08+3	15	1.86	5.63	1.31+3	17	1.89	5.66	
HN	67.0	<1.90+2	25	< .89	<4.67	<2.40+2	25	< .98	<4.76	
BE	73.2	<5.50+2	20	<1.44	<5.22	3.80+2	19	1.30	5.08	
					~4.70				~5.34	

TABLE VI (Continued)

S_H and S_V Measurements

		S_H		M_{SH}		S_V		M_{SV}	Comments
$\Delta°$	A	T	Log(A/T)		A	T	Log(A/T)		

Milrow (8)

LC	56.0	2.14+2	19	1.05	4.63	<2.50+2	20	<1.16	<4.74
PG	34.6	2.42+2	21	1.06	4.49	8.00+1	20	~.60	<4.03
FB	21.5	NA	12	1.91	4.45	NA	14	2.18	4.72	Rotated
NP	34.0						20	1.54	4.97	Rotated
LAO	47.2	1.37+2	20	.84	4.29	2.71+2	26.7	.99	4.44	Rotated
KN	49.2	NA	15	1.37	4.92	NA	16	1.53	4.98	Rotated
RK	51.6	NA	~26	< .70	<4.16	NA	26	1.00	4.46	Rotated
					~4.47				~4.73	

Piledriver (9)

RK		1.14+2	18	.86	3.29	<4.0 +1	~20	< .32	<2.85	Noise Measurements
HN		<2.77+2	~24	<1.06	<4.50	<4.76+2	~24	<1.30	<4.74	Noise Measurements
NP		<4.50+2	~20	<1.35	<4.79	<4.90+2	~20	<1.39	<4.83	
					~3.29				<2.85	

-27-

S waves for the same events and stations used by Der, Massé, and Gurski (1974) to analyze short-period S, shows less than a 10% variation between stations. This would seem to rule out a low-Q zone as a source of low long-period S waves.

While a low-velocity surface layer might result in a steeper emergence angle for short-period S waves, one would not expect such an effect for 20-second waves with wavelengths on the order of 60-100 km. Therefore the angles given by Chandra are appropriate.

A dip of the strain-release fault-plane to the northeast cannot be ruled out with the present data. It is, however, a rather adhoc explanation. Also, sS would not be near a node in this case and should contribute heavily to the signal.

Not only is the overall level of the S wave excitation for explosions lower than that to be expected for earthquakes, but also the relative amplitudes of S waves recorded at RKON from NTS shots cannot be predicted by use of Toksöz and Kehrer's (1972) fault azimuths and F factors.

If we assume that M_s, or a "tectonic" M_s^T given by

$$M_s^T = \log_{10}(\frac{F}{1+F} 10^{M_s})$$

adequately measures the strength of the released strain, and that the shear radiation pattern is as described by Ben-Menahem et al. (1965) and Helmberger (1974), then we may form the quantity $M_{SH} - (M_s^T + \log|\cos 2\theta|)$ where θ is the angle between the strike of the vertical strike-slip earthquake as given by Toksöz and Kehrer (1972) and the epicenter-station azimuth. This quantity should be nearly the same for all explosions from NTS observed at a single station. Effects due to distance may be neglected, since the distance from NTS to any single station is nearly constant. In Table VII we see that at RKON this quantity is no more constant using $M_s^T + \log|\cos 2\theta|$ as the normalizing factor than using M_s itself, and this suggests that the SH body wave radiation does not fit naturally into the double-couple vertical strike-slip source model suggested by Toksöz and Kehrer. Considering the expected variance of the data, however, we do not have a very strong test of the hypothesis.

We mention that one possibly large error in Table VII is that our original measurement of M_s for PILEDRIVER may have been seriously too small because of the cancellation of the direct explosion LR by the strain release (Toksöz and Kehrer, 1972). However, if M_s were made larger for PILEDRIVER the variance about the mean of the numbers in the $M_{SH}^{RK} - M_s^T - \log|\cos \theta|$ column of Table VII would increase while decreasing in the column $M_{SH}^{RK} - M_s$.

Before a definite conclusion can be reached that these data do not support a double-couple source a more careful analysis is needed. For example, it would be desirable to correct the LR measurements at each observing station for each event for the effects due to strain release in order to determine a more accurate M_s^T.

To gain further insight into the problem we decided to analyze earthquakes near NTS. We chose all events between 1962 and 1970 on the USGS seismicity list within a circle of radius 2° around BENHAM, with $m_b \geq 5.0$ which were not aftershocks of either an explosion or another earthquake. We found three events. In Table VIII are the source parameters for two of them. The third, a USGS m_b 5.0 event on October 23, 1970, had long-period LR and S radiation so weak that it could not be analyzed. In Table IX we see the calculated M_s, M_{SH}, and M_{SV} values; and the results, plotted on Figure 41a, place the earthquakes on the border between the earthquakes and explosions. M_s values were calculated with the same procedures used for NTS explosions including the -0.52 M_s dispersion correction.

As a parallel effort we analyzed two of the four NOS events with NOS M_s values between 5.1 and 5.3 between 1962 and 1970 which lay within 2° of MILROW, and which are closest in time to MILROW. These events are listed in Table VIII. The magnitude restriction was imposed in order to ensure good signal-to-noise ratios without clipping.

The measurements and magnitude estimates are given in Table IX, and the results are plotted in Figure 41a for those stations for which components were oriented radial and transverse to Amchitka. We see that these earthquakes are typical of the world-wide population (Gutenberg's distance-amplitude formula was used to calculate M_s from LR).

TABLE VII

M_{SH} at RKON Corrected for the Tectonic Strain Release as
Predicted from F Values Deduced by Toksöz and Kehrer (1972)

Event No.	Event	M_s	F	M_s^T	RK M_{SH}	RK $M_{SH}-M_s$	RK $M_{SH}-M_s^T$	Fault Azimuth	θ	$|\cos2\theta|$	$\log|\cos2\theta|$	$M_{SH}-(M_s^T + \log|\cos2\theta|)$
1	Benham	5.42	.85	5.08	4.74	− .68	− .34	345	−57	.41	− .39	+ .05
2	Boxcar	5.52	.59	5.09	4.41	−1.11	− .68	346	−56	.37	− .43	− .25
3	Faultless	5.36	.50	4.83	4.53	− .83	− .30	344	−58	.44	− .36	+ .06
4	Greeley	5.31	1.60	5.10	4.17	−1.16	− .93	355	−47	.07	−1.15	+ .22
9	Piledriver	4.05	3.20	3.93	3.29	− .76	− .64	340	−62	.56	− .25	− .39
5	Handley	5.35			4.47							
6	Jorum	5.12			4.12							

Azimuth NTS − RKON, 42°

−30−

TABLE VIII

Earthquakes Near Amchitka and NTS

	Date	Origin Time	Lat	Long	Depth	NOS m_b	This Study M_s
Near Amchitka	June 22, 1969	10:45:24.2	51.5N	179.9W	56	6.1	5.3
	August 4, 1969	10:23:28.9	51.4N	179.6W	41	5.3	5.1
Near NTS	August 16, 1966	18:02:36.6	37.4N	114.2W	33	5.6	5.5
	May 22, 1968	13:21:55.7	38.6N	116.2W	13	5.1	4.2

-31-

TABLE IX

LR and S Measurements of Earthquakes near Amchitka and NTS

Event and Distance to Station	Station and Installed Azimuth of LPR	Component	Gain in K at X10 view	Arrival Time	At X20 view Millimeters Amplitude P-P	Period in Seconds	Phase	Station M_S	Comments
69/06/22 55.2°	LCNM (133°)	LPZ	7.65	11:13:50	74	28	LR	4.98	
		LPR	31.50	11:02:31	58	20	S	4.91	
		LPT	48.60	11:02:40	221	25	S	5.20	
48.3°	KNUT (95°)	LPZ	4.98	11:10:10	212	26	LR	5.54	
		LPR	34.10	11:00:57	172	24	S	5.17	
		LPT	30.40	11:01:00	56	16	S	5.06	
66.2°	HNME (93°)	LPZ	5.50	11:25:50	145	23	LR	5.60	
		LPR	49.80	11:04:53	82	30	S	5.00	
		LPT	74.00	11:05:20	85	30	S	4.84	
50.8°	RKON (58°)	LPZ	6.84	11:14:50	198	24	LR	5.40	
		LPR	50.10	11:01:30	187	28	S	5.02	
		LPT	54.40	11:01:40	189	23	S	5.03	
33.6°	NPNT (356°)	LPZ	1.80	11:04:30	50	26	LR	5.10	
		LPR	16.90	10:57:20	74	32	S	5.09	
		LPT	14.90	10:57:10	53	33	S	4.99	
26.1°	WH2YK (325°)	LPZ	1.22	11:04:00	45	19	LR	5.19	
		LPR	.73	10:55:19	< 1				later phase with T=32
		LPT	2.70	10:55:19	14	28	S	5.21	
33.9°	PG2BC (110°)	LPZ	12.60	11:03:40	315	24	LR	5.18	Transverse to Event
		LPR	113.80						Radial to Event
		LPT	112.80	10:57:50	∿540	28	S	5.11	Traces mixed
69/08/04 48.1°	KNUT (95°)	LPZ	3.40	10:48:30	69	23	LR	5.25	
		LPR	35.50	10:39:10	114	23	S	4.99	
		LPT	31.70	10:39:12	25	15	S	4.78	

LCNM, KNUT, NPNT oriented radial and transverse to Amchitka.

TABLE IX (Continued)

LR and S Measurements of Earthquakes near Amchitka and NTS

Event and Distance to Station	Station and Installed Azimuth of LPR	Component	Gain in K at X10 view	Arrival Time	At X20 view Millimeters Amplitude P-P	Period in Seconds	Phase	Station M_S	Comments
66.1°	HNME (93°)	LPZ	5.50	11:06:40	56	19	LR	5.19	late measurement strange looking phase
		LPR	54.80	10:42:57	96	25	S	5.02	
		LPT	57.00	10:42:57	45	28	S	4.68	
50.6°	RKON (58°)	LPZ	7.23	10:52:20	99	25	LR	5.08	
		LPR	52.00	10:39:35	120	26	S	4.82	shorter period earlier
		LPT	55.60	10:39:40	54	35	S	4.44	
33.6°	NPNT (356°)	LPZ	1.90	10:45:15	26	23	LR	4.83	
		LPR	17.30	10:35:40	50	35	S	4.89	Transverse to Event
		LPT	16.10	10:36:00	64	26	S	5.03	Radial to Event
26.0°	WH2YK (325°)	LPZ	12.90	10:41:20	406	18	LR	5.16	
		LPR	11.10	10:34:20	38	20	S	5.08	
		LPT	6.40	10:34:20	28	27	S	5.18	
33.7°	PG2BC (110°)	LPZ	11.00	10:41:30	178	25	LR	4.87	
		LPR	121.00	10:35:30	330	24	S	4.88	time picked after first motion
		LPT	129.00	10:35:20	380	26	S	4.92	

KNUT, NPNT PG2BC oriented radial and transverse to Amchitka

Event and Distance to Station	Station and Installed Azimuth of LPR	Component	Gain in K at X10 view	Arrival Time	At X20 view Millimeters Amplitude P-P	Period in Seconds	Phase	Station M_S	Comments
66/08/16 38.9°	NPNT (356°)	LPZ	1.4K	18:25:30	53	20	LR	4.98	
		LPR	8.1K	18:16:00	27	26	S	5.14	
		LPT	16.50	18:16:00	44	17	S	4.97	
19.8°	RKON (58°)	LPZ	4.92	18:15:00	220	20	LR	5.00	
		LPR	36.00	18:10:45	130	17	S	4.32	
		LPT	48.00	18:10:45	289	24	S	4.29	
35.0°	HNME (93°)	LPZ	7.16	18:23:50	229	19	LR	5.09	
		LPR	45.8	18:15:20	226	25	S	5.14	
		LPT	57.7	18:15:00	24	19	S	4.21	

TABLE IX (Continued)

LR and S Measurements of Earthquakes near Amchitka and NTS

Event and Distance to Station	Station and Installed Azimuth of LPR	Component	Gain in K at X10 view	Arrival Time	At X20 view Millimeters Amplitude P-P	Period in Seconds	Phase	Station M_S	Comments
68/05/22 20.0°	RKON (58°)	LPZ	6.3	13:34:20	7	17	LR	3.48	
		LPR	58.5	13:30:00	< 16	20	S	<3.59	
		LPT	57.2	13:30:15	11	12	S	3.04	
25.0°	WH2YK (325°)	LPZ	12.0	13:37:50	46	16	LR	3.87	
		LPR	5.5	13:32:00	11	19	S	4.32	
		LPT	13.9	13:32:00	< 7	20	S?	<3.68	
35.8°	HNME (93°)	LPZ	70.2	13:44:10	88	19	LR	3.69	
		LPR	69.7	13:34:30	< 5	20?	S?	<3.74	
		LPT	63.4	13:34:30	<| 10	20	S?	<3.46	
		LPT	63.4	13:41:20	145	30	LQ		
37.7°	NPNT (356°)	LPZ	30.8	13:45:40	86	20	LR	3.83	
		I.PR	27.2	13:35:40	6	27	S?	<3.74	PcS?
		LPT	29.0	13:35:40	4	25	S?	<3.58	PcS?

Except for the signal recorded at SJTX, we see that CANNIKIN amplitudes are in relatively good agreement with NTS events. The signal recorded at SJTX has a signal-to-noise ratio of almost 10, and there can be little doubt as to its reality. MILROW has a number of relatively large S waves, and at most of the stations the signal-to-noise ratio was large enough to make measurement unambiguous. However the most anomalous measurement, at KNUT, was at a low signal-to-noise ratio; and so may well be biased toward too high an amplitude.

The rather striking difference between MILROW and CANNIKIN is hard to understand. CANNIKIN was exploded in a fifty-foot diameter mined cavity, whereas MILROW was simply lowered down a borehole (N. Pruvost, personal communication). This suggests that CANNIKIN with its low-amplitude Love waves (see, e.g., Willis et al. 1972), and S waves as seen in this report may be the anomalous event, and that MILROW may be the more normal event for the Amchitka test site. Engdahl (1972) has suggested that there is very little tectonic stress near the surface of the crust at Amchitka.

As a preliminary investigation into the performance of the S/LR discrimination for Asian explosions we beamed NORSAR on the large August 28, 1972 event at Novaya Zemlya. The resulting point is plotted on Figure 41a. The normalizing M_s was determined by von Seggern (1974) using LPE data. We see that it fits nicely into the NTS population. Further investigation of Asian explosions and earthquakes is underway at this time.

To attempt to reduce the scatter in Figure 41a, we have averaged the individual station M_{SH} and M_{SV} values for each event. (If in a series of M_{SH} or M_{SV} measurements for a given event there were noise measurements which yielded low upper-limit magnitude estimates, then the average magnitude was replaced by the median magnitude with the low noise measurements included in the histogram.) The results are plotted in Figure 41b. We see that the best line we can draw still misclassifies the MILROW explosion and that BENHAM is perilously close to misclassification.

All the sample earthquakes fall below the point $(0,0)$ on Figure 41b, as would be expected since this normalizing point corresponds to M_{SHEAR} determined

-35-

from the maximum observed shear wave on either component, as discussed previously. To examine the discrimination which would result if such a procedure had been followed for the earthquakes and explosions analyzed in this report, we have computed the average magnitude for each event obtained by averaging the maximum magnitude component at each station. Since SH/SV does not appear from Figures 41a and 41b to be a good discriminant, little should be lost by this procedure. The result is plotted in Figure 41c. We see that not only do the earthquakes now cluster about the origin as they should, but the discrimination has improved such that perfect discrimination is possible with a suitably chosen line. It must be admitted, however, that the populations are so close that a false classification rate of several percent must be expected in practice.

APPLICATION OF NEGATIVE DISCRIMINANTS

If, as Figure 41 suggests, there is ∿0.5 magnitude difference between the amplitudes ratio S/LR for explosions and earthquakes, then application of this technique for positive discrimination (measurement of the LR and S amplitudes are used to determine the nature of the event) for explosions will be severely limited. Therefore we investigate here some of the general requirements for the application of negative discriminants in which the absence of detectible S waves is an indication of an explosion. The theory as developed will have application not only to negative discrimination by S/LR, but also by $M_s : m_b$.

One may say that negative discrimination is possible when no stations detect S waves from an event. We must note, however, that in this case if S waves are not detected from an earthquake then there is a false alarm. Routine network evaluation programs, e.g. NETWORTH (Wirth, 1970), can calculate the probability of a zero-station detection and can therefore determine the threshold magnitude for any desired false alarm rate. Thus, to determine the capability of negative discrimination it is only necessary to compare the threshold magnitude for some reasonable false alarm rate with the detection threshold required for positive discrimination.

Let us imagine that an event has occurred at 50° N, 155° E (Kamchatka). Let us further suppose that our 25-station long-period network is similar to that of Romney (1971), and has zero-to-peak median long-period noise levels of 19 mμ except that it has 15 mμ noise levels at LASA, ALPA, and NORSAR. Let us also assume a standard deviation of 0.3 magnitude units in the signal and noise amplitudes - and a requirement of a signal-to-noise ratio of 1.5 for detection. Then program NETWORTH enables us to calculate the probability of detection of S waves by K or more stations as a function of magnitude. The results are plotted in Figure 42.

We see that the magnitude for a false alarm probability of 0.01 is almost exactly equal to the magnitude for 90% probability of detection by two or more stations. Thus the M_s negative discrimination threshold for explosions is about equal to the positive discrimination threshold for earthquakes. The

positive discrimination threshold for explosions is 0.5 M_s units higher than for earthquakes because of the mean separation of the two populations as seen in Figure 41a,b,c.

Some discussion is required of the particular probability levels we have chosen for false alarm rate and probability of detection. Since there are several thousand worldwide M_s = 3.4 or larger earthquakes each year; there will be several tens of false alarms. However, this technique is only to be regarded as a screening mechanism, and each of the events could be investigated further. In addition, the chief application of the technique will be against shot arrays; and the possible locations for these have only several hundreds of candidate earthquakes per year.

The requirement for detection by 2 or more stations has several justifications:

o The probability is reduced of picking an arrival from a different event not detected by the short-period network.

o The amplitude of an isolated detection may be anomalously large because of multipath focussing or other unknown cause; and may result in an explosion being classified as an earthquake.

We should note that the differences between the thresholds for negative and positive discrimination would be substantially reduced if the requirement were for .001 probability of a false alarm and 90% probability of detection by 1 or more stations. The conclusions would, of course, be completely reversed were we to look at the question through the eye of a cautious evader and not allow even .01 probability of detection by 1 or more stations.

In Figure 42 we see that the 90% threshold for detection by 4 or more stations is 3.62, about 0.2 magnitude units higher than the thresholds discussed above. The same relationships between thresholds are generally valid at all points on the globe, as can be seen by comparing Figures 43-45.

Figure 43 gives contours of the M_s magnitude for which there is a .01 probability of a false alarm. Figures 44 and 45 give contours of the M_s magnitude for which there is a 90% probability of detection by 2 or 4 stations

-38-

respectively. The star on each of these Figures indicates the epicenter for which Figure 42 was calculated. The triangles indicate the station locations. One station is off the map at the South Pole.

While the standard deviations of 0.3 magnitude units used for the foregoing calculations are reasonable for ensembles of noise amplitudes measured over the course of a year (von Seggern, 1974) and for S wave signals with respect to their mean (see Figure 25) there are certain situations where 0.1 magnitude units is more reasonable; we next investigate the relationship between thresholds in this case.

Such a situation arises when one considers discrimination of a particular event in a well-studied location. In this case the rms noise amplitude is known exactly, and station-epicenter amplitude anomalies may have been determined. From von Seggern and Blandford (1974), von Seggern (1973), and Blandford and Wirth (1973), it is then reasonable to assume a standard deviation of 0.1 magnitude units for both noise and signal.

To look at such a situation from another point of view, consider the case of evaders attempting to avoid discrimination by the S/LR criterion. We may presume that they know the rms noise levels at each detecting station, as well as the station amplitude anomalies. They could therefore attempt very precisely to just slip under the detection threshold.

In Figure 46 we see the curves of 0.1 standard deviations corresponding to Figure 42. We note that the curves are much steeper and that the magnitude for 0.01 probability of a false alarm is about 0.2 unit below the magnitude for 90% probability of detection by 2 or more stations. Thus the negative discrimination threshold for explosions is 0.2 magnitude units lower than the positive discrimination threshold for earthquakes. The positive discrimination threshold for explosions is $0.7 = 0.2 + 0.5$ units higher than for earthquakes because of the mean separation of the two populations as seen in Figure 41. Inspection of Figures 47-49 will show that conclusions drawn from Figure 46 are qualitatively valid at most geographical locations. Furthermore, while these figures are in general similar to Figures 43-45, they are more complicated and show sharper gradients in threshold magnitude. This is because

the sharp maximum in the distance-amplitude relationship of Figure 25 has not been "smoothed out" by the large values of σ. For example, in Figure 47 compare the deep minimum around 15° S, 150° E with the corresponding point in Figure 43, and compare the minima in Figure 49 with the corresponding positions in Figure 45.

The existence of an isolated station can lead to very large threshold differences if $\sigma = 0.1$. Note the difference of 0.8 magnitude units between Figures 47 and 48 at 75°S, 180°E. This is due to the isolated station at the South Pole. In this case the negative threshold for explosions is 1.3 magnitude units below the explosion positive threshold.

Figures 50-57 tell a similar story for detection of Rayleigh waves for use in positive and negative discrimination by use of LR in $M_s:m_b$. In these calculations we used the distance-amplitude formula

$$M_s = \log_{10}(A/T) + \log \Delta + 1.12$$

where A is peak-to-peak amplitude in $m\mu$, and T was taken to be 20 seconds. For $\Delta < 10$ degrees the B factor was taken equal to its value at 10 degrees in order to avoid concentric threshold contours around each station for the case of detection by one or more stations. The main difference observed between LR and S waves is that for LR we do not find the dramatic spread in thresholds for $\sigma = 0.1$ that we found for S.

While we have found great value in the concept of negative discrimination, it must be remembered that the theory relies on an extrapolation of the distribution of recorded amplitudes to probability levels such as 0.01, 0.001, where the supporting data bases are just beginning to reach. Furthermore, the application of negative discrimination in practice requires careful attention to details of system failure, a very careful review of all records, and careful noise amplitude measurements at selected periods by experienced analysts. Finally, the resulting discrimination is often felt to be unsatisfactory for various reasons probably closely related to these difficulties.

Further study of the actual operation of a network using negative and positive discriminants is currently planned by using the network simulation capabilities recently developed by von Seggern and Blandford (1974).

SUMMARY AND SUGGESTIONS FOR FURTHER RESEARCH

We have developed a distance-amplitude formula for S waves and found it to be in good agreement with the data of Nuttli (1969) and the distance-amplitude relation of Gutenberg and Richter (1956), except near 20° where our maximum is more pronounced. This amplitude maximum suggests that stations in the distance range 15°-25° would be very valuable for application of the S/LR ratio discriminant.

We find the 50% and 90% thresholds for detection of S waves at LASA to be m_b = 5.0 and 5.2 respectively, using either beamforming or FKCOMB. These values are consistent with the values 4.2 and 4.7 from Strauss's (1973) ALPA data when consideration is taken of the noise levels and distance-amplitude relation for S waves.

Application of our distance-amplitude relationship made it possible to evaluate M_{SH} and M_{SV} versus M_s as a discriminant, and the results shown in Figures 41a, b, c, suggest that it is a good discriminant. Such a discriminant should work as well for shot arrays as for individual explosions. The success of this discriminant for explosions with high F values suggests that the SH waves from explosions are not due to tectonic strain release, although this conclusion is probably not well-established without better azimuthal converge. The preferred discriminant is to measure the maximum S on any component, see Table IV to compute M_{SHEAR} and discriminate on M_s - M_{SHEAR}.

From Figure 41a, b we can also see that the ratio SH/SV also is not a good discriminant. Figures 32 and 33 suggest that one explanation for this is a substantial amount of site-to-site "rotation" of SV into SH; possibly due to ray refraction out of the great-circle path.

Investigation of negative discrimination as a technique has shown that its threshold for explosions, assuming about 0.01 probability of a false alarm, is within 0.1-0.2 M_s magnitude units of the earthquake threshold for 90% probability of detection by 2 or more stations for a 25-station world-wide network.

Topics for future research include:

- Investigation of long-period P/LR ratios;
- Improved distance-amplitude relations using more LPE data;
- Intensive investigation of Asian earthquakes and explosions using NORSAR;
- Investigation of such puzzles as: Why are MILROW and CANNIKIN so different: Why does SJTX have such a large S wave for CANNIKIN? What is the cause of the large SH on F1 and E2 at LASA for CANNIKIN?
- Better azimuthal coverage of NTS events using WWSSN data.

ACKNOWLEDGEMENTS

REFERENCES

Ben-Menahem, A., S. W. Smith, and T. Teng, 1965, A procedure for source studies from spectrums of long-period seismic body waves, Bull. Seism. Soc. Am., v. 55, p. 203-236.

Blandford, R. and M. H. Wirth, 1973, Automatic array and network detection in the presence of signal variability, Seismic Data Laboratory Report No. 308, Teledyne Geotech, Alexandria, Virginia, AD.

Booker, A. and W. Mitronovas, 1964, An application of statistical discrimination to classify seismic events, Bull. Seism. Soc. Am., v. 54, p. 961-972.

Brune, J. N. and P. W. Pomeroy, 1963, Surface wave radiation patterns for underground nuclear explosions and small-magnitude earthquakes, J. Geophys. Res., v. 68, p. 5005-5028.

Chandra, U., 1972, Angles of incidence of S waves, Bull. Seism. Soc. Am., v. 62, p. 903-916.

Clark, D., 1968, FAULTLESS, Seismic Data Laboratory Report 215, Teledyne Geotech, Alexandria, Virginia. AD 830 474.

Clark, D. M., R. P. Massé, and J. E. Dunavant, 1972, Preliminary evaluation of the Alaskan Long-Period Array, Seismic Data Laboratory Report 281, Teledyne Geotech, Alexandria, Virginia. AD 745 596.

Der, Z. A., R. P. Massé, J. P. Gurski, 1974, Regional attenuation of short-period P and S waves in the United States, SDAC-TR-74-1, Teledyne Geotech, Alexandria, Virginia.

Engdahl, E. R., 1972, Seismic effects of the MILROW and CANNIKIN nuclear explosion, Bull. Seism. Soc. Am., v. 62, p. 1411-1423.

Evernden, J., 1969, Identification of earthquakes and explosions by use of teleseismic data, J. Geophys. Res., v. 74, p. 3828-3856.

Evernden, J. F., 1971, Variation of Rayleigh wave amplitude with distance, Bull. Seism. Soc. Am., v. 61, p. 231-240.

REFERENCES (Continued)

Farnham, P. R., 1968, A study to evaluate the efficiency of beamforming the LASA long-period array, Seismic Data Laboratory Report 226, Teledyne Geotech, Alexandria, Virginia. AD 844 265.

Geyer, R. L. and S. T. Martner, 1969, SH waves from explosive sources, Geophysics, v. 34, p. 893-905.

Gudzin, M. G. and F. M. Hennen, 1967, LASA LP system, TR-67-17, Teledyne Geotech, Alexandria, Virginia.

Gutenberg, B., 1945, Amplitudes of surface waves and magnitude of shallow earthquakes, Bull. Seism. Soc. Am., v. 35, p. 3-12.

Gutenberg, B., 1945a, Amplitudes of surface waves and magnitude of shallow earthquakes, Bull. Seism. Soc. Am., v. 35, p. 85-102.

Gutenberg, B., 1945b, Amplitudes of P, PP, and S and magnitude of shallow earthquakes, Bull. Seism. Soc. Am., v. 35, p. 57-69.

Gutenberg, B., 1945c, Magnitude determination for deep-focus earthquakes, Bull. Seism. Soc. Am., v. 35, p. 117-130.

Gutenberg, B. and C. F. Richter, 1956, Magnitude and energy of earthquakes, Annali de Geoficica, v. 9, p. 1-15.

Haskell, N. A., 1962, Crustal reflection of plane P and SV waves, J. Geophys. Res., v. 67, p. 4751-4768.

Helmberger, D. V., 1974, Generalized ray theory for shear dislocations, Bull. Seism. Soc. Am., v. 64, p. 45-64.

Helmberger, D. V. and G. R. Engen, 1974, Upper-mantle shear structure, J. Geophys. Res., v. 19, p. 4017-4028.

Johns, F. H., 1971, Preliminary analysis of data resulting from the CANNIKIN event, Geotech Technical Memorandum, 17 December.

Kim, W. H. and Kisslinger, C., 1967, Model investigation of explosions in prestressed media, Geophysics, v. 32, p. 633-651.

REFERENCES (Continued)

Kisslinger, C., E. J. Mateker, Jr., and T. V. McEvilly, 1961, SH motion from explosions in soil, J. Geophys. Res., v. 66, p. 3487-3496.

Kogan, S. D., 1960, Travel-times of longitudinal and transverse waves, calculated from data on nuclear explosions made in the region of the Marshall Islands, Bull. Acad. Sci., USSR Geophys. Serv., English Trans., p. 246-253.

Lambert, D. G., E. A. Flinn, and C. B. Archambeau, 1972, Geophys. J. R. astr. Soc., v. 29, p. 403-432.

Marshall, P. D. and P. W. Basham, 1972, Discrimination between earthquakes and underground explosions employing an improved M_s scale, Geophys. J. R. astr. Soc., v. 28, p. 431-458.

Massé, R. P., D. M. Clark, and H. J. Mecklenberg, 1970, Analysis of long period seismic signals and noise recorded at LASA, TFO, and UBO, Seismic Data Laboratory Report 254, Teledyne Geotech, Alexandria, Virginia. AD 874 843.

Nuttli, O., 1959, The particle motion of the S wave, Bull. Seism. Soc. Am., v. 49, p. 49-56.

Nuttli, O. and J. D. Whitmore, 1962, On the determination of the polarization angle of the S wave, Bull. Seism. Soc. Am., v. 52, p. 95-107.

Nuttli, O., 1964, The determination of S wave polarization angles for an earth model with crustal layering, Bull. Seism. Soc. Am., v. 54, p. 1429-1440.

Nuttli, O., 1969, Travel times and amplitudes of S waves from nuclear explosions in Nevada, Bull. Seism. Soc. Am., v. 59, p. 385-398.

Oliver, J., 1971, On the long-period character of shear waves, Bull. Seism. Soc. Am., v. 51, p. 1-12.

REFERENCES (Continued)

Perret, W. R., 1967, Free-field particle motion from a nuclear explosion in salt, Part I, Project Dribble, SALMON event, VUF-3012, Sandia Laboratory, Albuquerque, New Mexico.

Perret, W. R., 1968, Shear waves from a nuclear explosion in a salt cavity, Bull. Seism. Soc. Am., v. 58, p. 2043-2051.

Perret, W. R., 1970, Gasbuggy seismic source and surface motion, PNE-1002, Sandia Laboratory, Albuquerque, New Mexico.

Perret, W. R., 1972a, Close-in ground motion from the MILROW and CANNIKIN events, Bull. Seism. Soc. Am., v. 62, p. 1489-1504.

Perret, W. R., 1972b, Gasbuggy seismic source measurements, Geophysics, v. 37, p. 301-312.

Richter, C. F., 1958, Elementary Seismology, Freeman, W. H., San Francisco.

Romney, C. F., 1971, Seismic system improvement, Presentation to the Joint Committee on Atomic Energy, 27 October 1971.

Short, N. M., 1960, Fracturing of rock salt by a contained high explosive, UCRL 6054, published by Office of Technical Services, U. S. Department of Commerce, Washington, 1960.

Short, N. M., 1961, Excavation of contained TNT explosions in tuff, UCRL 6445, published by Office of Technical Services, U. S. Department of Commerce, Washington, 1961.

Singh, S. J., 1973, Generation of SH-type motion by torsion-free sources, Bull. Seism. Soc. Am., v. 63, p. 1189-1201.

Smart, E. and E. Flinn, 1971, Fast frequency-wavenumber analysis and Fisher signal detection in real-time infrasonic array data processing, Geophys. J. R. Astr. Soc., v. 26, p. 279-284.

Smart, E., 1972, FKCOMB, a fast general-purpose array processor, Seismic Array Analysis Center Report No. 9, Teledyne Geotech, Alexandria, Virginia.

REFERENCES (Continued)

Springer, D. L. and R. L. Kinnaman, 1971, Seismic source summary for U. S. underground nuclear explosions, 1961-1970, <u>Bull. Seism. Soc. Am.</u>, v. 61, p. 1073-1098.

Strauss, A. C., 1973, Final evaluation of the detection and discrimination capability of the Alaskan long-period array, Special Report No. 8, Texas Instruments, Dallas, Texas. (Contract No. F33657-72-C-0725, ARPA Order No. 1714, ARPA Program Code No. 2F10).

Teledyne Geotech, 1964, SALMON. Seismic Data Laboratory Report 120, Teledyne Geotech, Alexandria, Virginia. AD 482 047.

Thomson, K. C., T. J. Ahrens, and M. N. Toksöz, 1969, Dynamic photoelastic studies of P and S wave propagation in prestressed media, <u>Geophysics</u>, v. 34, p. 696-712.

Toksöz, M. N., D. G. Harkrider, and A. Ben-Menahem, 1965, 2, Release of tectonic strain by underground nuclear explosions and mechanisms of earthquakes, <u>J. Geophys. Res.</u>, v. 70, p. 907-922.

Toksöz, M. N., K. C. Thomson, and T. J. Ahrens, 1971, Generation of seismic waves by explosions in prestressed media, <u>Bull. Seism. Soc. Am.</u>, v. 61, p. 1589-1623.

Toksöz, M. N. and H. H. Kehrer, 1972, Tectonic strain release by underground nuclear explosions and its effect on seismic discrimination, <u>Geophys. J. Roy. Astr. Soc.</u>, v. 31, p. 141-161.

United States Atomic Energy Commission, 1969, AEC Press Release No. M-225 24 September.

von Seggern, D. H., 1970, Surface-wave amplitude-versus-distance relation in the western United States, Seismic Data Laboratory Report No. 249, Teledyne Geotech, Alexandria, Virginia. AD 870 769.

von Seggern, D. H., 1971, Effects of propagation paths on surface-wave magnitude estimates, Seismic Data Laboratory Report 279, Teleydne, Geotech, Alexandria, Virginia.

REFERENCES (Continued)

von Seggern, D. H., 1972, Seismic shear waves as a discriminant between earth-
quakes and underground nuclear explosions, Seismic Data Laboratory
Report 295, Teledyne Geotech, Alexandria, Virginia. AD 747 763.

von Seggern, D. H. and D. G. Lambert, 1972, Analysis of teleseismic data for
the nuclear explosion MIIROW, SDL Report 258, Teledyne Geotech,
Alexandria, Virginia. AD 743 072.

von Seggern, D. H., 1973, Joint magnitude determination and analysis of variance
for explosion magnitude estimates, Bull. Seism. Soc. Am., v. 63, p. 827-845.

von Seggern, D. H., 1974, Final report on the analysis of the Recordings of the
Very Long Period Experimental Network, Teledyne Geotech, Alexandria,
Virginia.

von Seggern, D. H. and R. R. Blandford, 1974, Seismic threshold determination,
SDAC-TR-74-3, Teledyne Geotech, Alexandria, Virginia.

White, J. E. and R. L. Sengbush, 1963, Shear waves from explosive sources,
Geophysics, v. 28, p. 1001-1019.

Willis, D. E., J. DeNoyer, and J. T. Wilson, 1963, Differentiation of earth-
quakes and underground nuclear explosions on the basis of amplitude
characteristics, Bull. Seism. Soc. Am., v. 53, p. 979-987.

Willis, D. E., G. D. George, K. G. Poetzl, C. E. Saltzer, A. F. Shakal,
R. D. Torfin, T. L. Woodzick, and C. Woiosin, 1972, Seismological
aspects of the CANNIKIN nuclear explosion, Bull. Seism. Soc. Am.,
v. 62, p. 1377-1395.

Wirth, M. H., 1970, Estimation of network detection and location capability,
Seismic Data Laboratory Research Memorandum, Teledyne Geotech,
Alexandria, Virginia.

Wright, J. K. and E. W. Carpenter, 1962, The generation of horizontally
polarized shear waves by underground explosions, J. Geophs. Res.,
v. 67, p. 1957-1963.
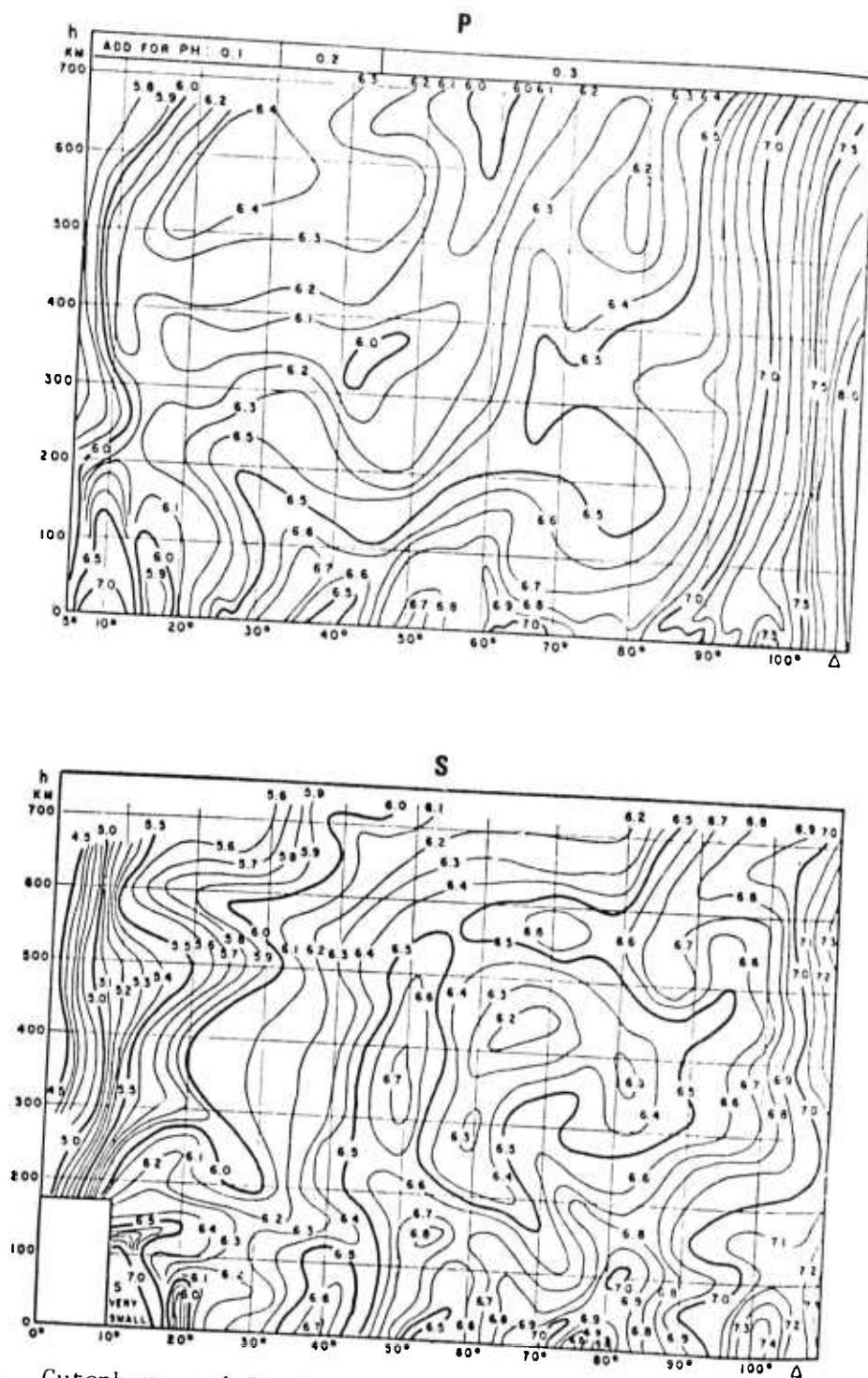
Figure 1. Gutenberg and Richter's (1956), (from Richter, 1958) B factors for P and S.
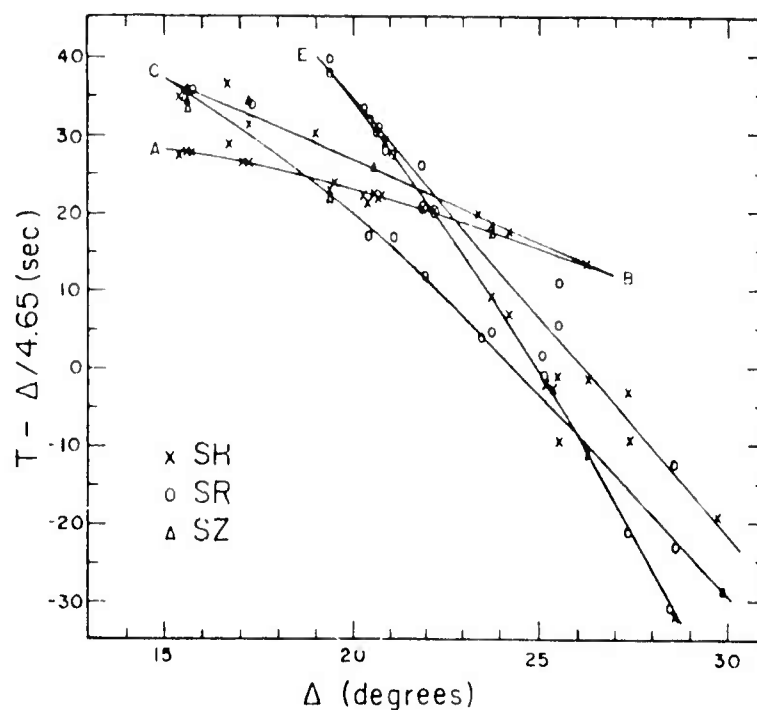
Figure 2. Travel times of S to thirty degrees as read at North American stations for the Nevada Test Site explosions HALFBEAK and GREELEY. The ordinates scale is in km. From Nuttli (1969).
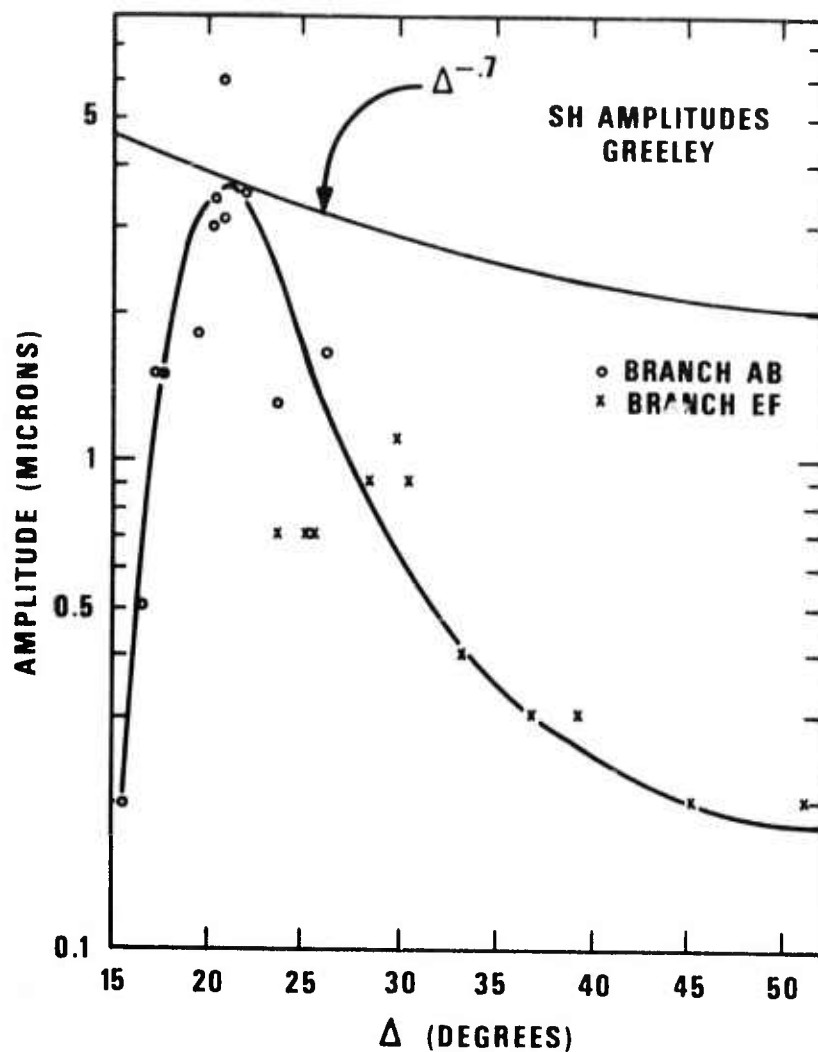
Figure 3. SH amplitudes for GREELEY from Nuttli (1969). The smooth curve through the data has been drawn by hand. The shallow sloping curve through the peak of the data is proportional to $\Delta^{-.7}$, the relation suggested by Evernden (1969).
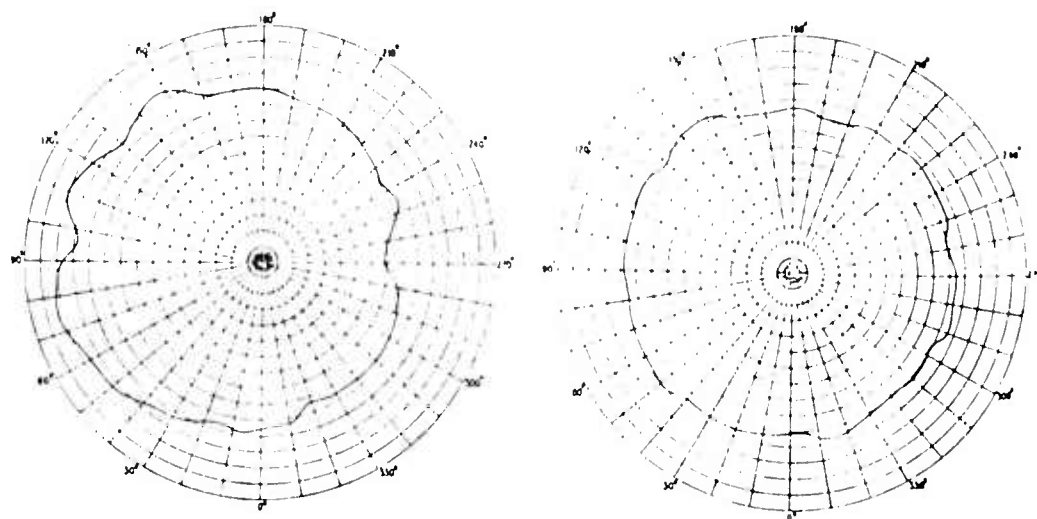
Figure 4. Polar diagrams of mid-horizontal section through plaster cast of cavity created by small explosion in soft clay. Illustrates asymmetrys to be expected. From Wright and Carpenter (1962).
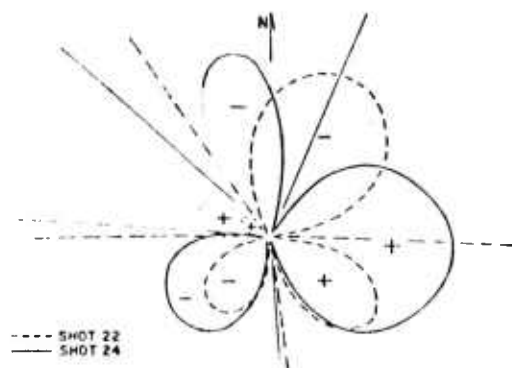
Figure 5a. Comparison of radiation patterns of SH motion from cratering shot (24) and contained shot (22). From Kisslinger et al. (1961).
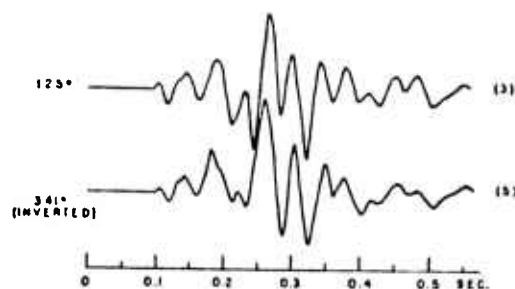
Figure 5b. Reversal of polarity of entire SH wave form at two stations 144° apart (shot 24). From Kisslinger et al. (1961).
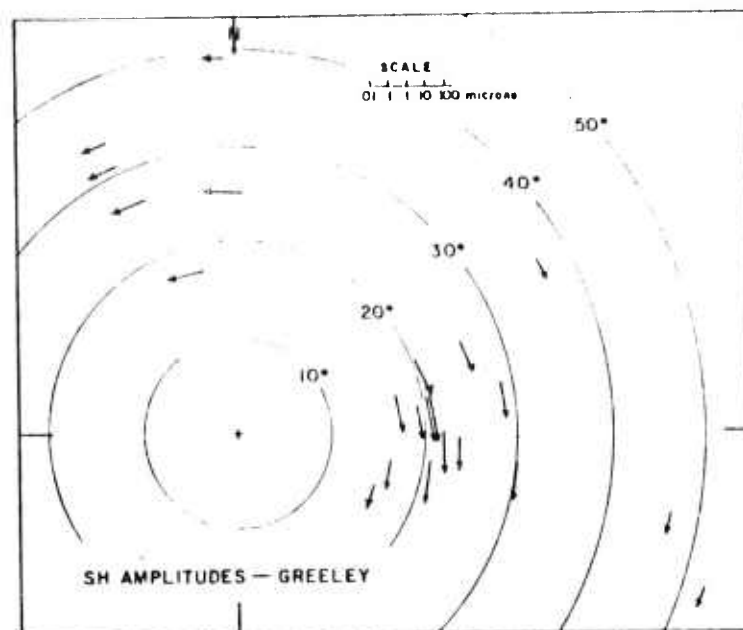
Figure 6a. Polar plot of the SH amplitudes for GREELEY. Note that the sense of motion is similar to that for HALFBEAK, as seen in Figure 6b. From Nuttli (1969).
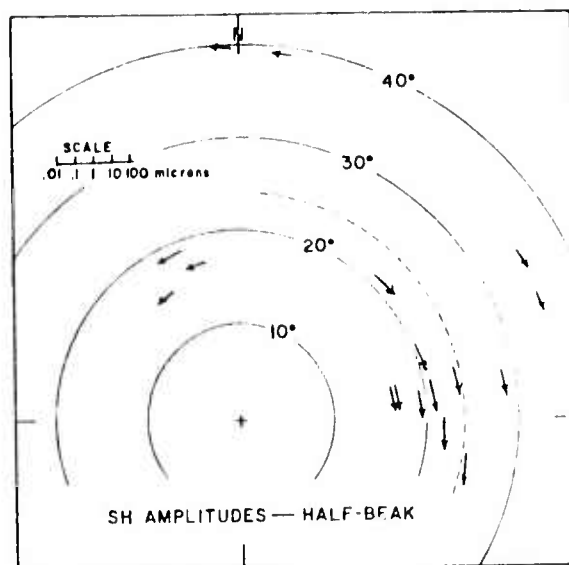
Figure 6b. Polar plot of the SH amplitudes for HALFBEAK. The dashed line separates branch AB arrivals at the shorter distances from branch EF arrivals. Note the reversal of the sense of motion. Nuttli (1969).

Subsurface Station Locations and Geology
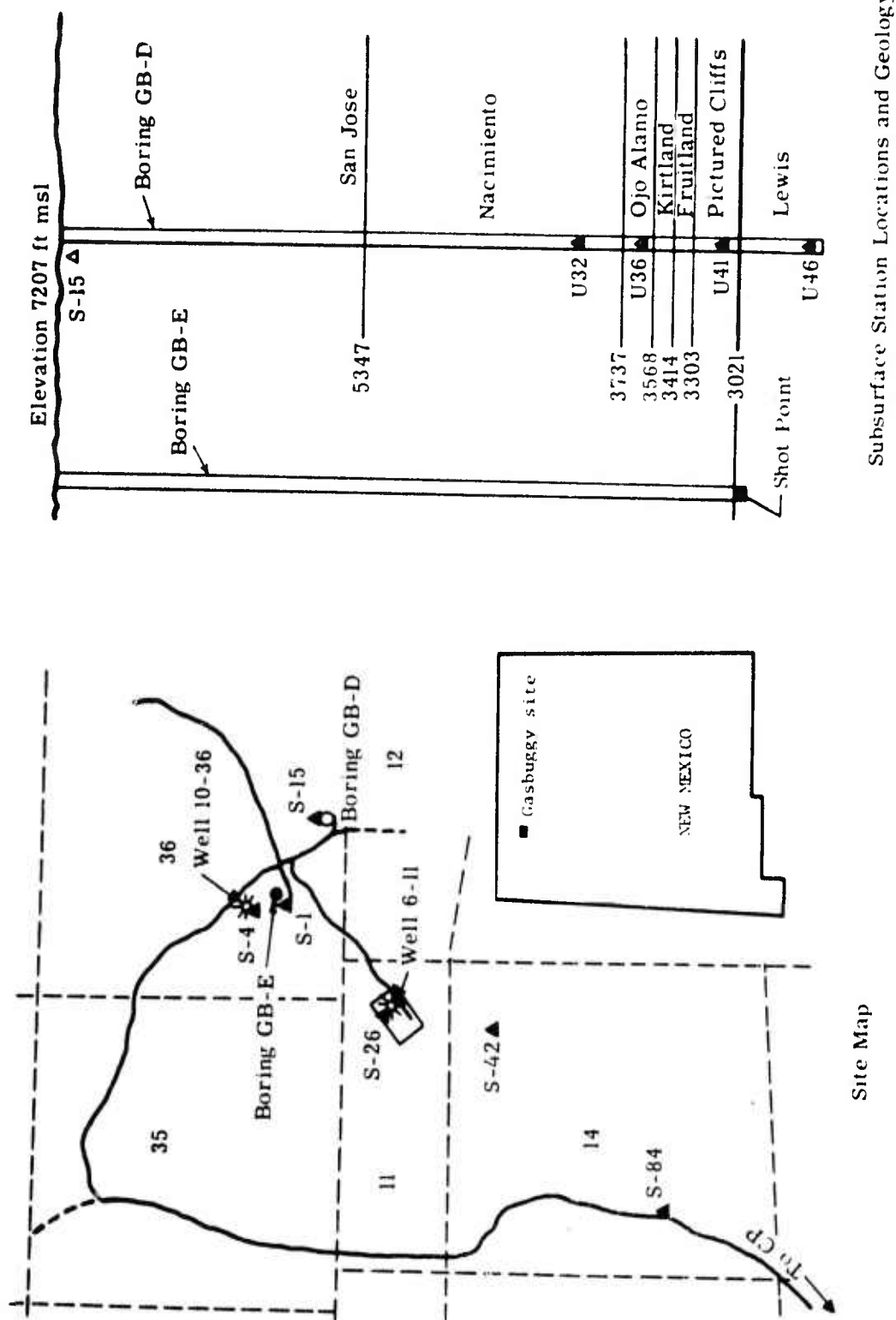
Site Map

Figure 7. Site map and instrument station locations for GASBUGGY from Perret (1972b).

-56-
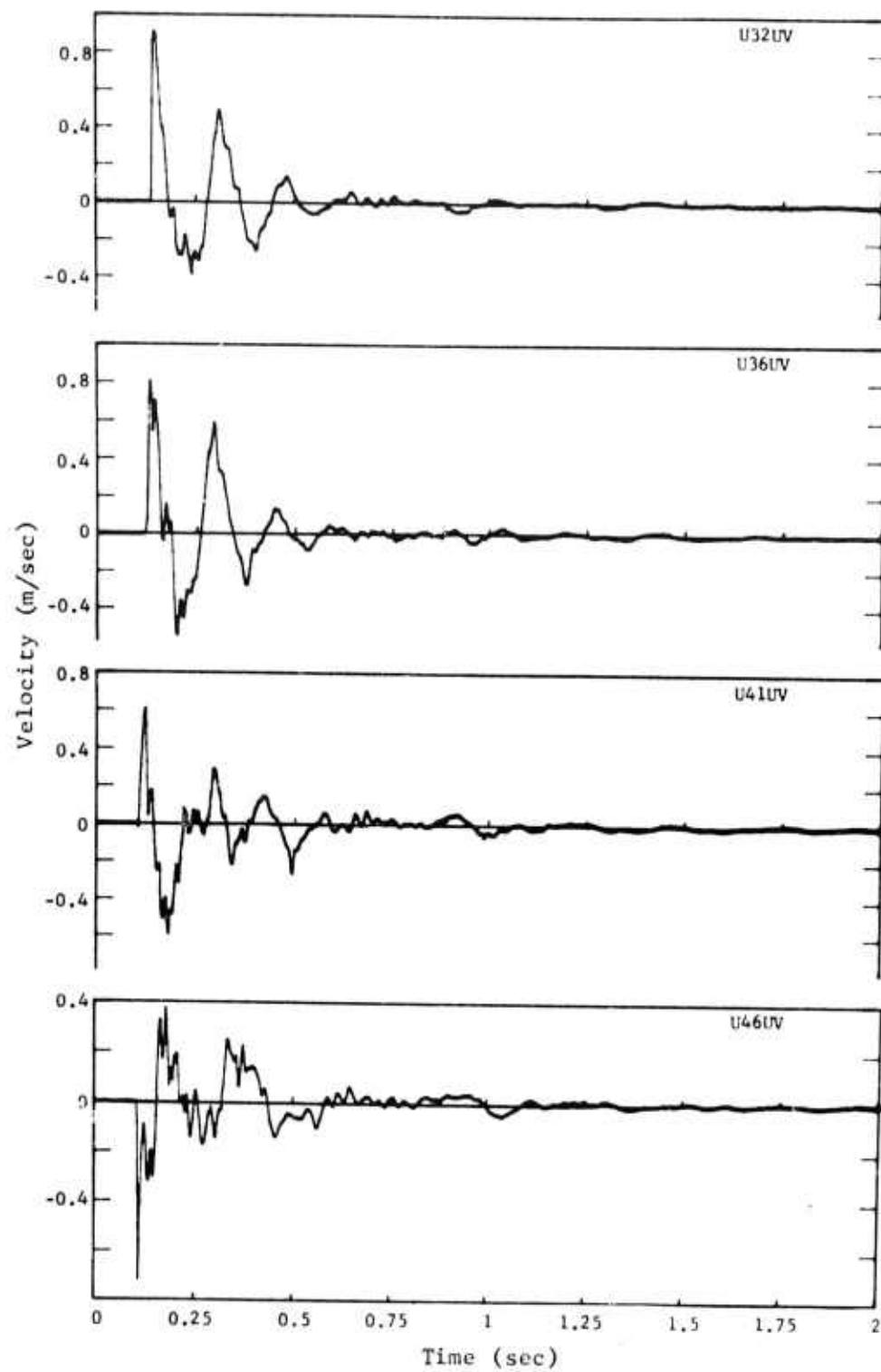
Figure 8. Subsurface vertical particle velocity record for GASBUGGY.
From Perret (1970).
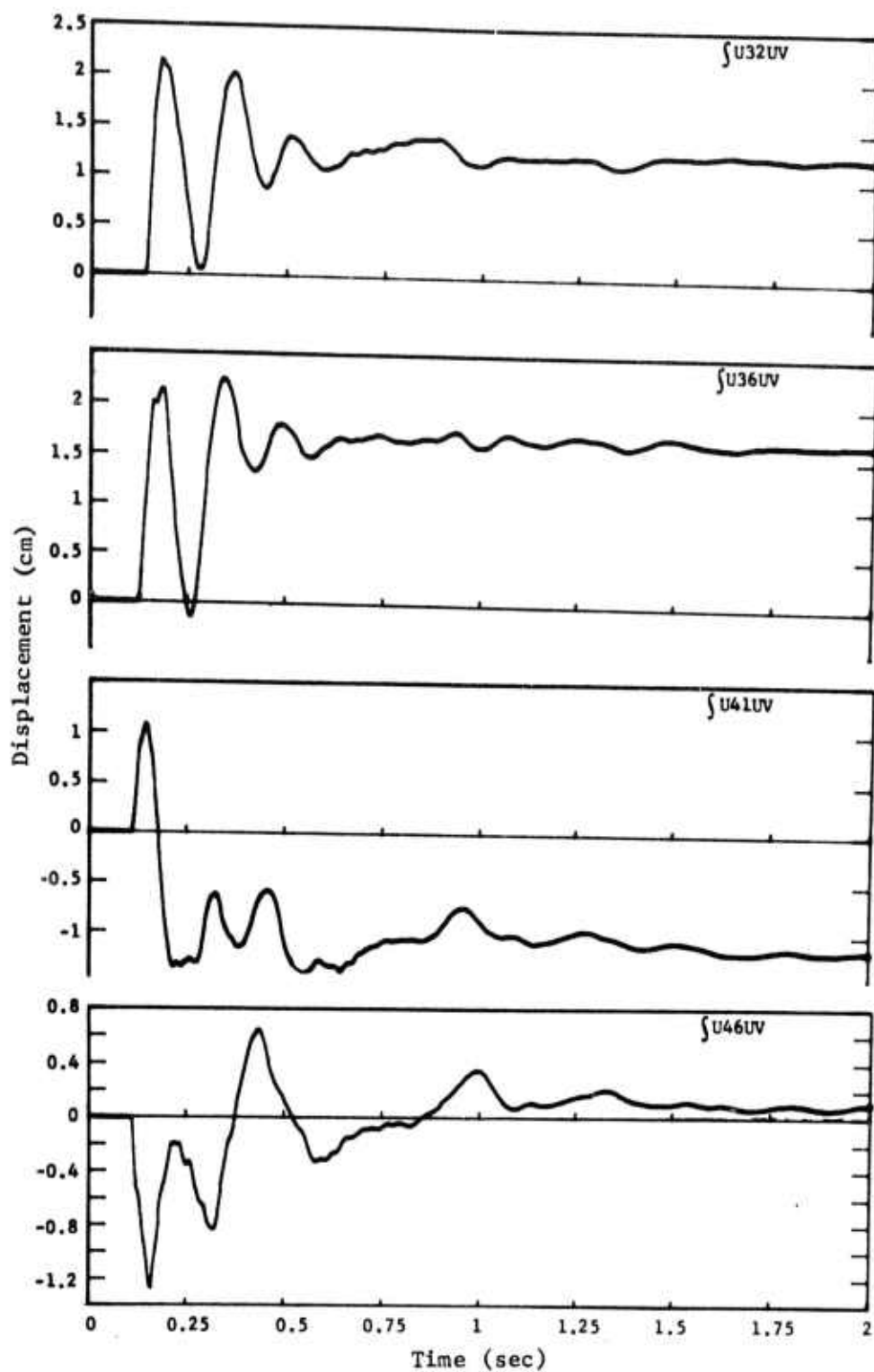
Figure 9. Subsurface vertical displacement records for GASBUGGY. From Perret (1970).
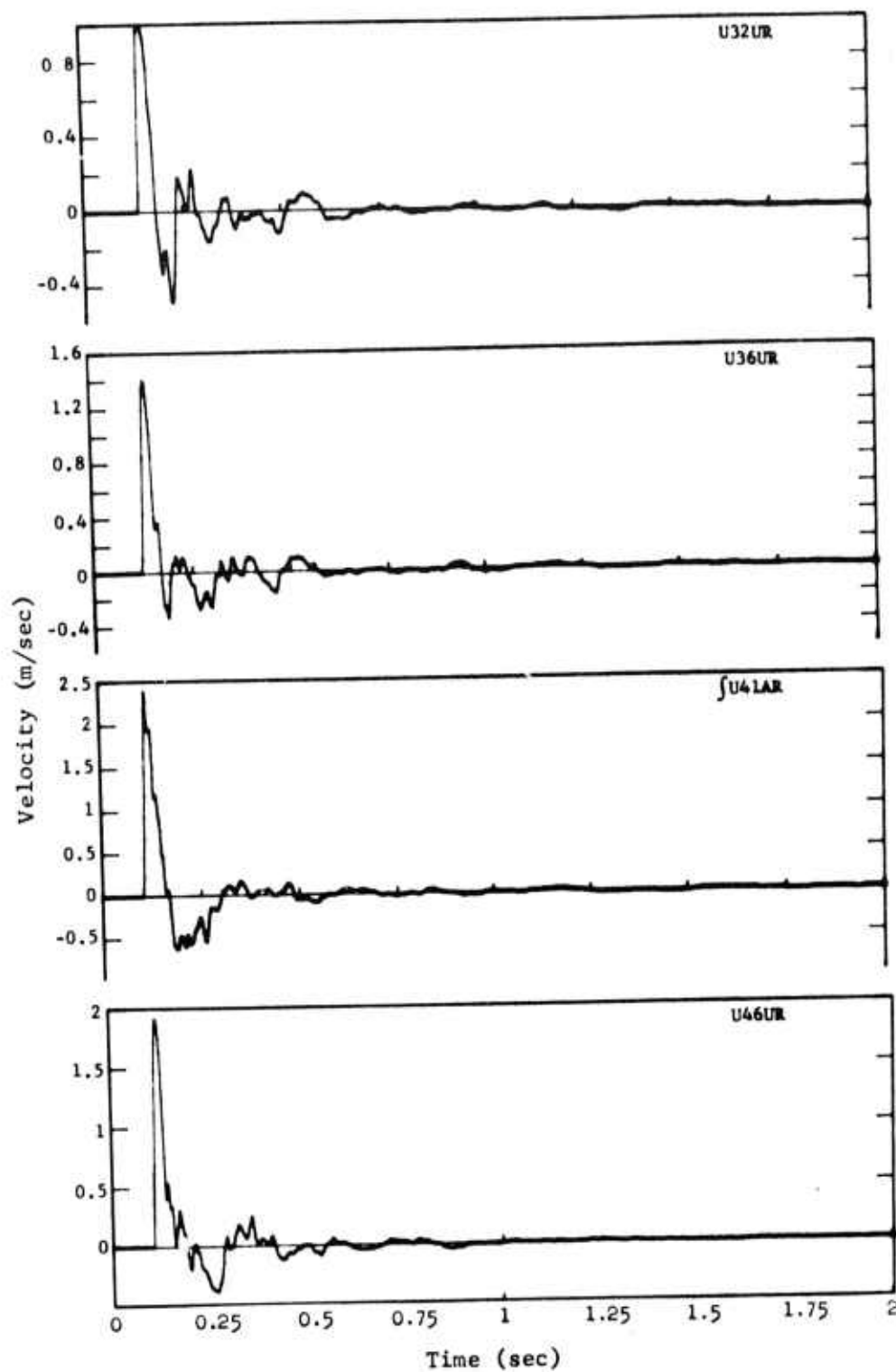
Figure 10. Subsurface radial particle velocity records for GASBUGGY. From Perret (1972b).
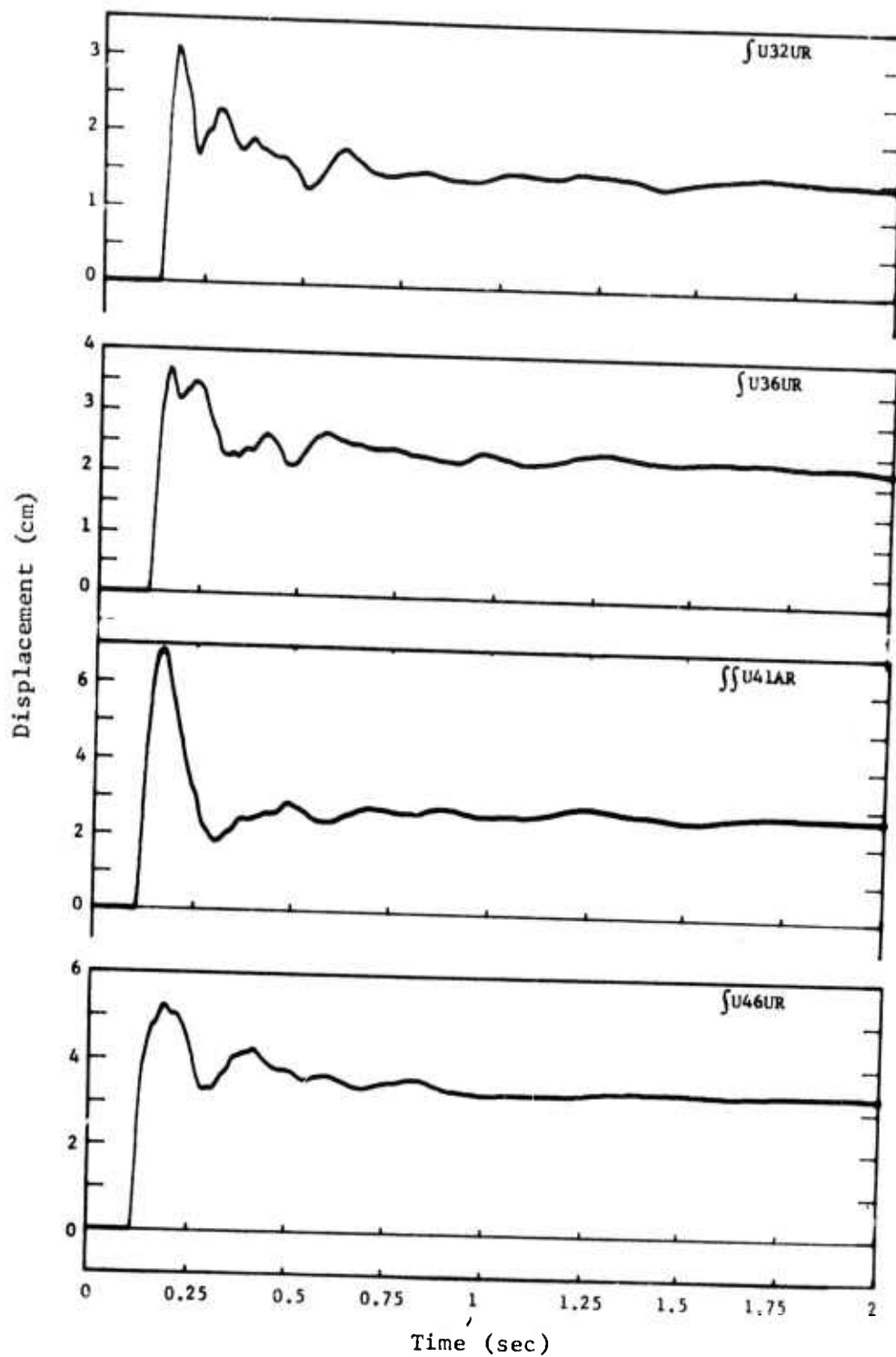
Figure 11. Subsurface radial displacement records for GASBUGGY. From Perret (1972b).
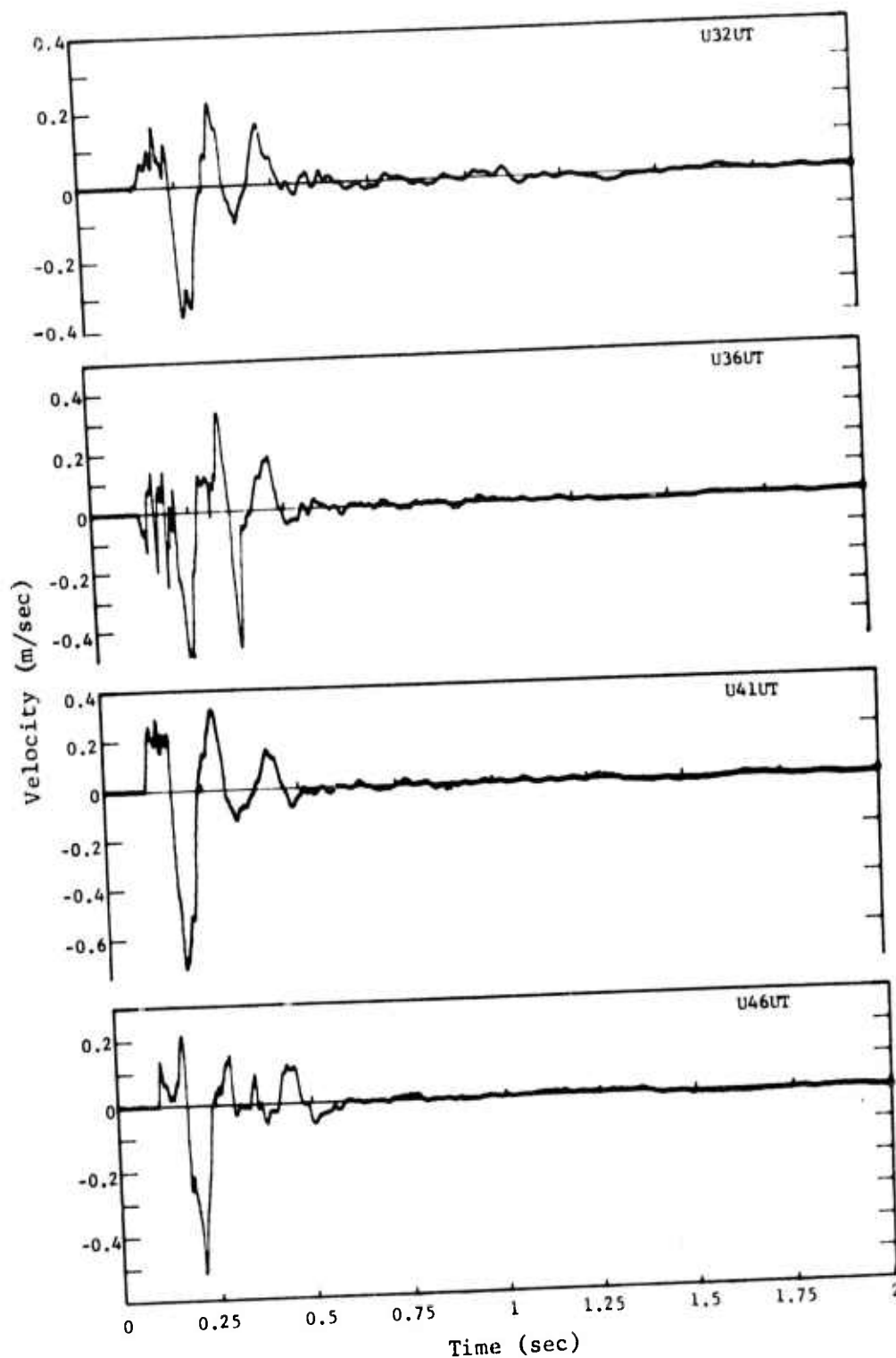
Figure 12. Subsurface tangential particle velocity records for GASBUGGY. From Perret (1970).
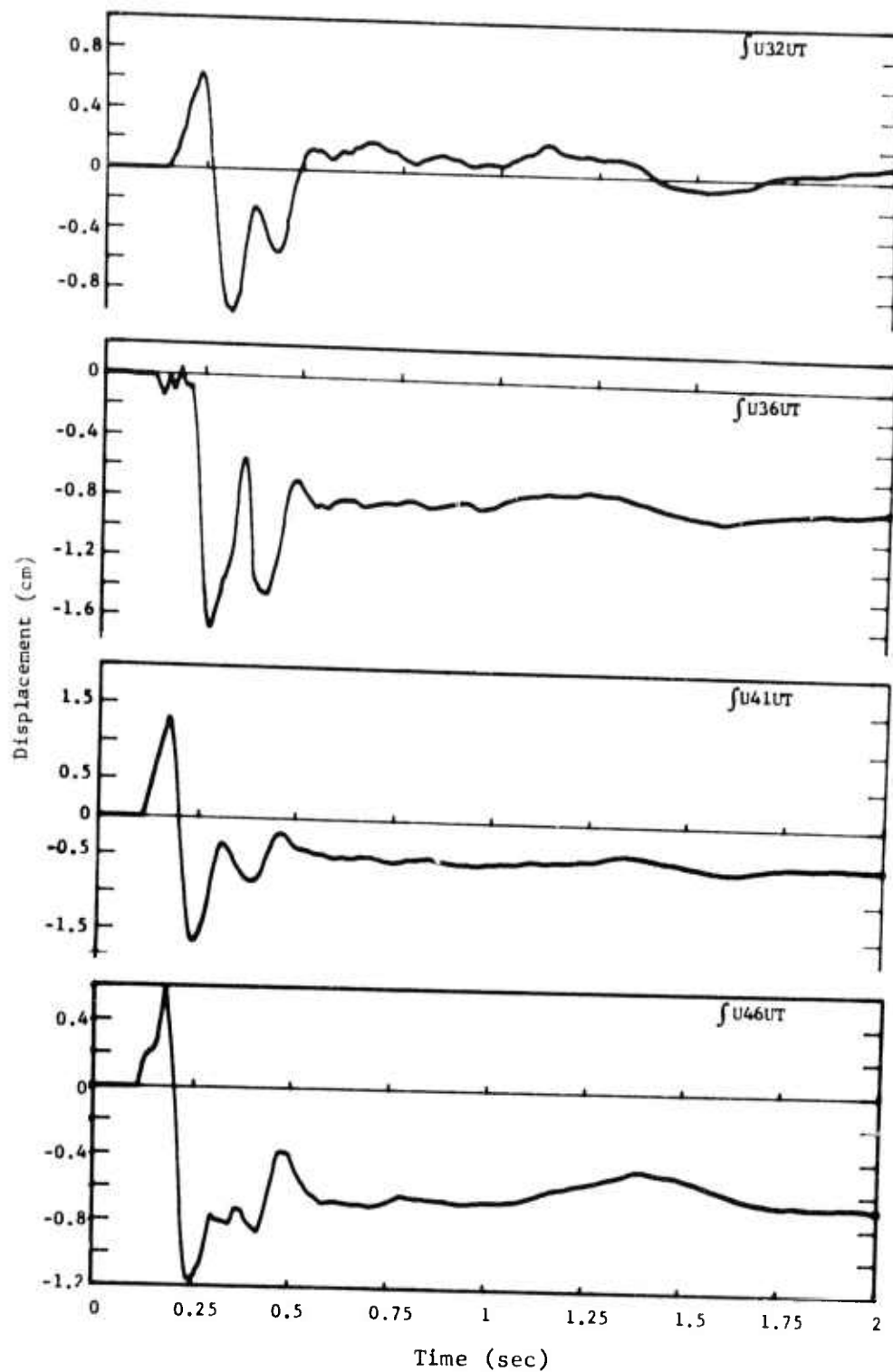
Figure 13. Subsurface tangential displacement records for GASBUGGY. From Perret (1970).
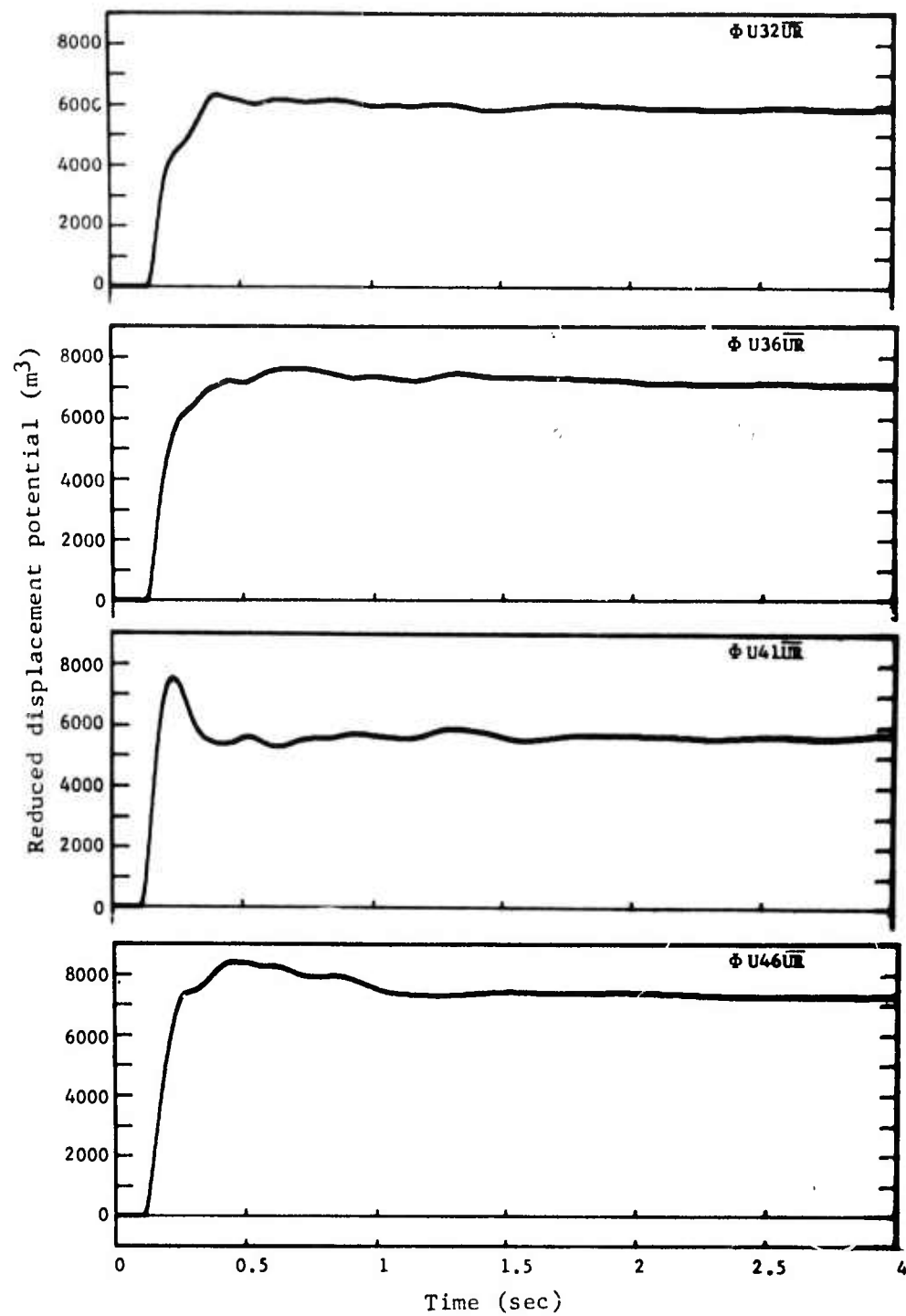
Figure 14. Reduced displacement potential records for GASBUGGY. From Perret (1972).
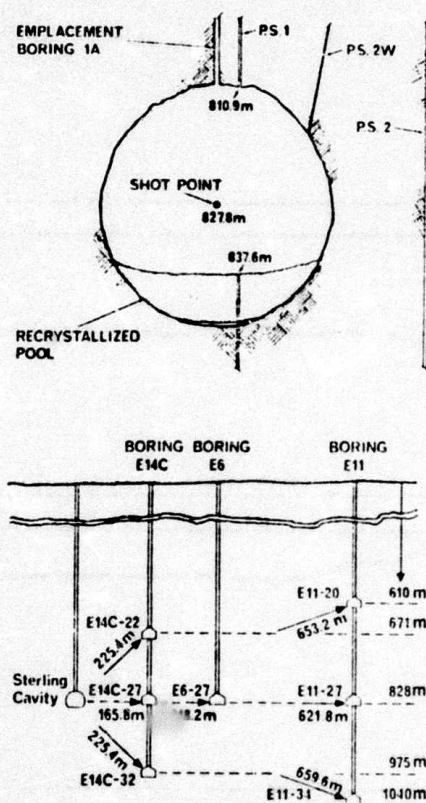
Figure 15. Schematic elevation of SALMON created cavity and location of instrument station for STERLING. From Perret (1968).
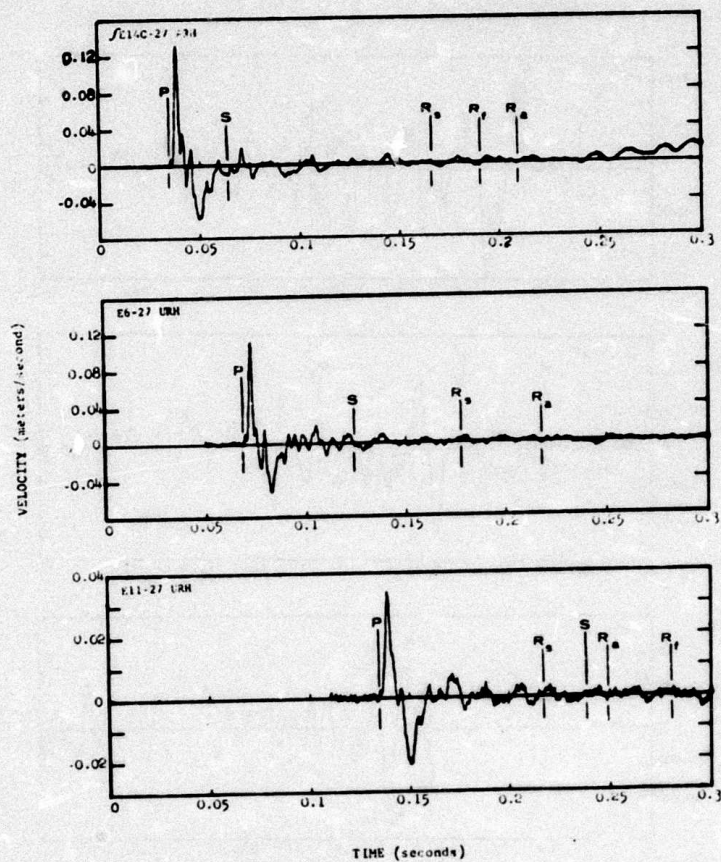
Figure 16. Radial particle velocity at shot-level stations for STERLING. From Perret (1968).
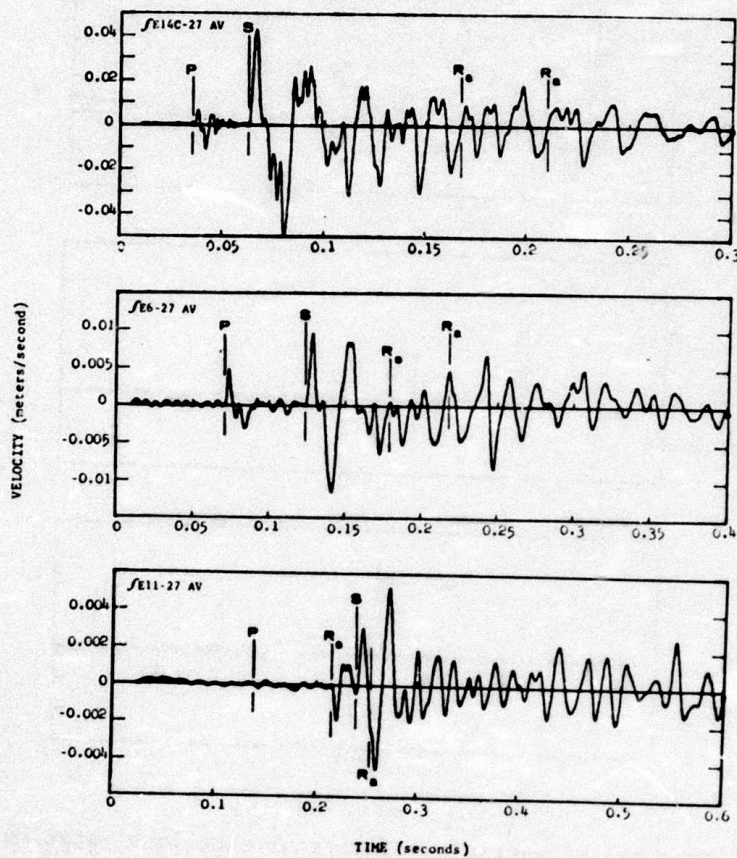
Figure 17. Vertical particle velocity at shot-level stations at STERLING. From Perret (1968).
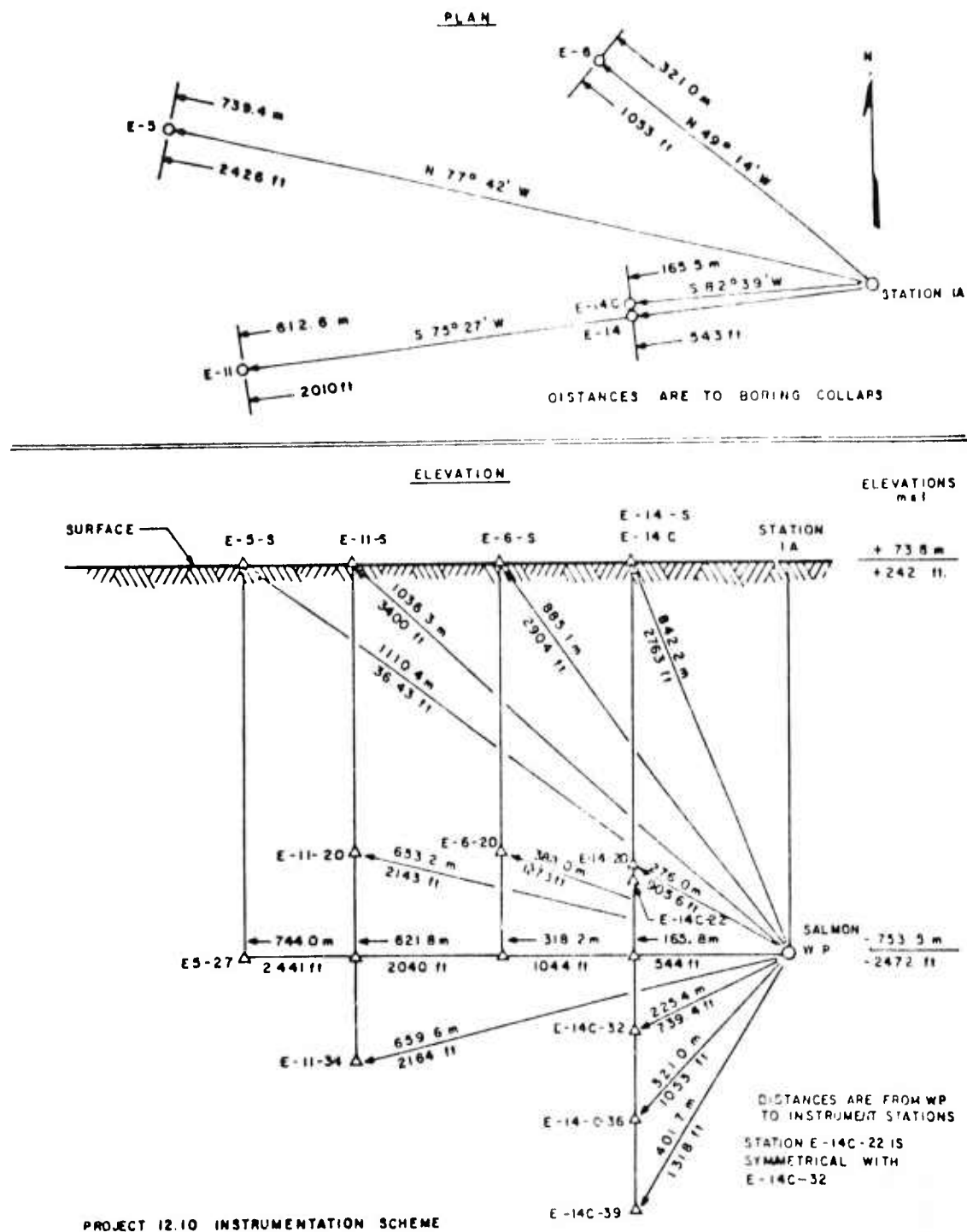
Figure 18. Instrumentation for SALMON. From Perret (1967).
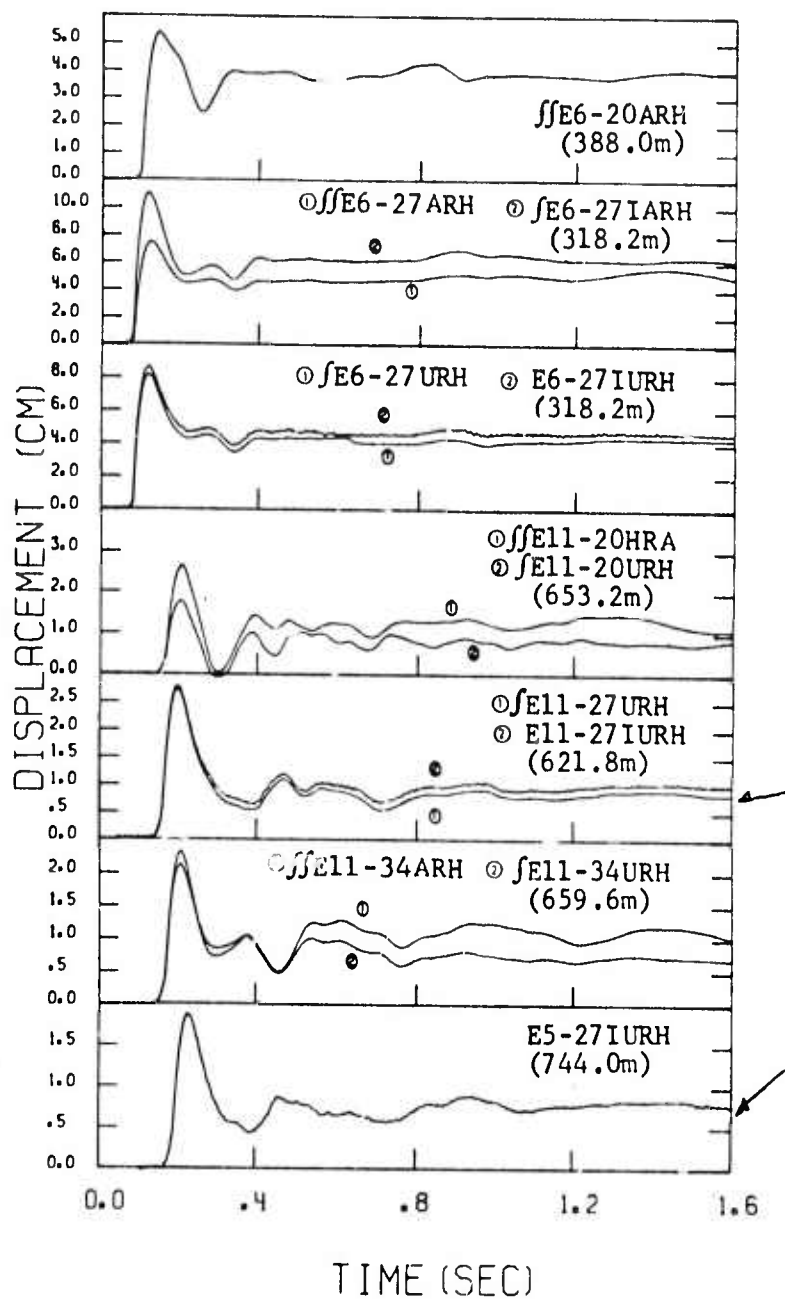
Figure 19. Horizontal radial displacement for SALMON. Pairs of traces show agreement between single and double integration of records from two different instruments and illustrate degree of data reliability. From Perret (1967).
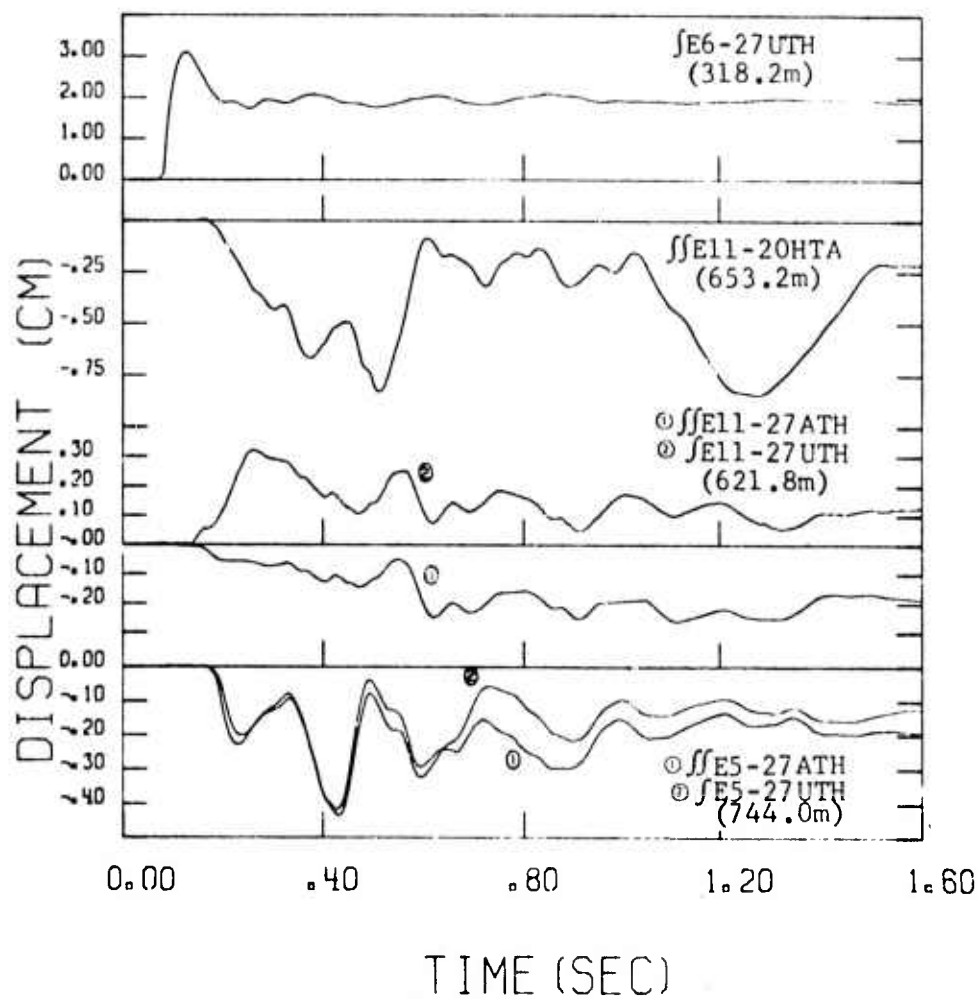
Figure 20. Horizontal tangential displacement from SALMON. Pairs of traces show agreement between single and double integration of records from two different instruments and illustrate degree of data reliability. From Perret (1967).
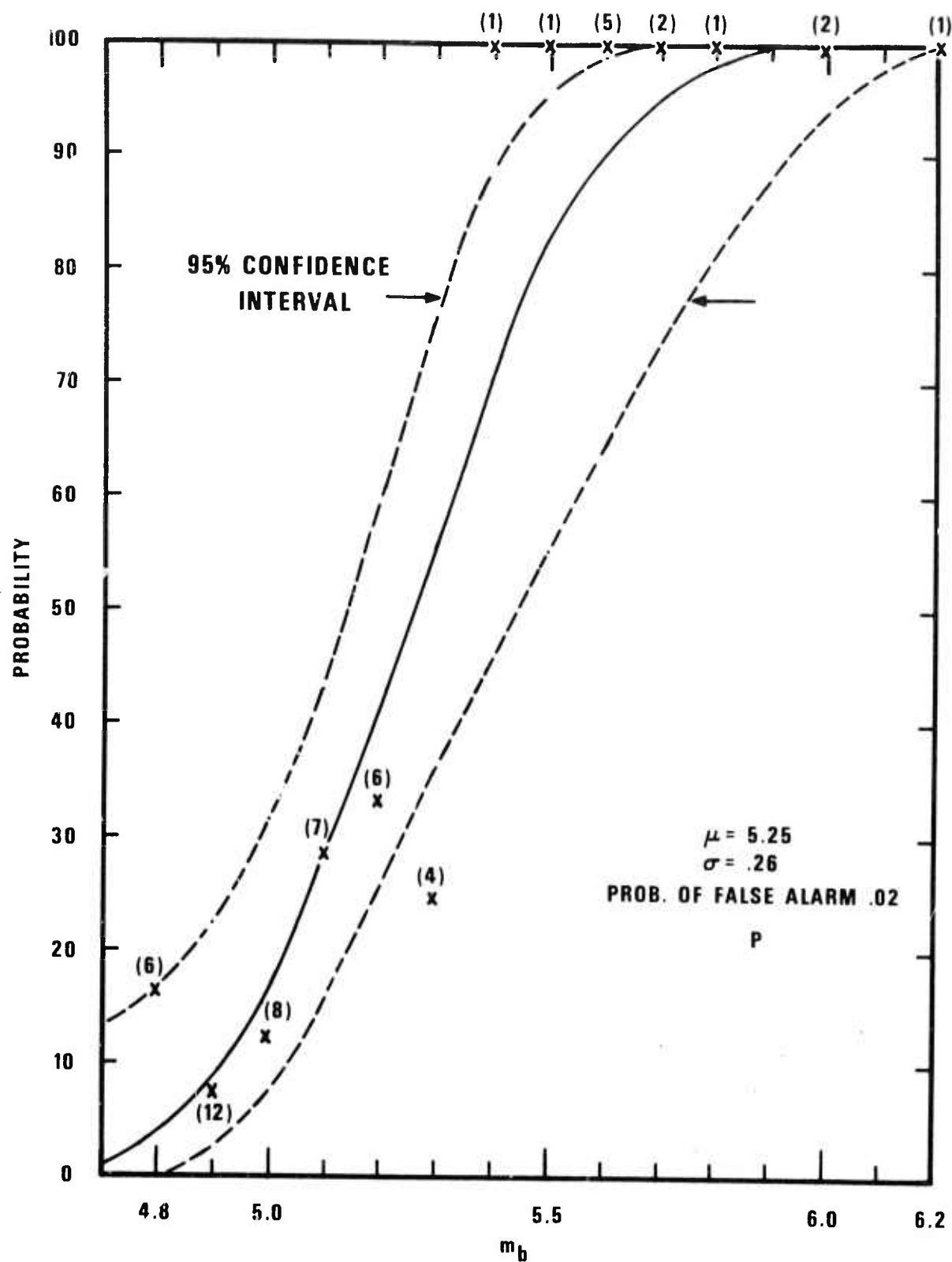
Figure 21. Probability of detection of long-period P at LASA using FKCOMB for events in the Kurils and Japan as a function of m_b.
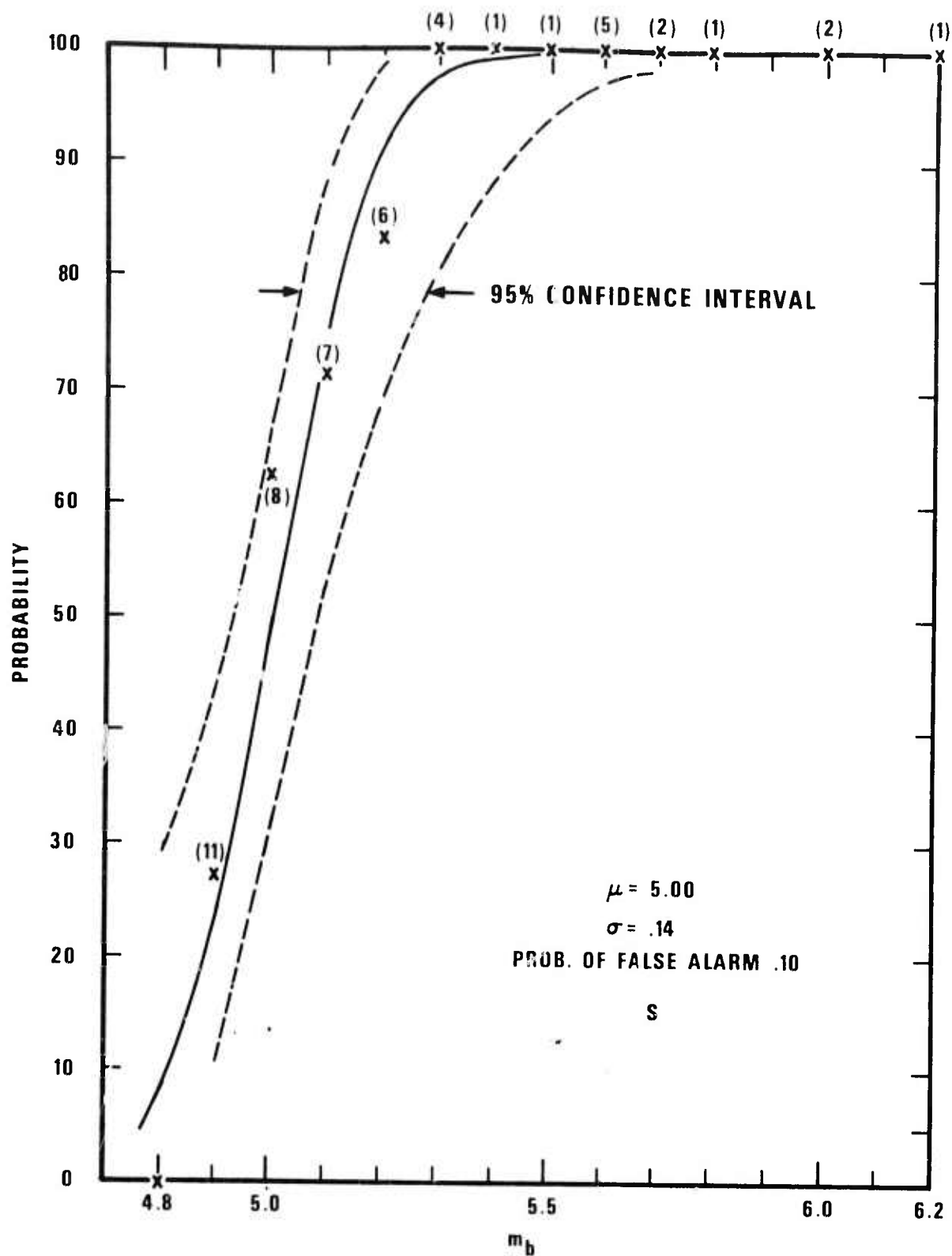
Figure 22. Probability of detection of long-period SH at LASA using FKCOMB for events in the Kurils and Japan as a function of m_b.

-71-

LASA "S" 18 DEC 71 KAM
START TIME FROM LASASITE F4
352 22 10 11 1971

BEAM 120 mμ

|◄——— 128 sec ———►|
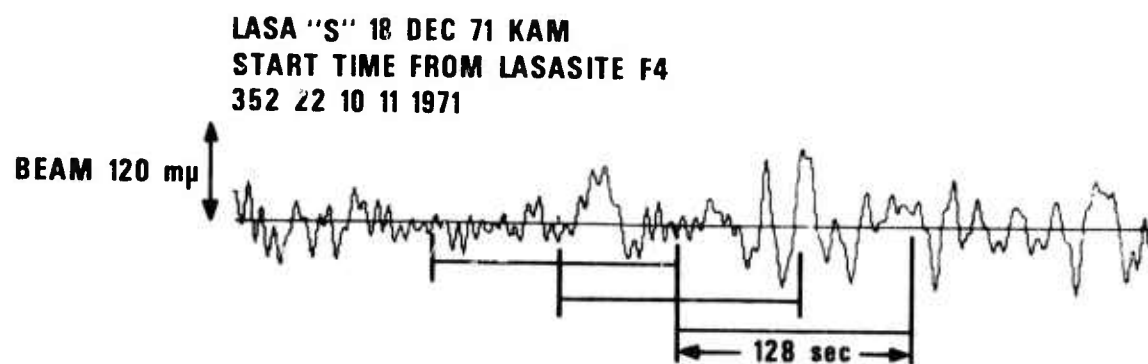
Figure 23.   An SH signal on a beam for an event in Kamchatka which was not detected by FKCOMB.

LL CANNIKAN "5"
START TIME FROM LASASITE F4
310 22 11 12 1971

548 mμ
VERTICAL

1807 mμ
RADIAL

309 mμ
TRANSVRS

100 sec
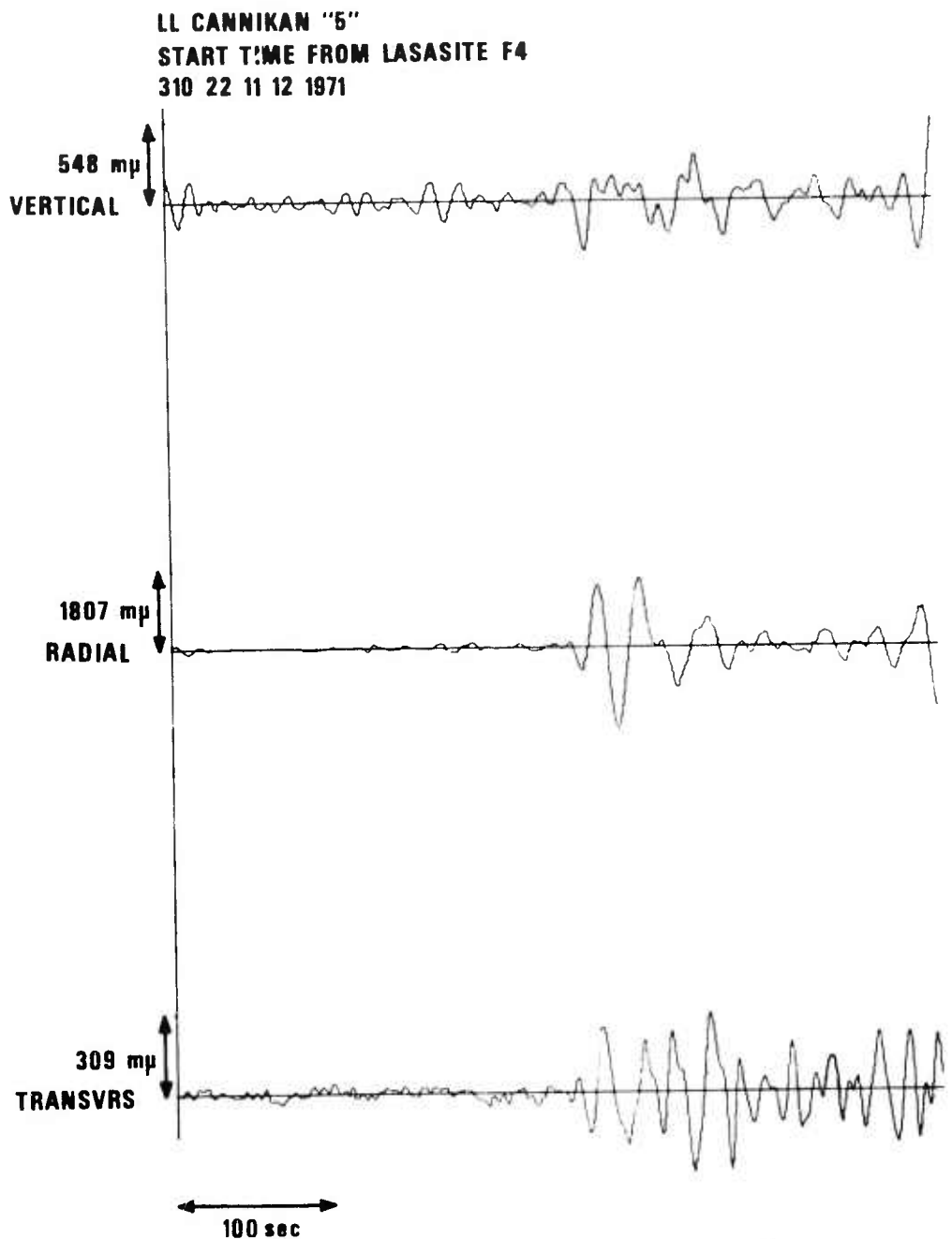
Figure 24. Vertical, radial, and transverse long-period S components
of CANNIKIN at LASA. FKCOMB failed to detect the SH component, presumably because the signal was substantially different between the individual channels.
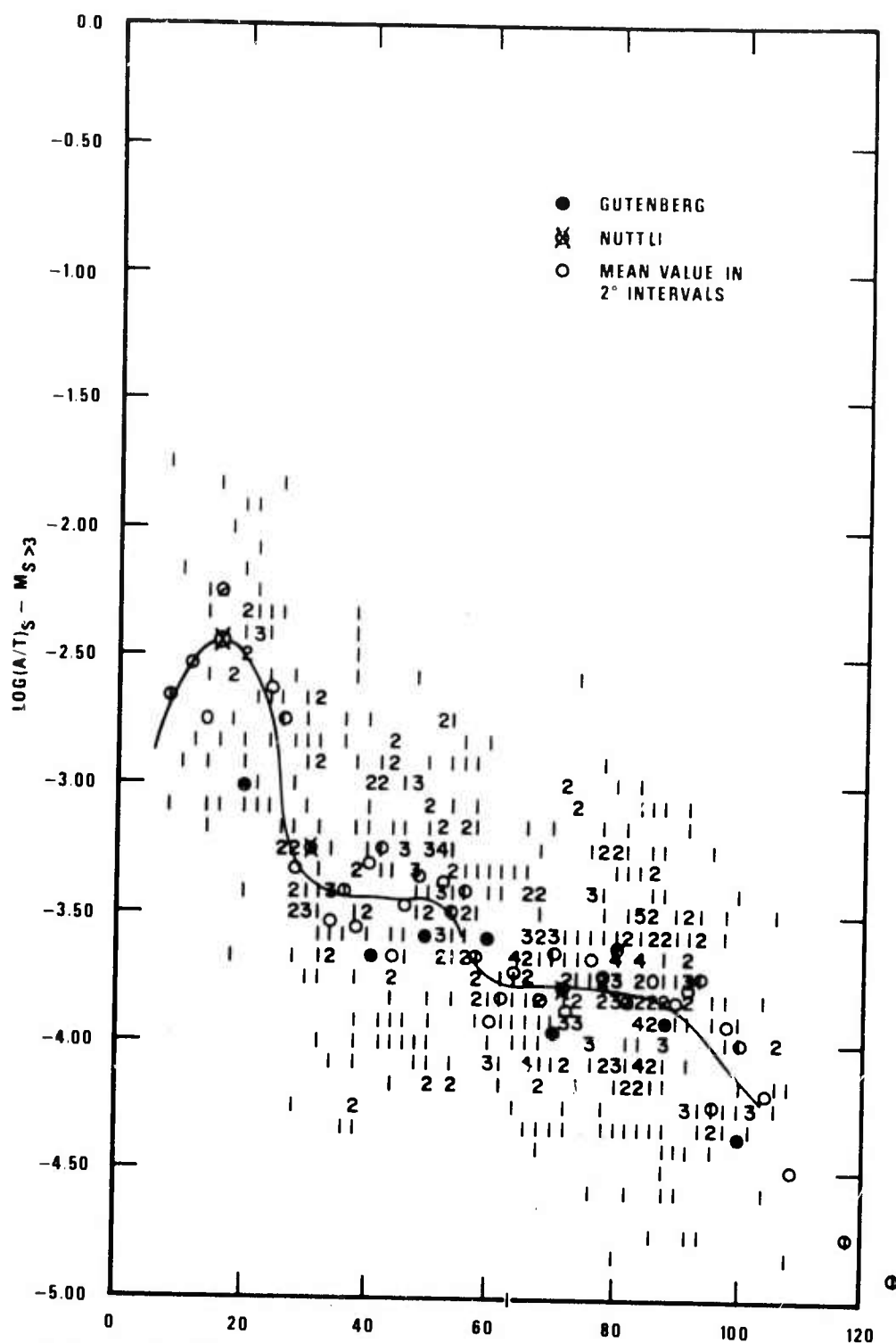
Figure 25. Distance-amplitude relationship for long-period S waves.
Data used was the largest component of all long-period S waves
detected at LPE stations January-April 1972 from events of depth less
than 60 km and with LR detected at three or more LPE stations. Smooth
curve is drawn by hand using mean values as indicated. Crosses are from
the smooth curve through Nuttli's (1969) data seen in Figure 3 normalized
at 20°, and the solid dots are from Gutenberg and Richters (1956) surface
relationship seen in Figure 1.
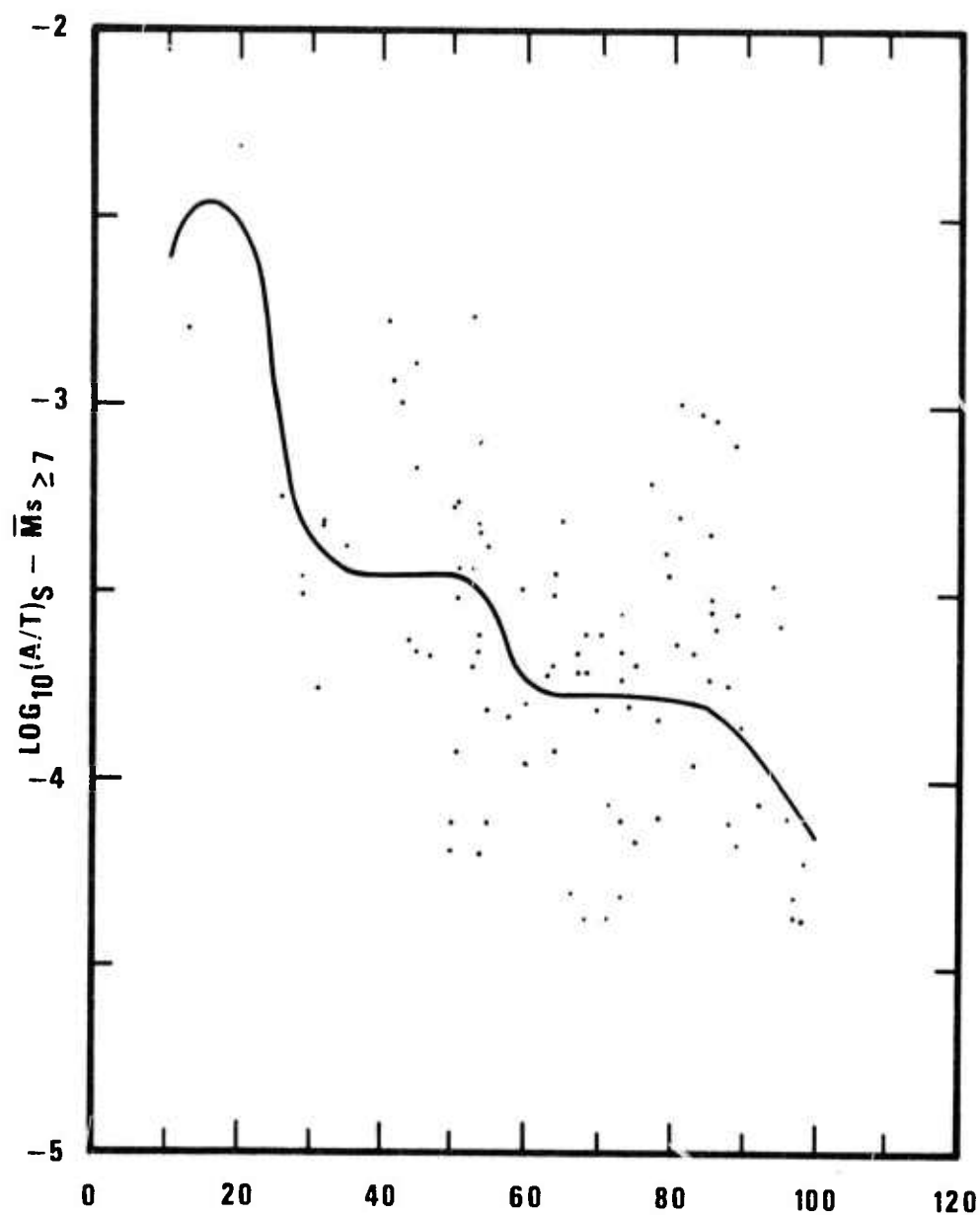
Figure 26. Data points from Figure 25 for events for which LR was detected at 7 or more out of 8 LPE stations. Data from these larger events suggests that the smooth curve as drawn here and in Figure 25 is not biased by use of smaller events for which only exceptionally large S waves are detected.
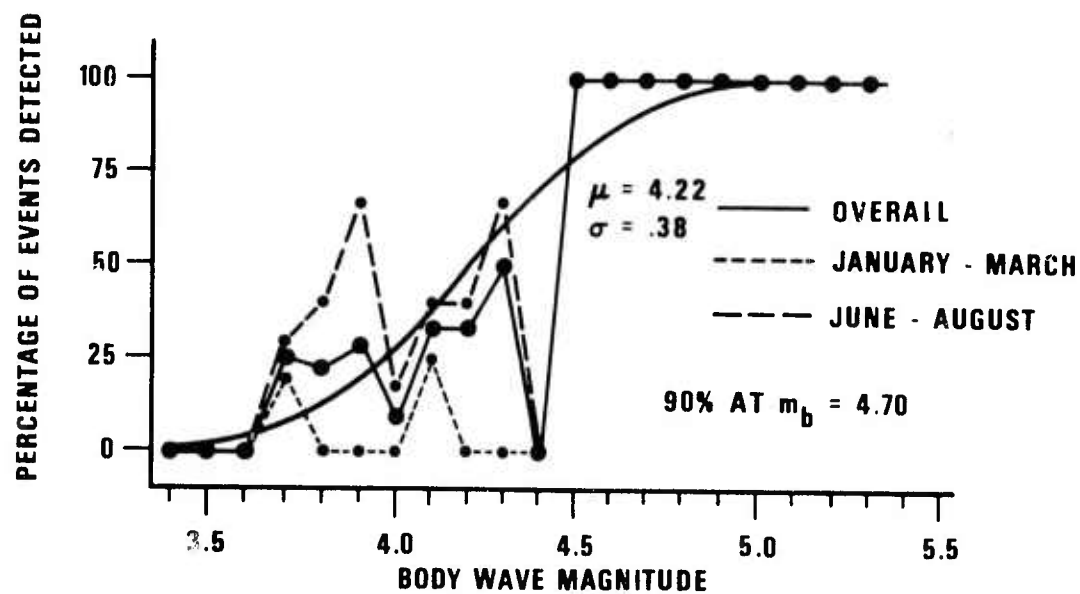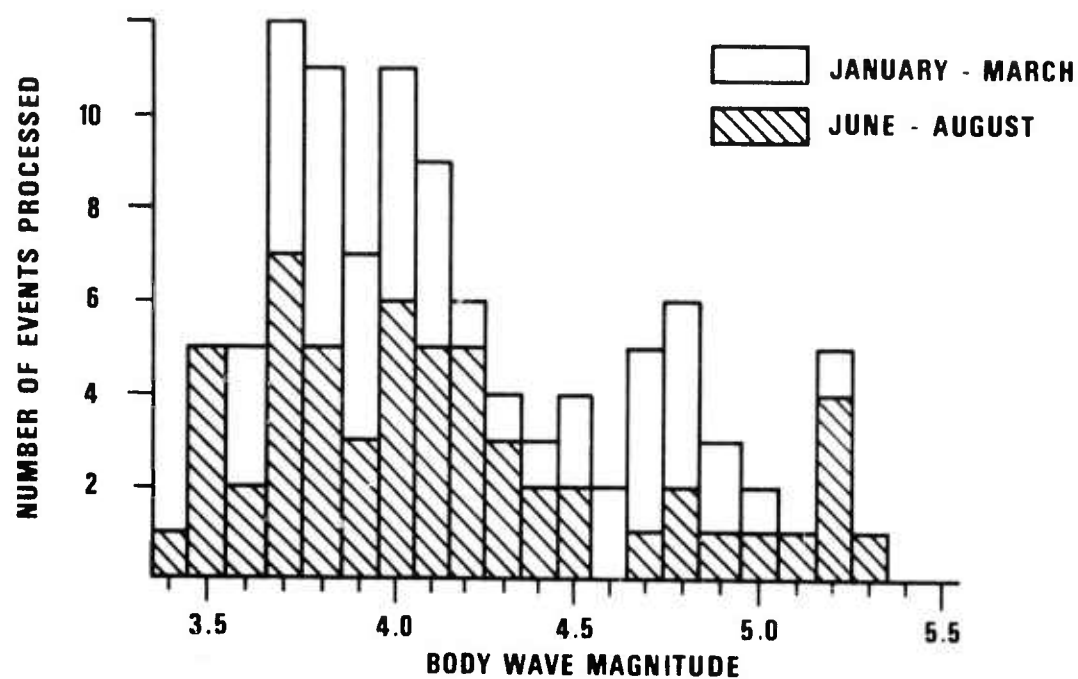
Figure 27. S-wave detection data for Kuril Island-Kamchatka area. From Strauss (1972). Smooth curve is fitted cumulative normal.

-76-

LASA CANNIKAN SITE A0 ONLY
START TIME FROM LASASITE F1
310 22 1 0 1971

VERTICAL 14501 mµ

RADIAL 9696 mµ

S

TRANSVRS 6074 mµ

100 sec
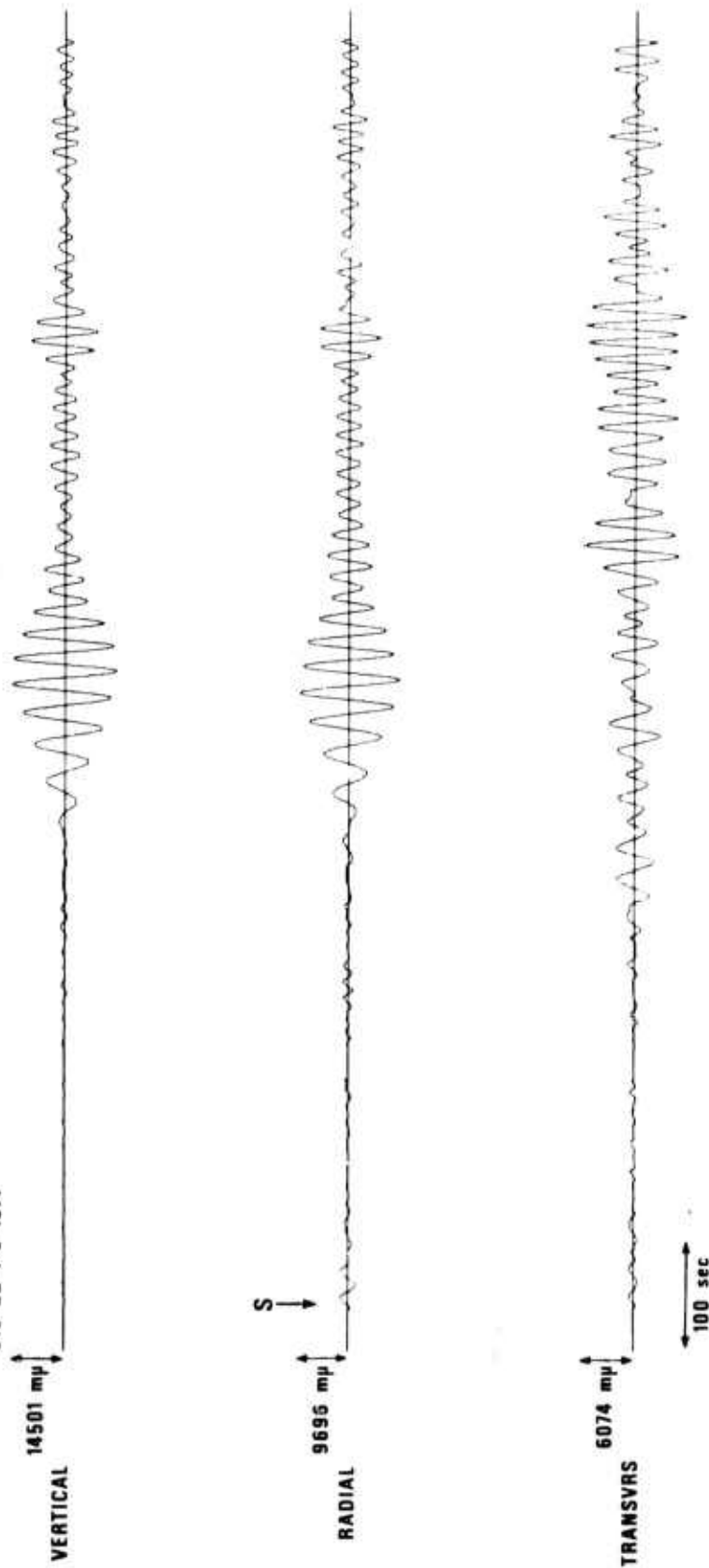
Figure 28. Vertical, radial, and transverse single-sensor long period data as seen at A0 at LASA for CANNIKIN.

-77-

Figure 29. Vertical beams and individual traces for the long-period P wave at LASA from CANNIKIN.

LL CANNIKAN "P" RADIAL & TRANS
START TIME FROM LASASITE F4
310 22 5 6 1971

BEAM 131 mµ

F3 241 mµ

F4 180 mµ

A0 390 mµ

C4 15 mµ

C3 180 mµ

D3 530 mµ

D4 16 mµ

D1 346 mµ

D2 220 mµ

E3 212 mµ

E4 145 mµ

E1 220 mµ

E3 992 mµ

E2 329 mµ

F2 452 mµ

100 sec
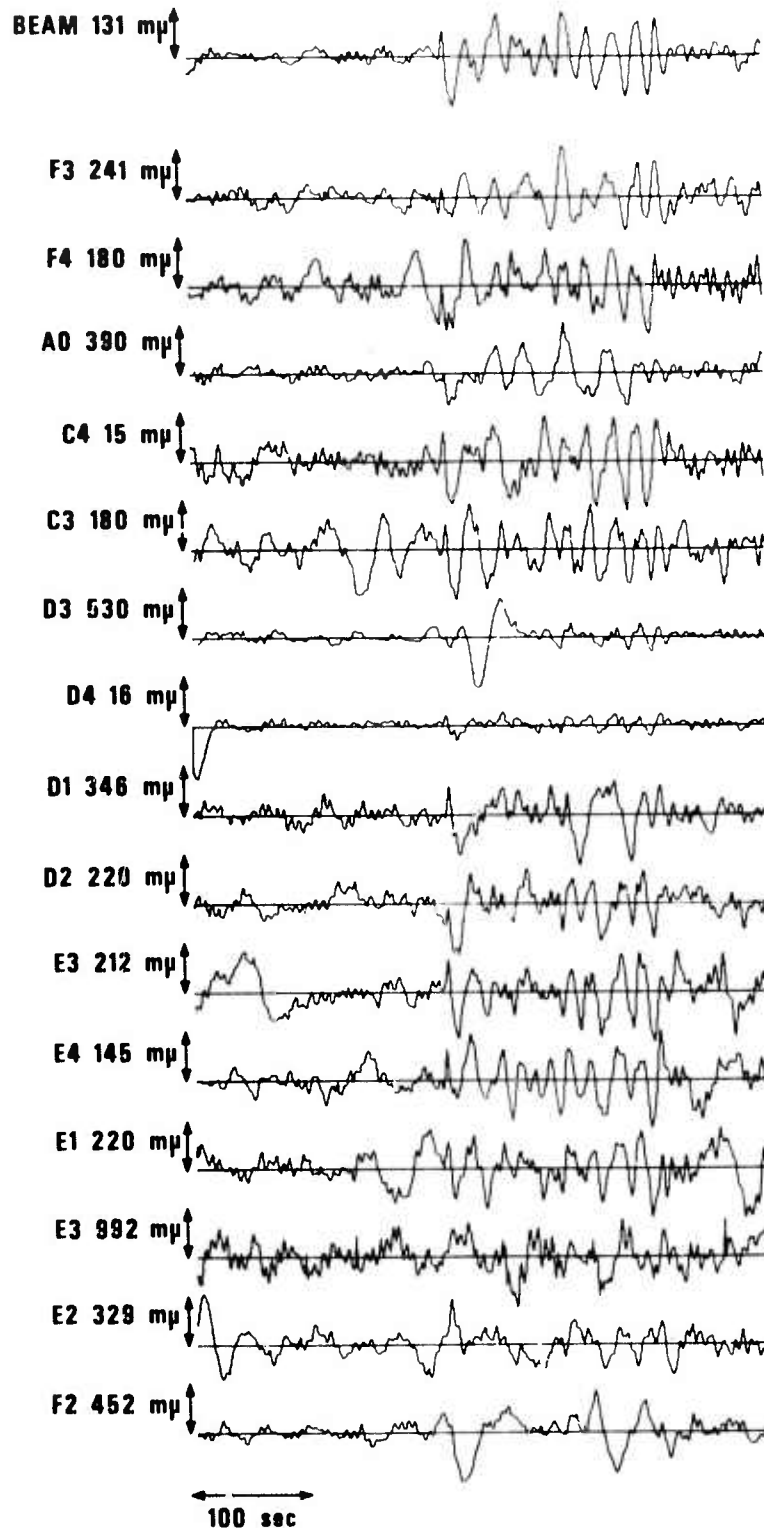
Figure 30. Radial beam and individual traces for the long-period P wave at LASA from CANNIKIN.
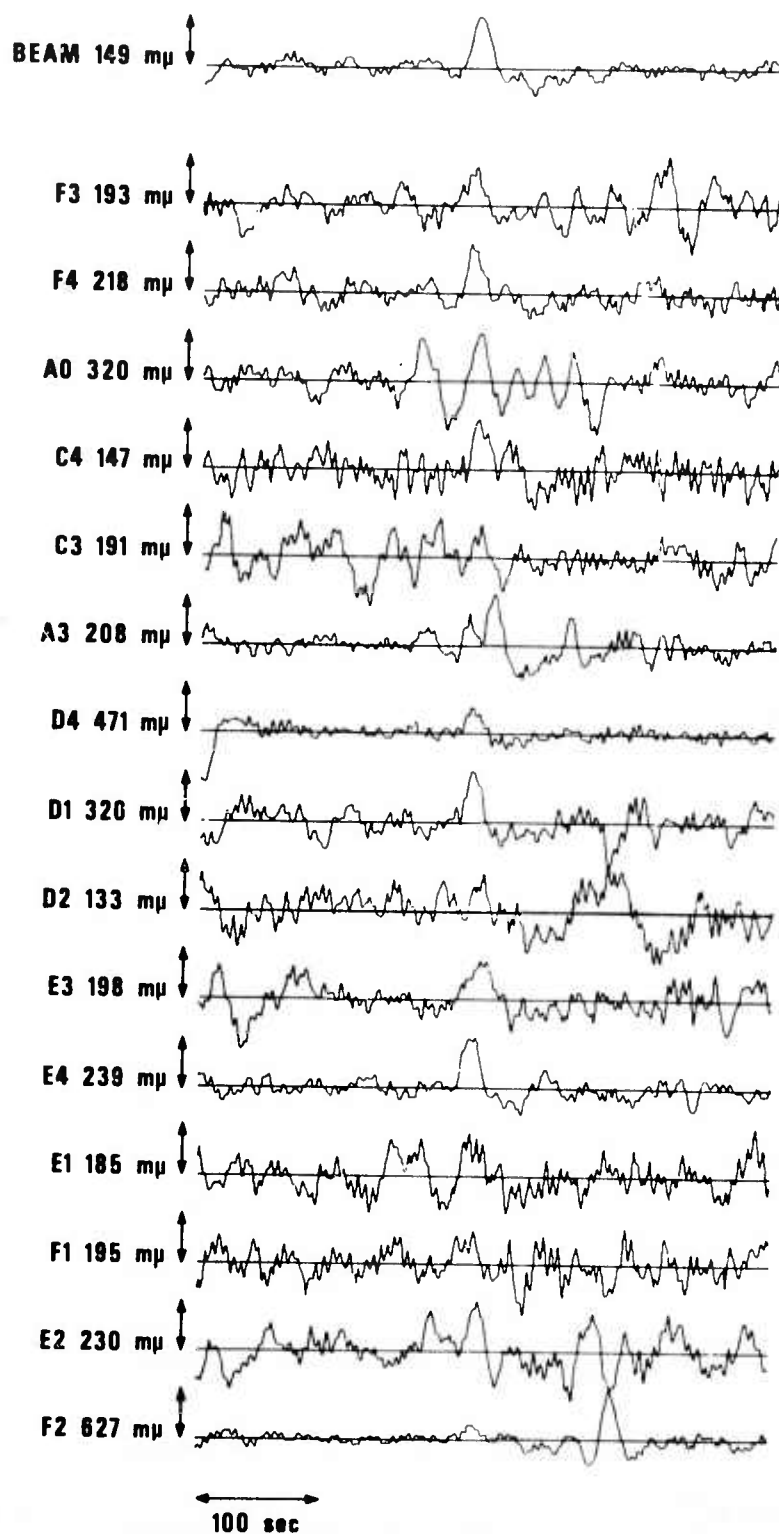
-79-

Figure 31. Transverse beams and individual traces for the long-period P wave at LASA from CANNIKIN.

LASA CANNIKAN "S" RADIAL AT 8 km/sec
START TIME FROM LASASITE F4
310 22 11 12 1971

BEAMS 1806 mμ

F3 2187 mμ

F4 2047 mμ

A0 1504 mμ

C4 2039 mμ

C3 1840 mμ

D3 1678 mμ

D4 1953 mμ

D1 2460 mμ

D2 1767 mμ

E3 2308 mμ

E4 2003 mμ

E1 1934 mμ

F1 1600 mμ

E2 1725 mμ

F2 1516 mμ

100 sec
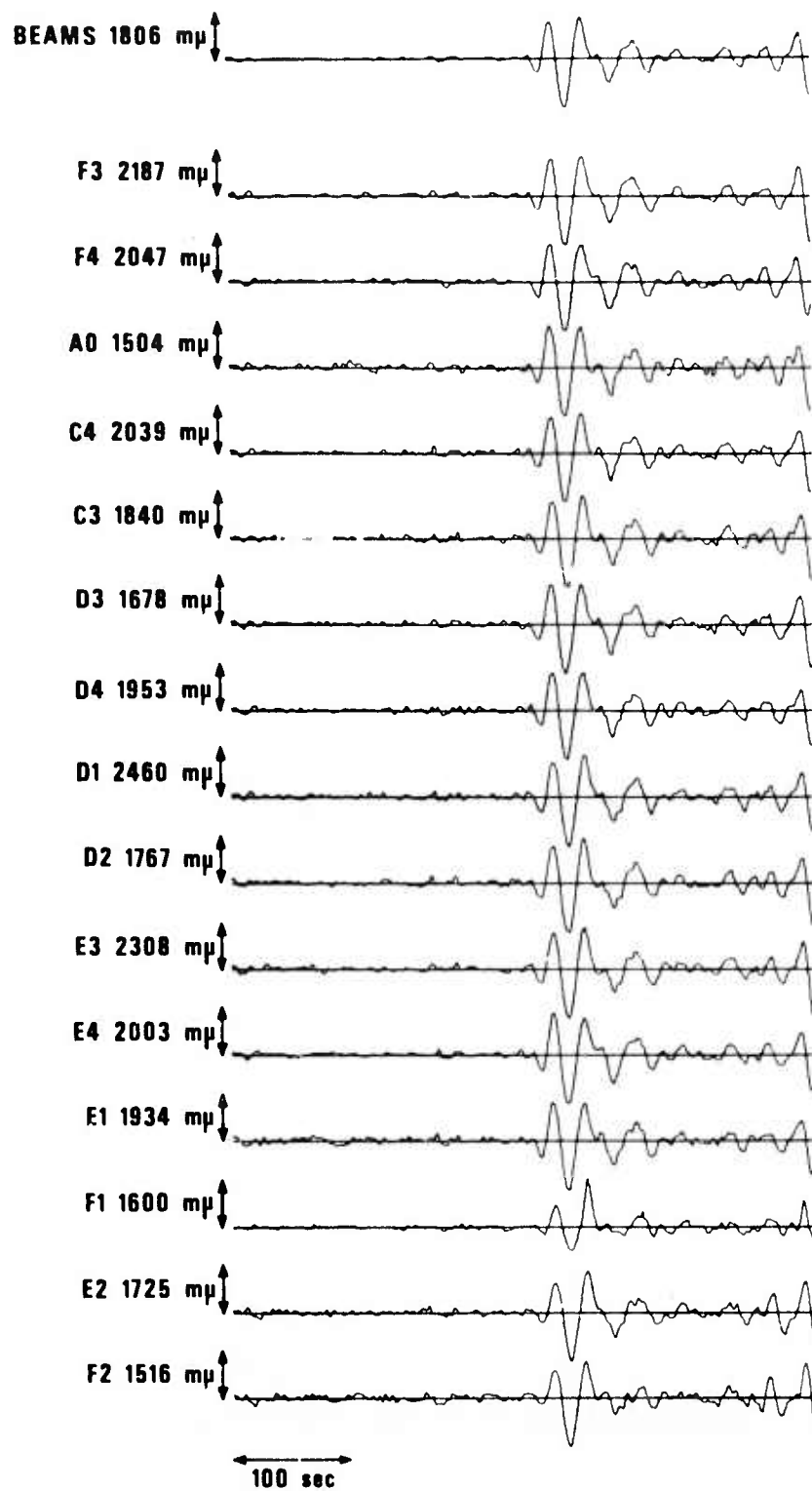
Figure 32. Radial beam and individual traces for the long-period S wave at LASA from CANNIKIN.

-81-
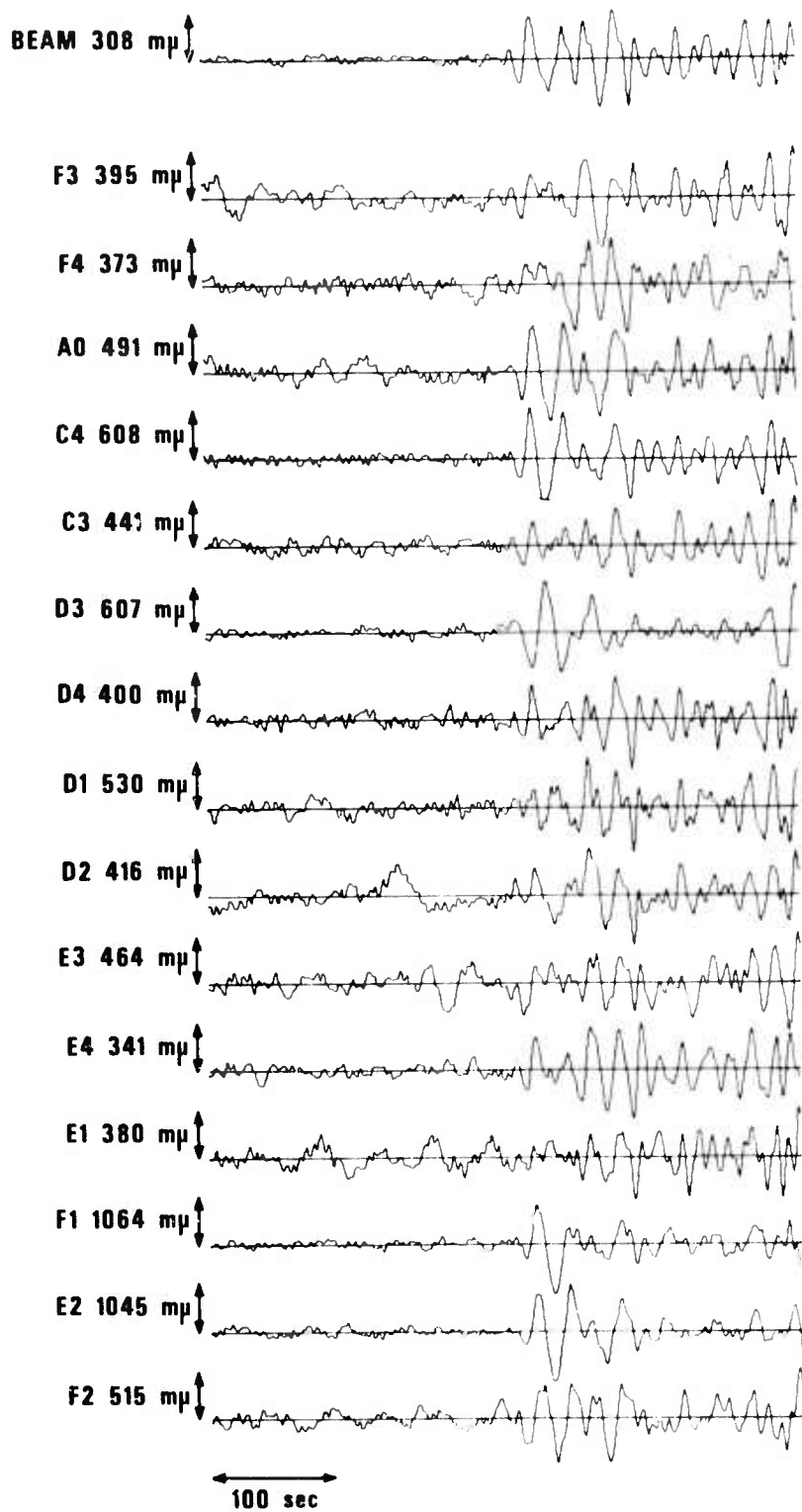
Figure 33. Transverse beams and individual traces for the long-period S wave at LASA from CANNIKIN.

Figure 34. Radial beam and individual traces for the long-period S wave at LASA from MILROW.

LL MILROW 9 OCT 69 S=222126 TRANSVERSE
START TIME FROM LASASITE F4
275 22 17 12 1969
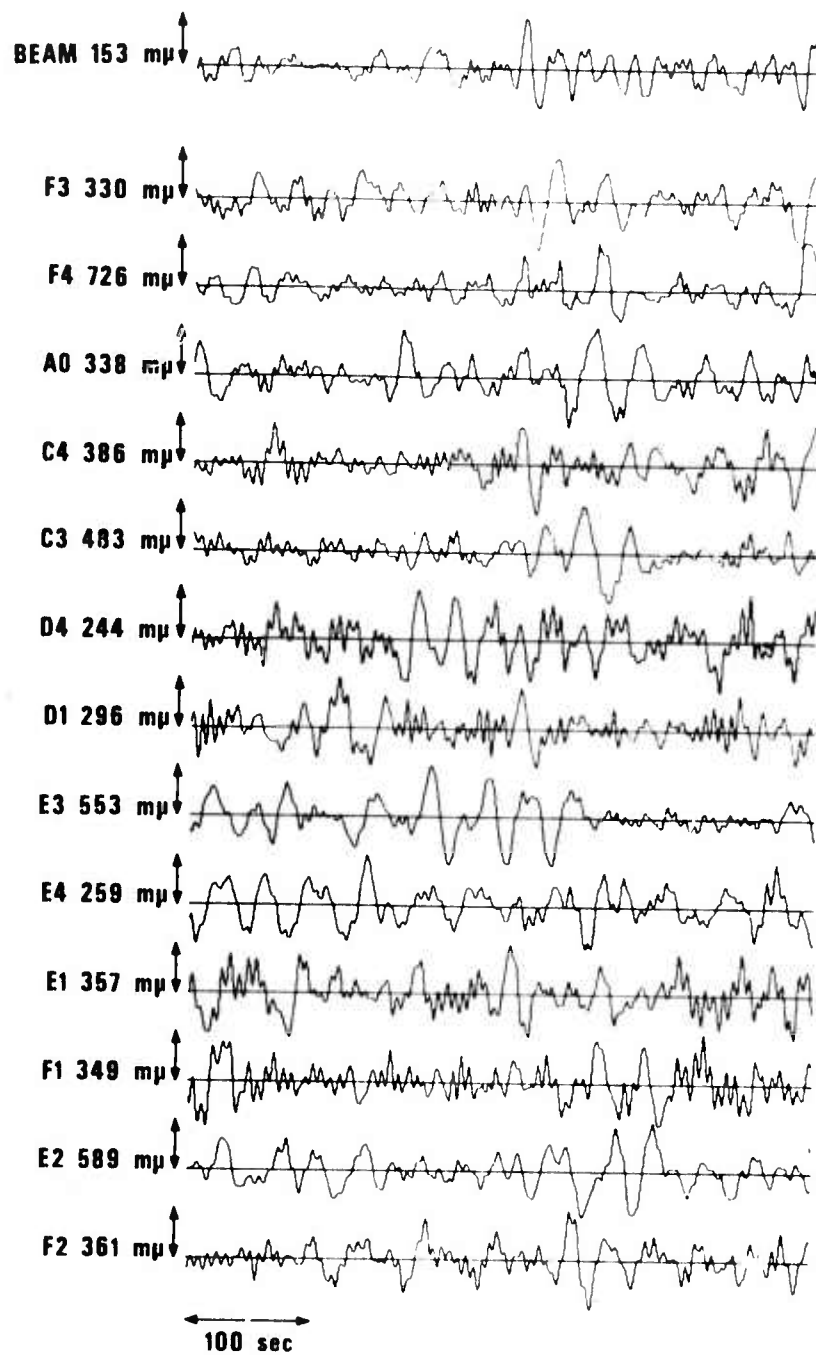
Figure 35. Transverse beam and individual traces for the long-period
S wave at LASA from MILROW.

-84-

Figure 36. Vertical, radial, and transverse long-period S at RKON from JORUM.

LPZ

15.8K X10

317 mμ

14:40

LPT

14.0K X10

358 mμ

14:40

LPR

40.0K X10

125 mμ

14:40

JORUM, WH2YK

SEPT. 16. 1969

LPZ

317 mµ ↕
14:40

15.8K X10

LPT

358 mµ ↕
14:40

14.0K X10

LPR

125 mµ ↕
14:40

40.0K X10
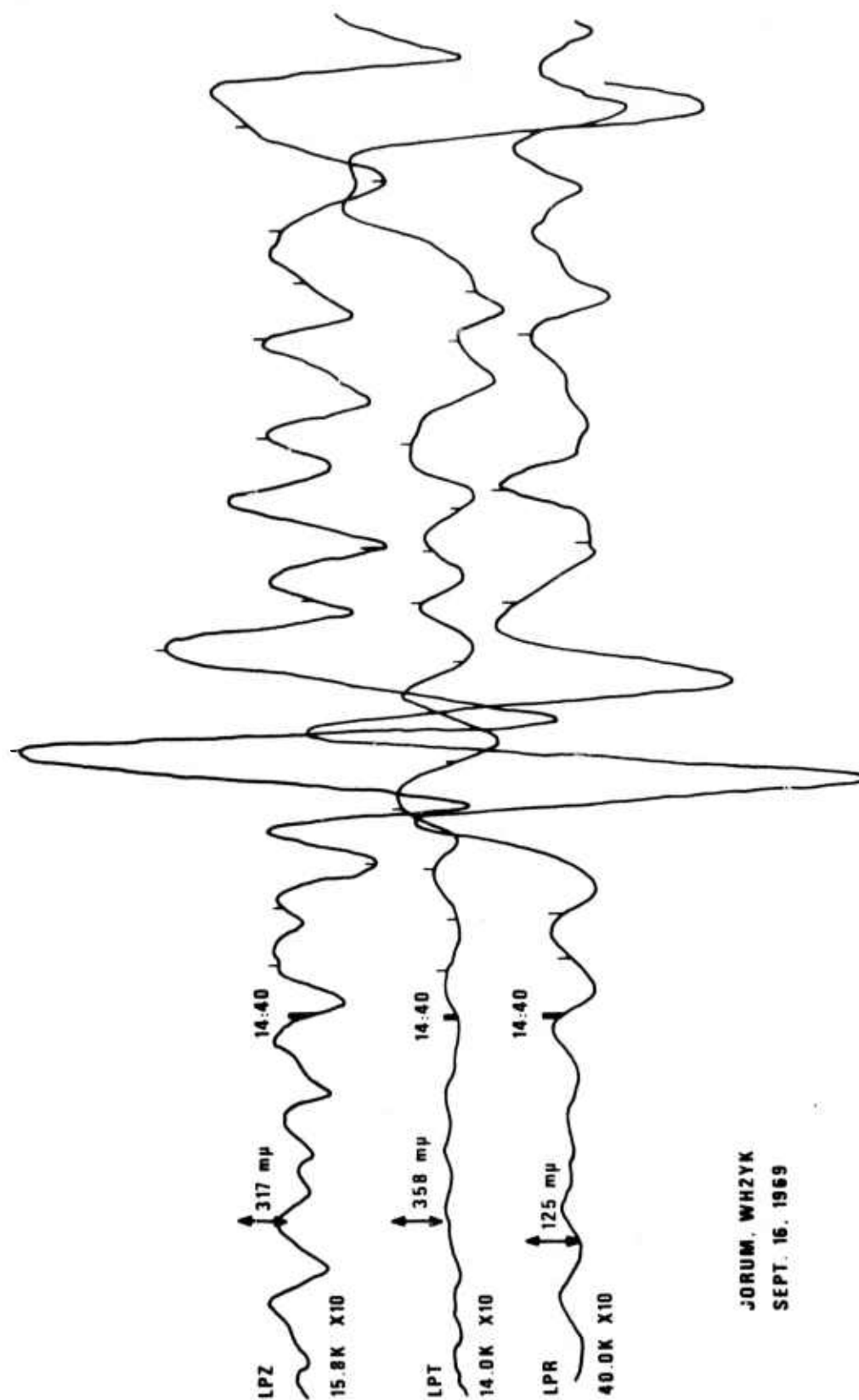
20X VIEW
JORUM. WH2YK
SEPT. 16. 1969
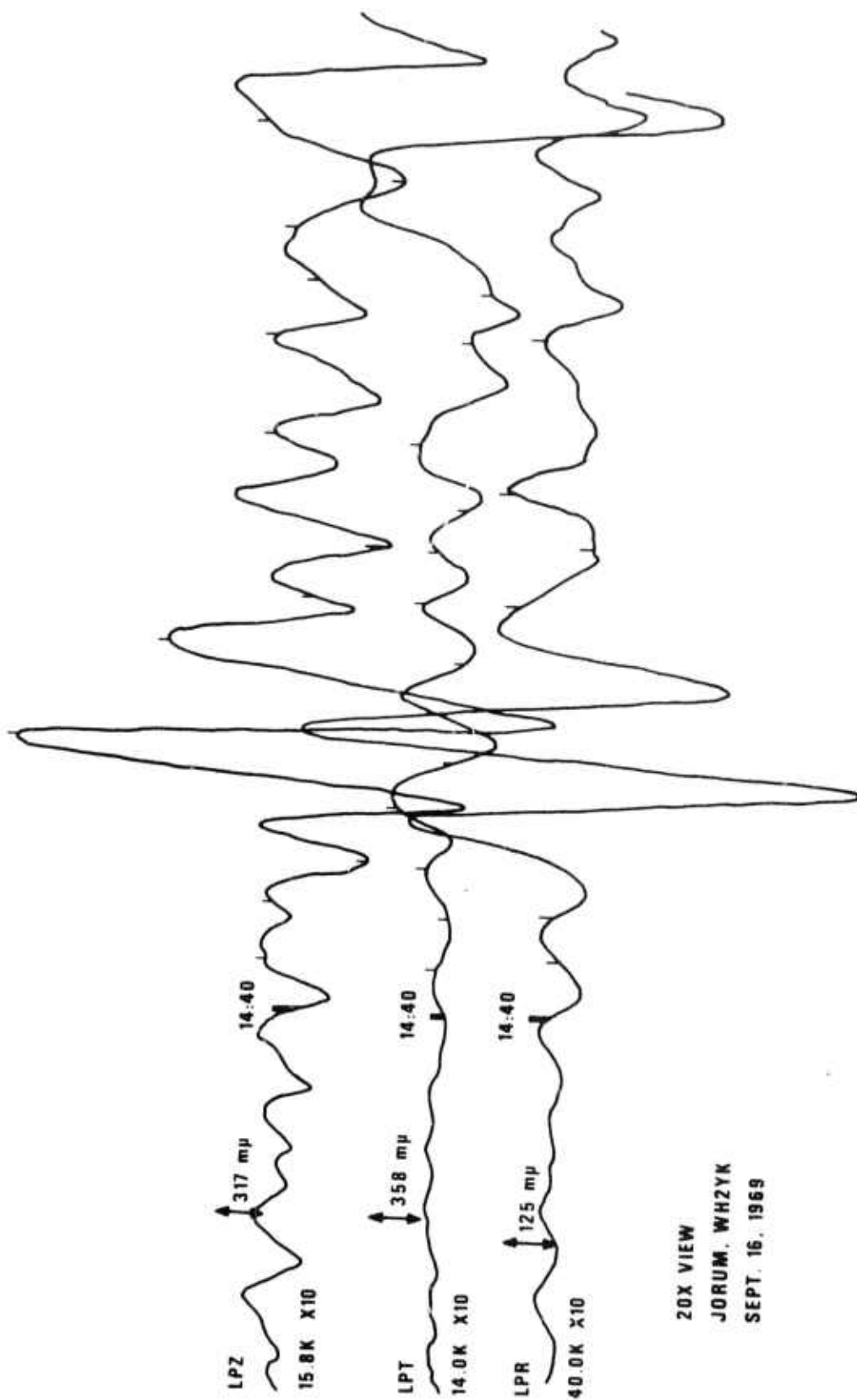
Figure 37. Vertical, radial, and transverse long-period S at WH2YK from JORUM.
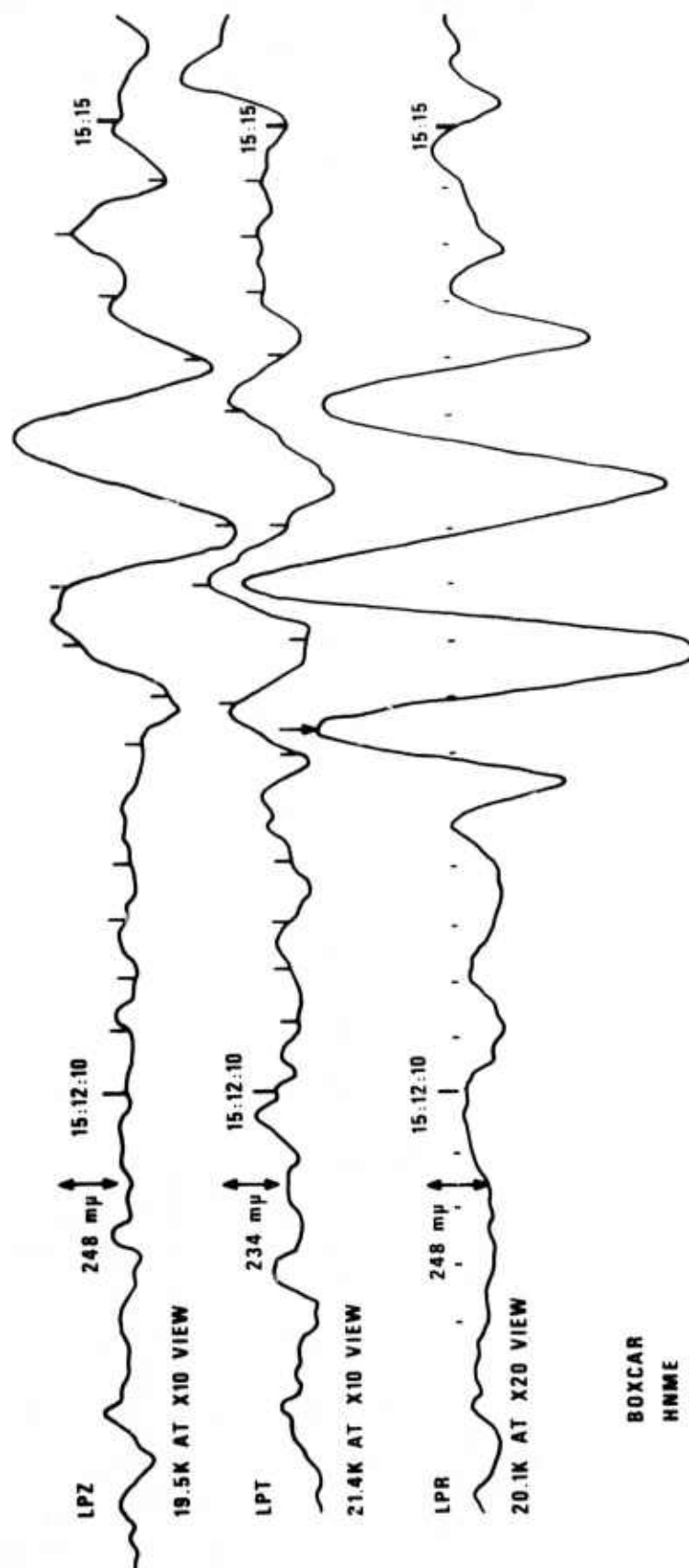
Figure 38. Vertical, radial, and transverse long-period S at HNME from BOXCAR.
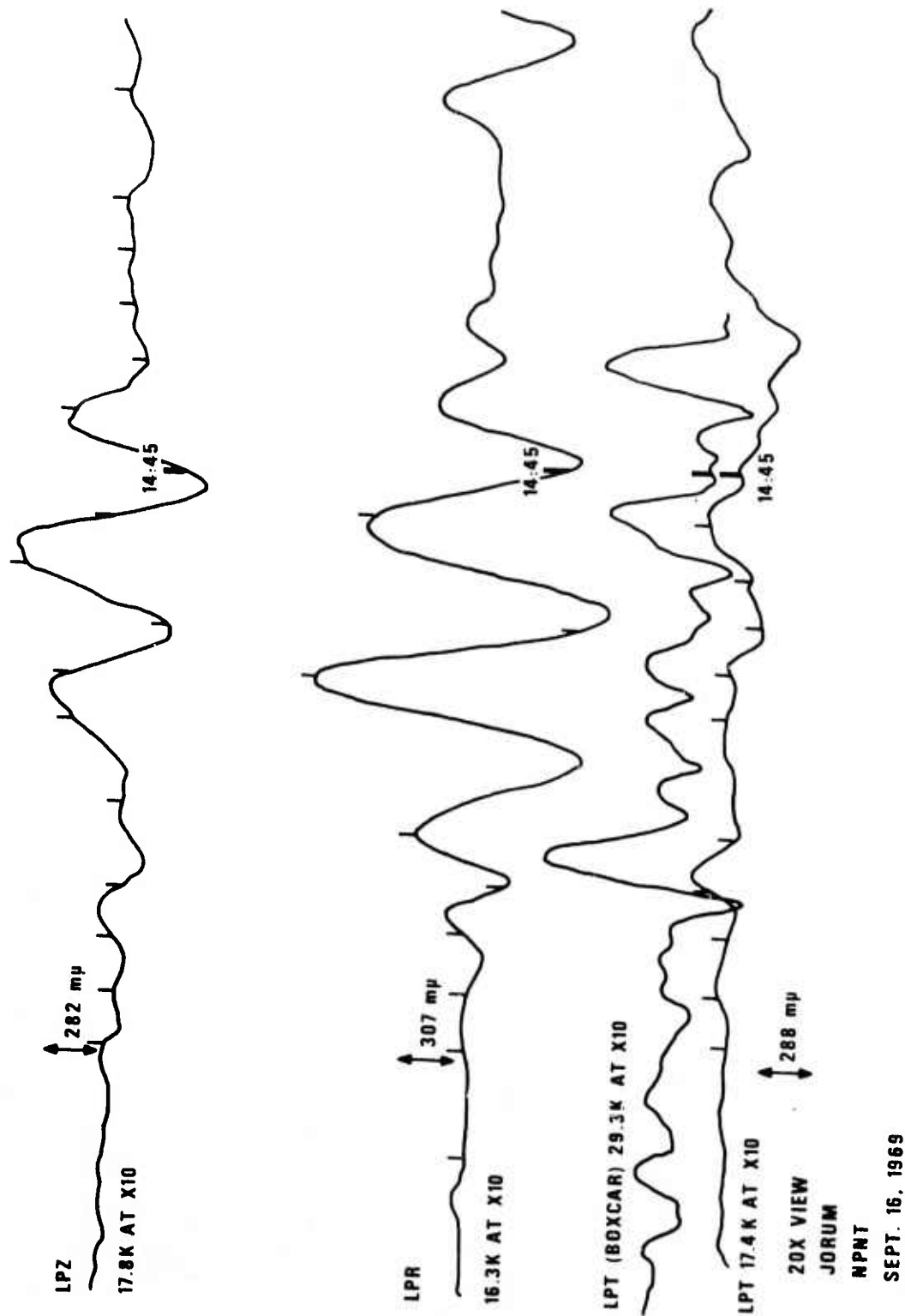
Figure 39a. Vertical, radial, and transverse long-period S at NPNT from JORUM. The transverse component from BOXCAR has also been traced.
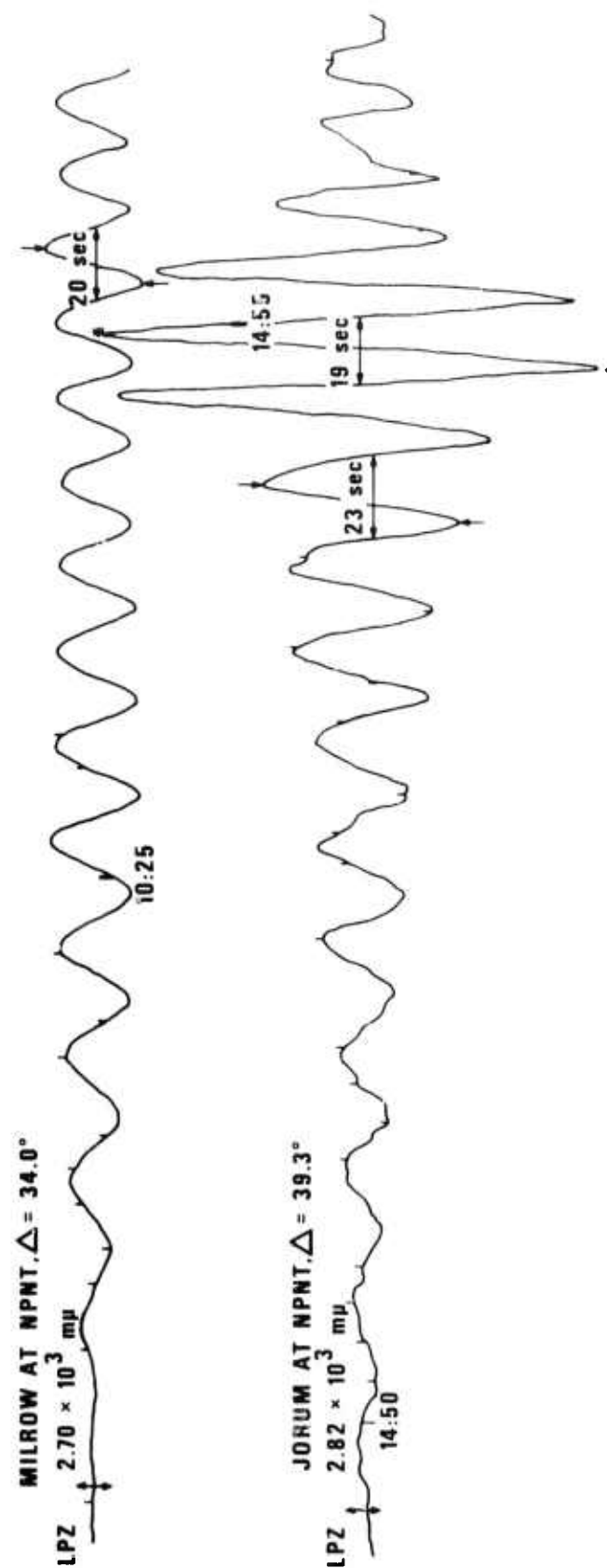
Figure 39b. Rayleigh waves from MILROW and JORUM at NPNT.
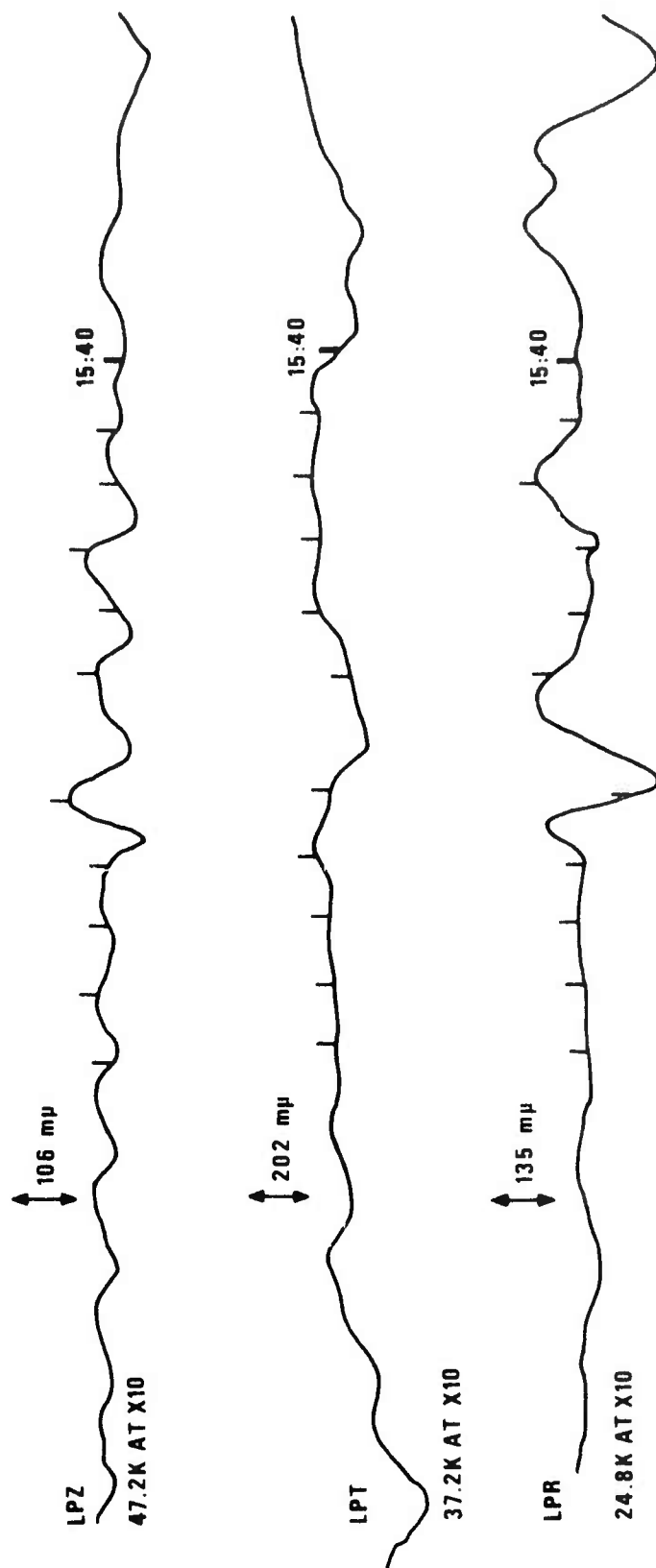
Figure 40. Vertical, radial, and transverse long-period S at RKON from PILEDRIVER.
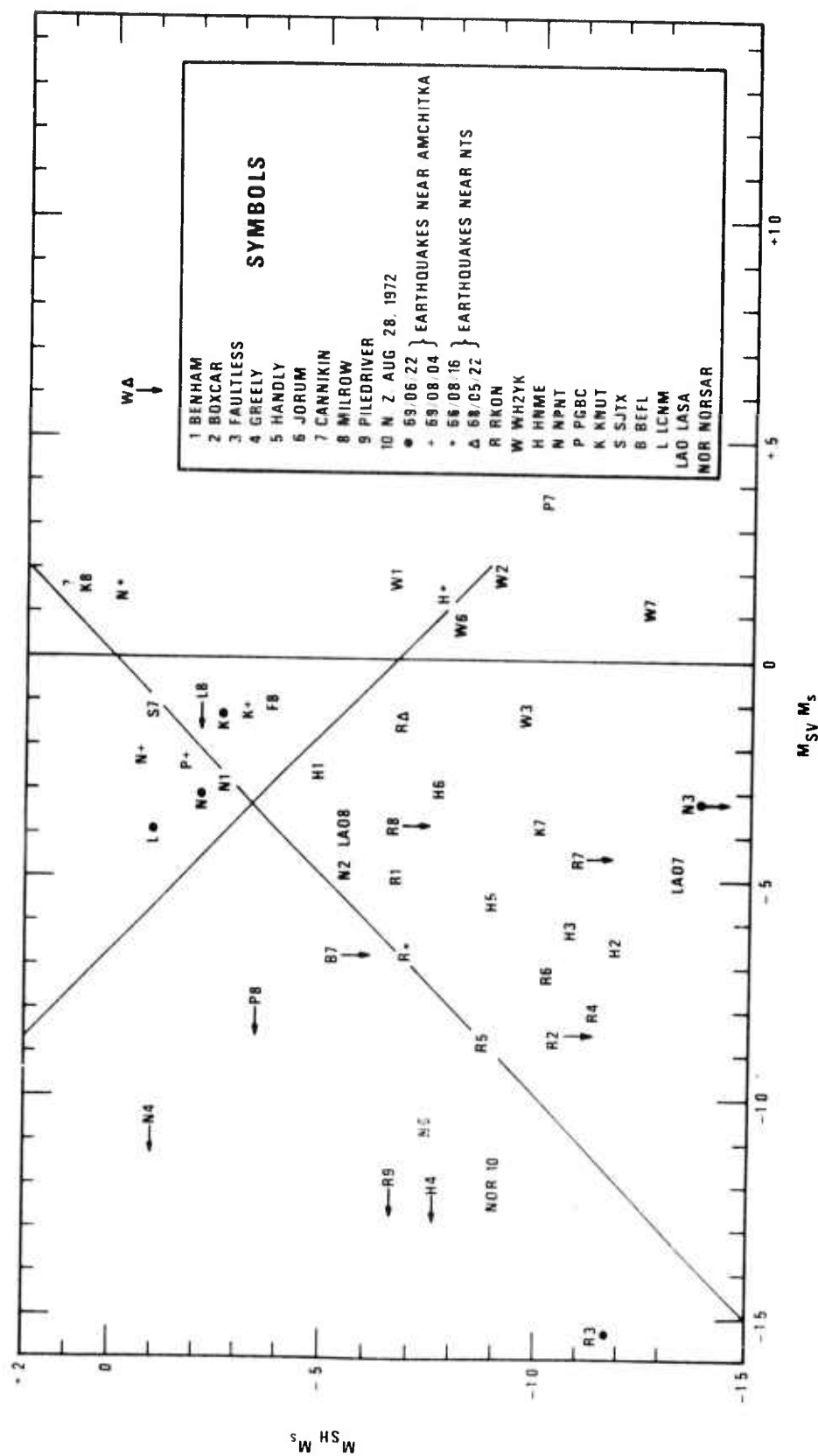
Figure 41a. $M_{SH}-\overline{M}_s$ versus $M_{SV}-\overline{M}_s$ for several explosion and earthquake event-station pairs. Worldwide earthquakes will cluster 0.1-0.2 magnitude units diagonally below the point (0,0).
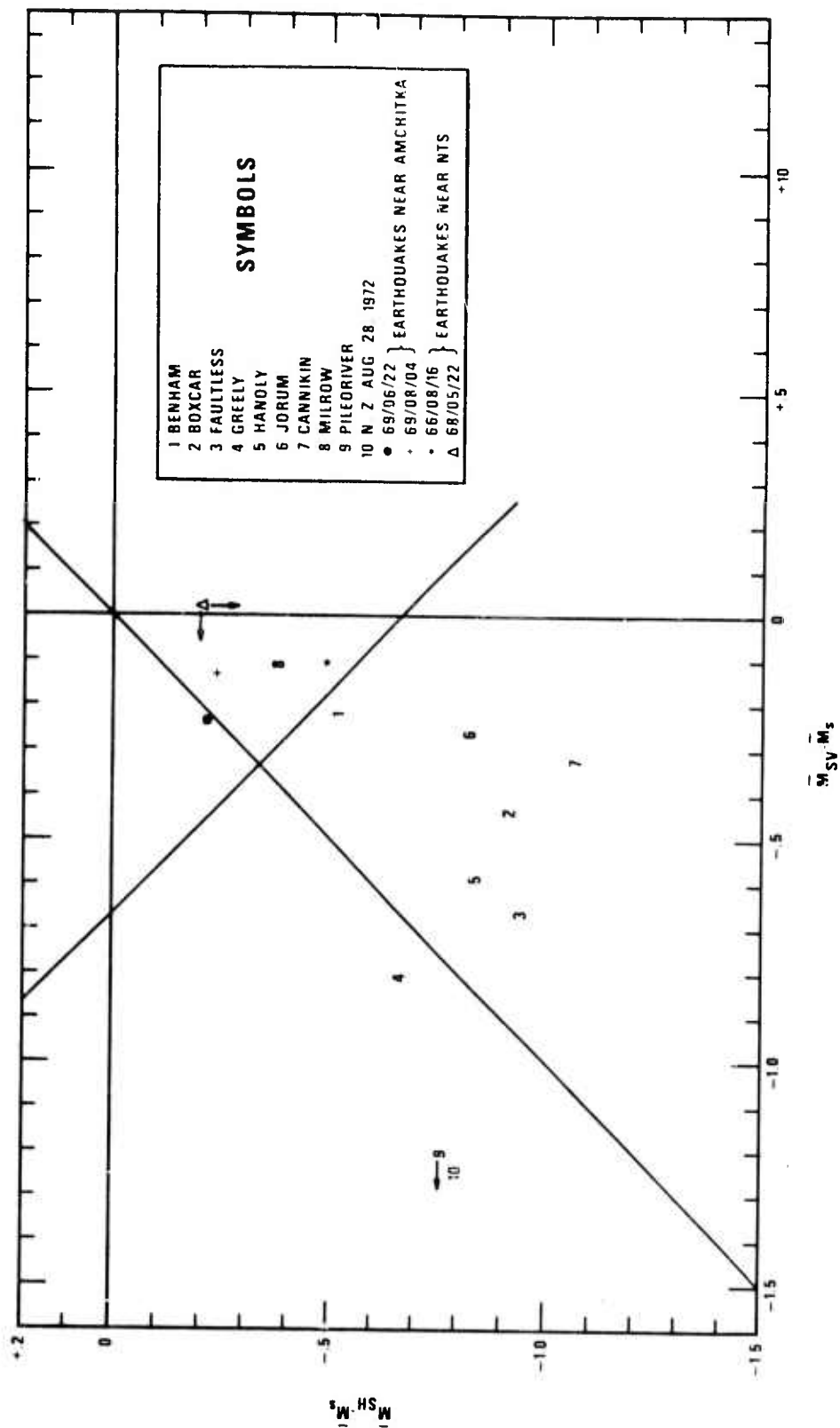
Figure 41b. $\overline{M}_{SH}-\overline{M}_s$ versus $\overline{M}_{SV}-\overline{M}_s$ for several earthquakes and explosions. Worldwide earthquakes will cluster about 0.1-0.2 magnitude units diagonally below the point (0,0).

SYMBOLS

1 BENHAM
2 BOXCAR
3 FAULTLESS
4 GREELY
5 HANDLY
6 JORUM
7 CANNIKIN
8 MILROW
9 PILEDRIVER
10 N Z AUG. 28, 1972
● 69/06/22 } EARTHQUAKES NEAR AMCHITKA
+ 69/08/04 }
· 66/08/16 } EARTHQUAKES NEAR NTS
△ 68/05/22 }

POSSIBLE DISCRIMINATION VALUE

EARTHQUAKE LARGE POPULATION MEAN

$\bar{M}_{SHEAR} - \bar{M}_s$

−1.0   −.5   0   +.5
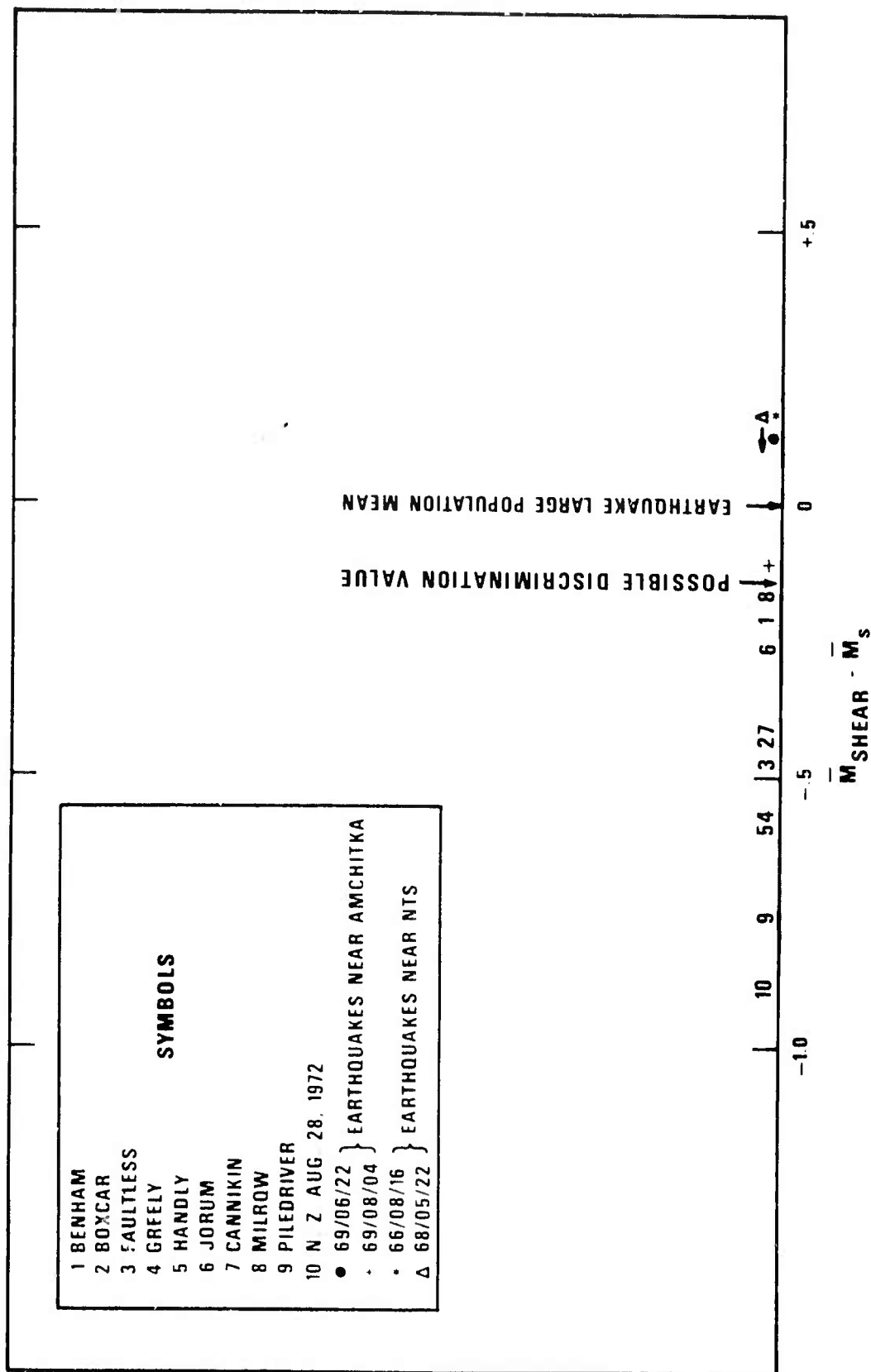
Figure 41c. $\bar{M}_{SHEAR} - \bar{M}_s$ for several earthquakes and explosions. Worldwide earthquakes will cluster about one point (0,0).
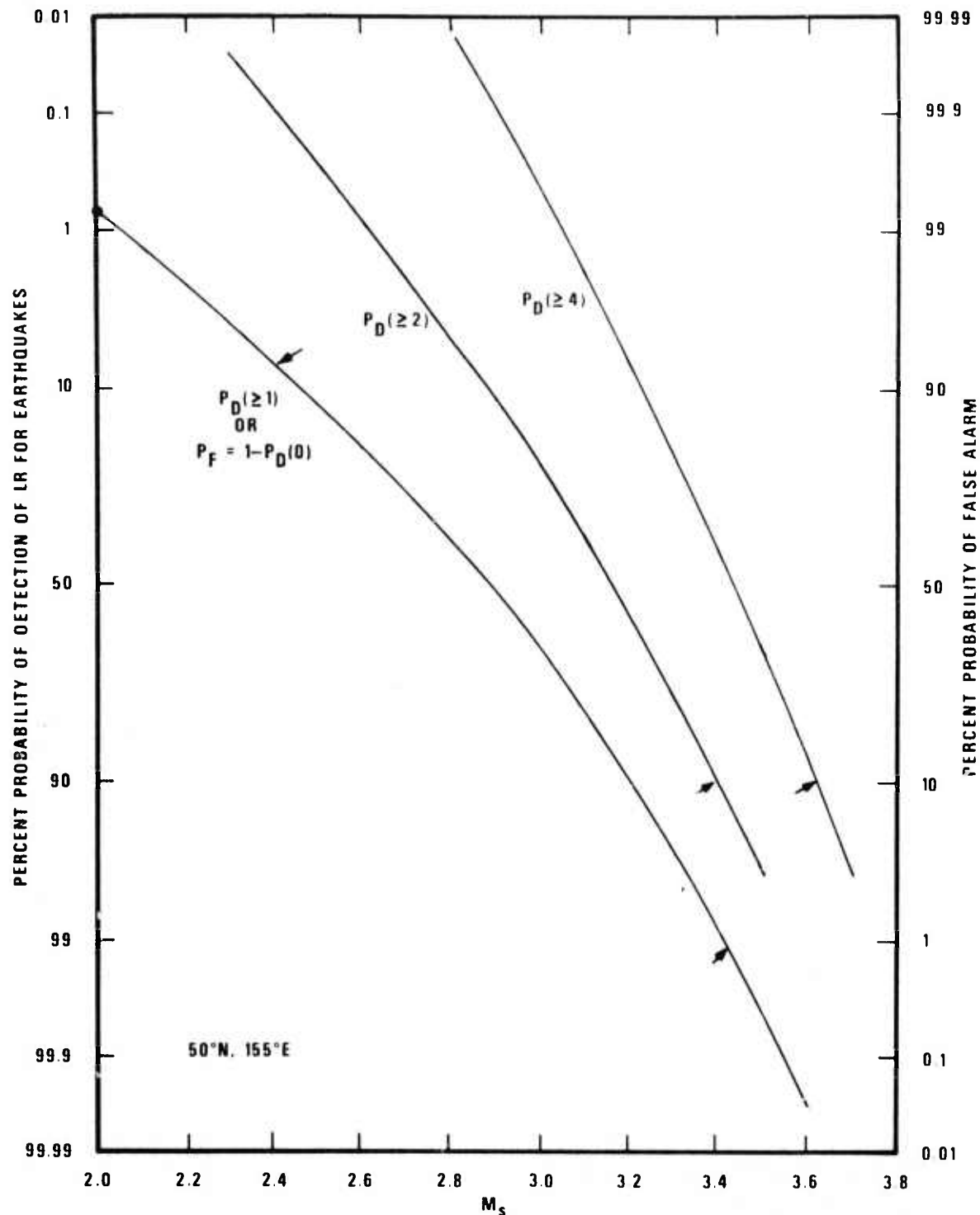
Figure 42. Probability of detection of S by $\geq$ 1, 2, or 4 stations out of 25 and probability of a false alarm (no detection, resulting in a decision that an earthquake is an explosion by means of negative discrimination) as a function of M_s for a 25-station worldwide network after Romney (1971) for an epicenter in Kamchatka. Noise and signal standard deviation is 0.3 magnitude units. Arrows indicate points referred to in the text.
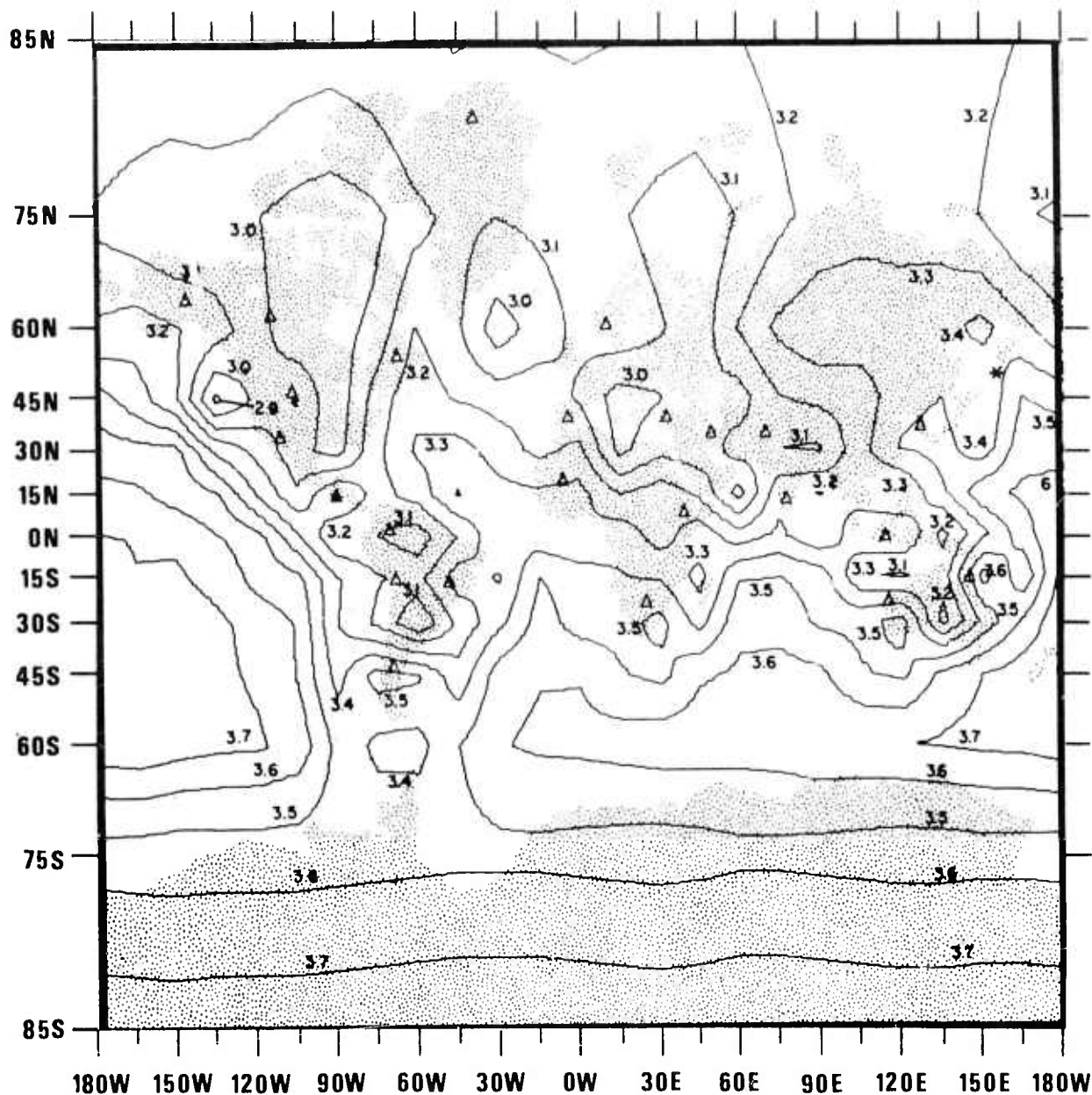
Figure 43. Threshold magnitude for 99% probability of detection of S by 1 or more stations by a worldwide network of 25 stations with mean zero-to-peak noise levels of 19 mμ except for 15 mμ for LASA, NORSAR, and ALPA, a signal-to-noise ratio for detection of r=1.5, and a standard deviation of signal and noise of 0.3 magnitude units. The star indicates the epicenter assumed for the probability of detection versus M_s plots such as Figure 42.
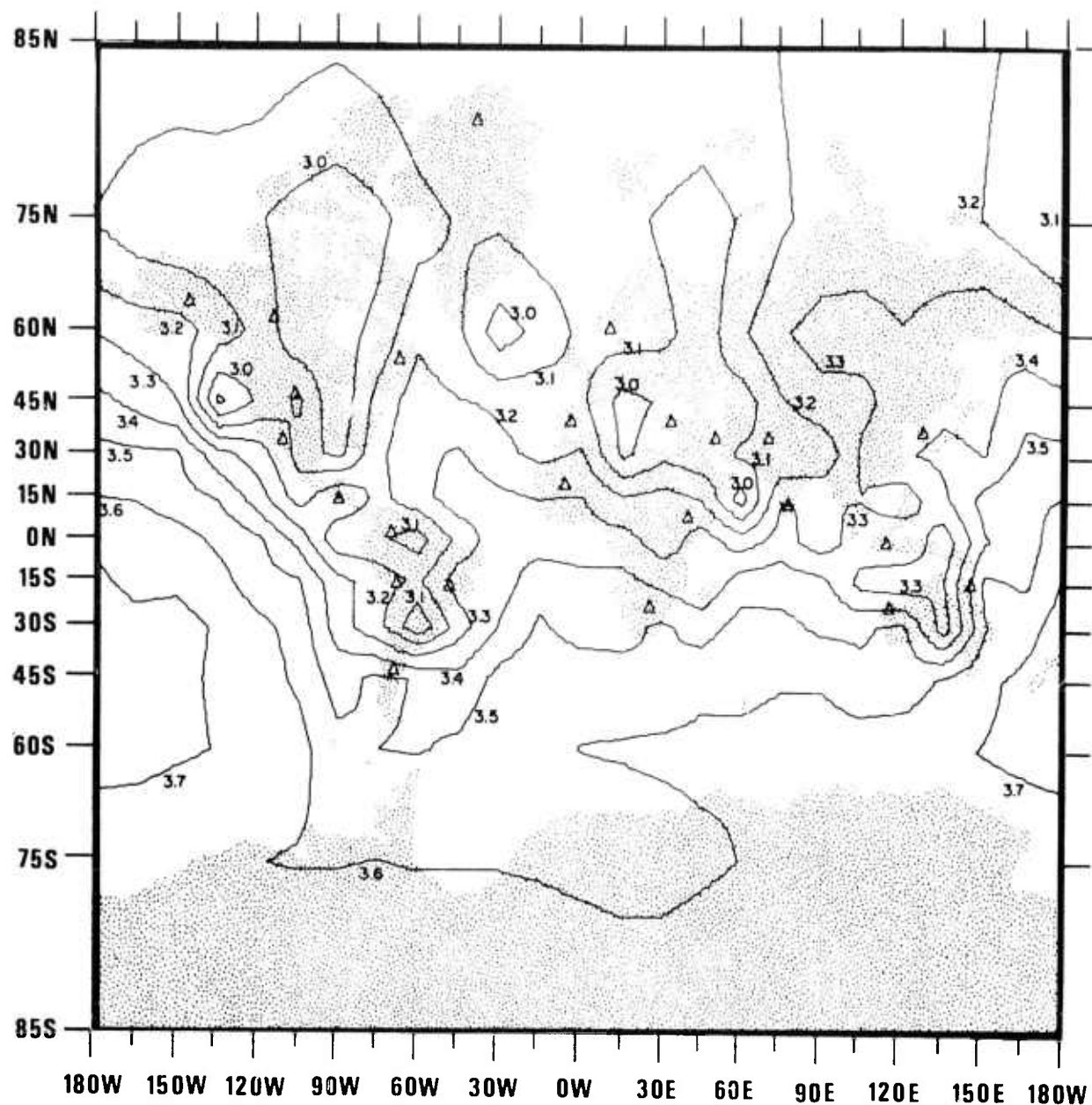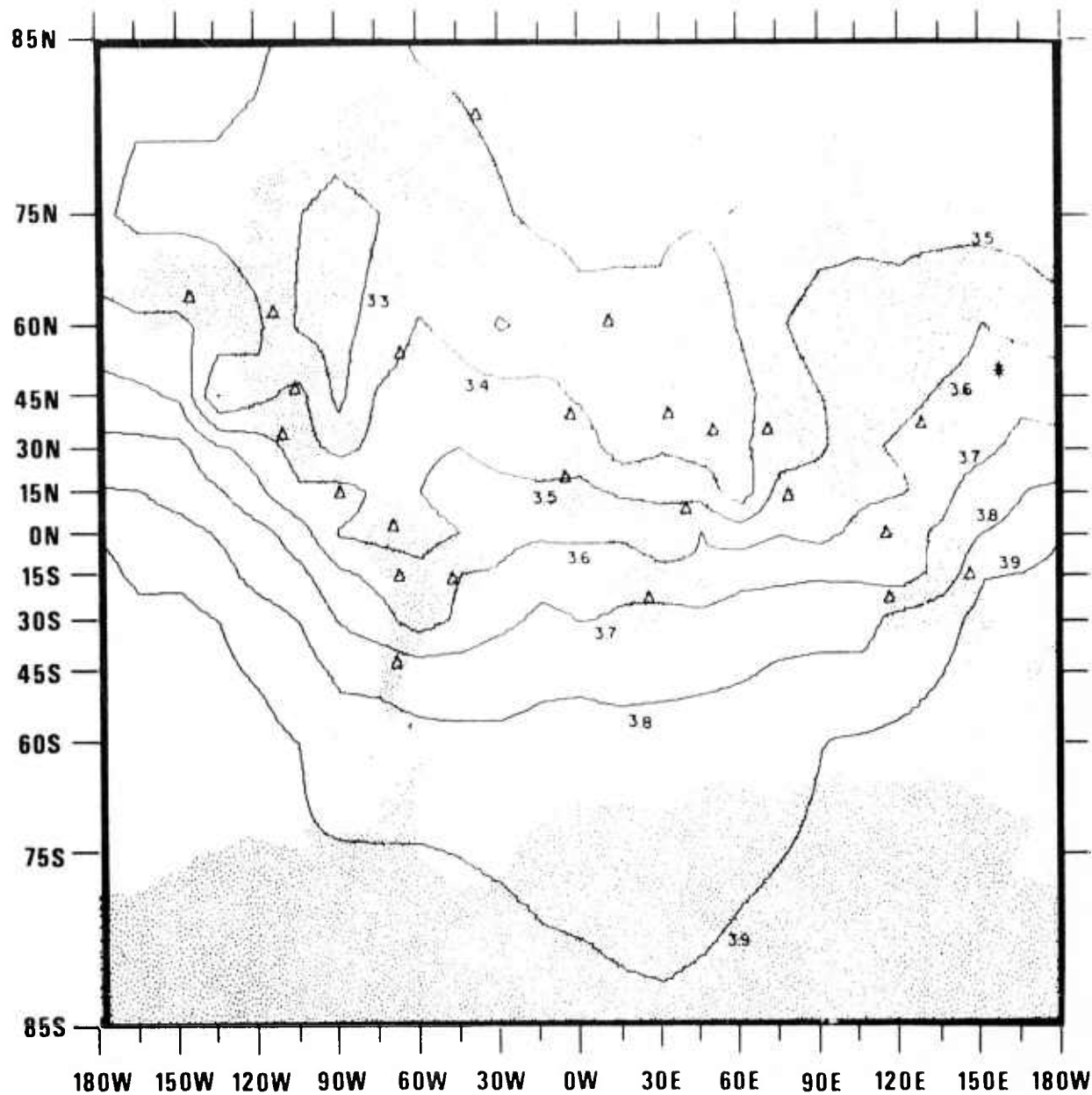
Figure 44. Threshold magnitude for 90% probability of detection of S by 2 or more stations by a worldwide network of 25 stations with mean zero-to-peak noise levels of 19 mμ except for 15 mμ for LASA, NORSAR, and ALPA, a signal-to-noise ratio for detection of r=1.5, and a standard deviation of signal and noise of 0.3 magnitude units. The star indicates the epicenter assumed for the probability of detection versus M_s plots such as Figure 42.
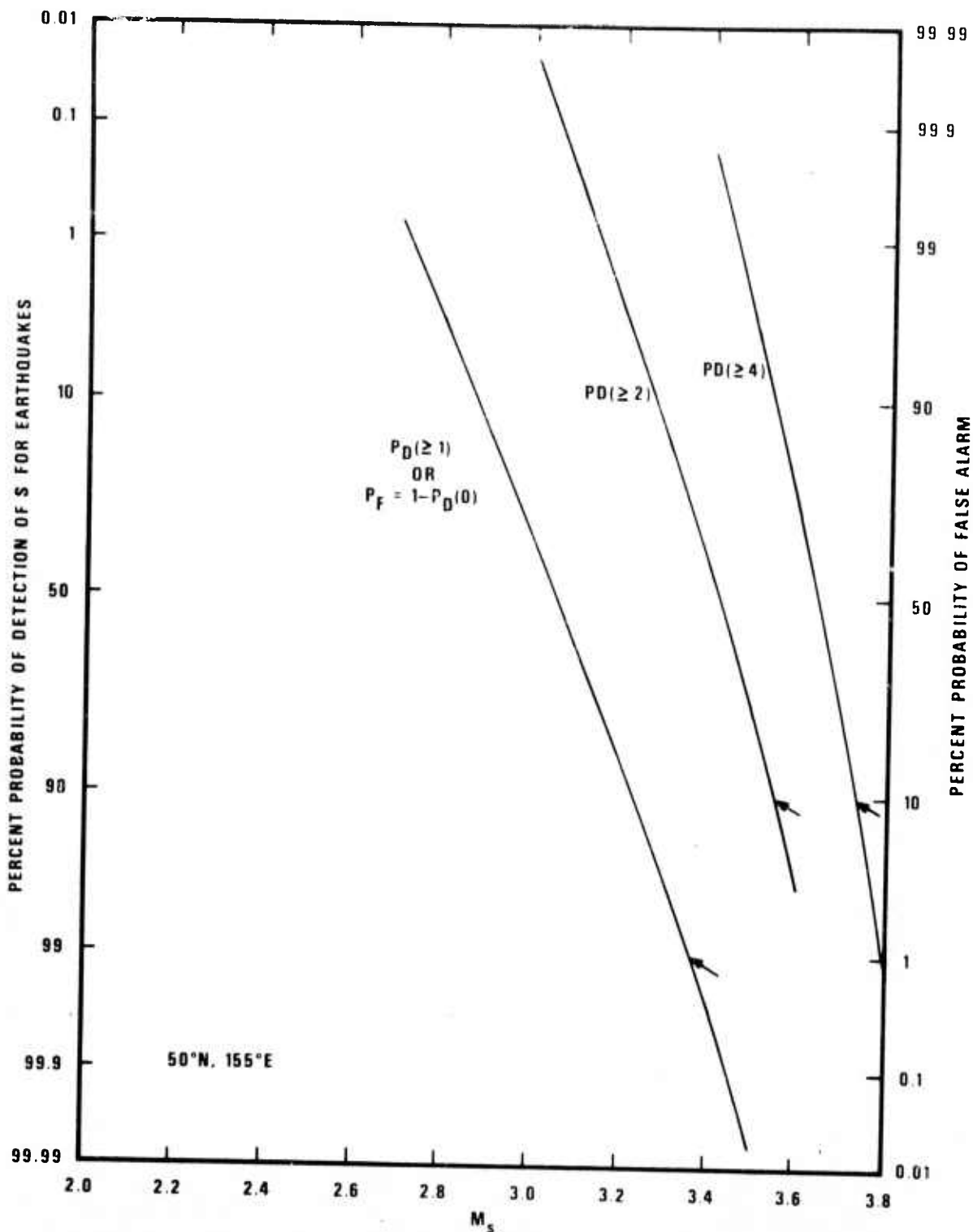
Figure 45. Threshold magnitude for 90% probability of detection of S by
4 or more stations by a worldwide network of 25 stations with mean zero-to-peak
noise levels of 19 mμ except for 15 mμ for LASA, NORSAR, and ALPA, a
signal-to-noise ratio for detection of r=1.5, and a standard deviation of
signal and noise of 0.3 magnitude units. The star indicates the epicenter
assumed for the probability of detection versus M_s plots such as Figure 42.

Figure 46.   Probability of detection of S by $\geq$ 1, 2, or 4 stations out of 25 and probability of a false alarm (no detection, resulting in a decision that an earthquake is an explosion by means of negative discrimination) as a function of M_s for a 25-station worldwide network after Romney (1971) for an epicenter in Kamchatka.   Noise and signal standard deviation 0.1 magnitude units.   Arrows indicate points referred to in the text.
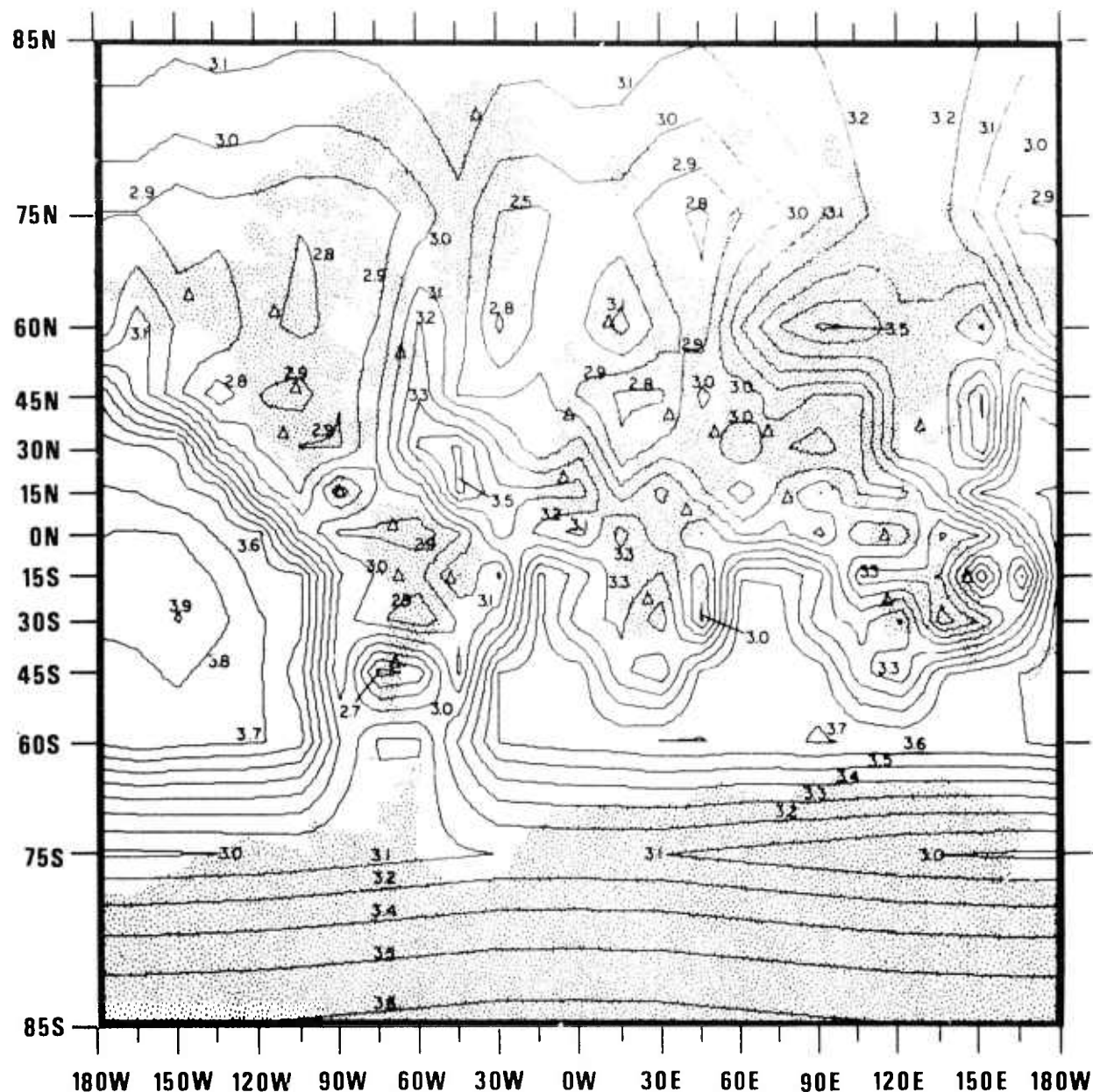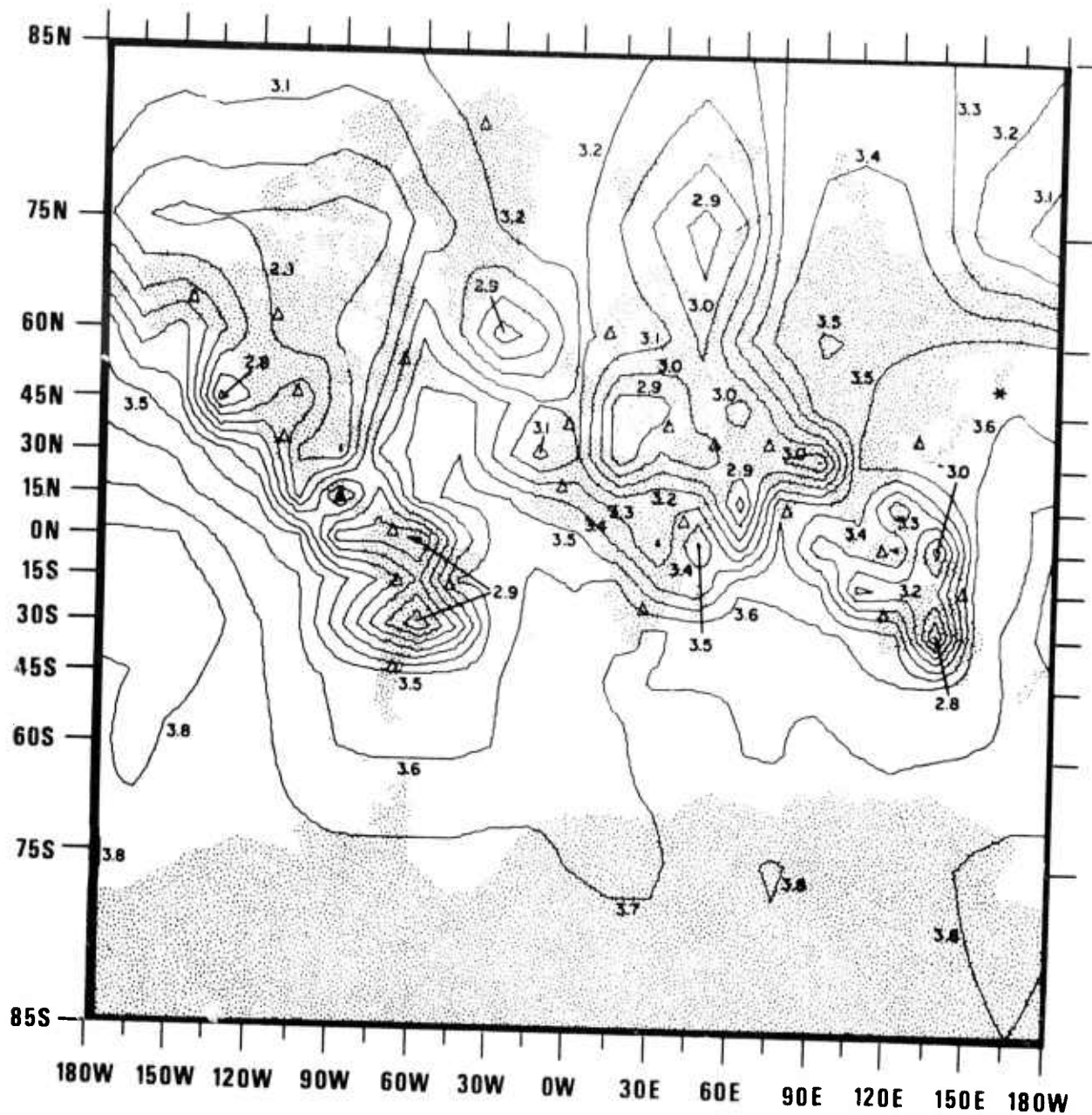
Figure 47. Threshold magnitude for 99% probability of detection of S by
1 or more stations by a worldwide network of 25 station with mean
zero-to-peak levels of 19 mμ except for 15 mμ for LASA, NORSAR, and ALPA,
a signal-to-noise ratio for detection of r=1.5, and a standard deviation
of signal and noise of 0.1 magnitude units. The star indicates the
epicenter assumed for the probability of detection versus M_s plots such
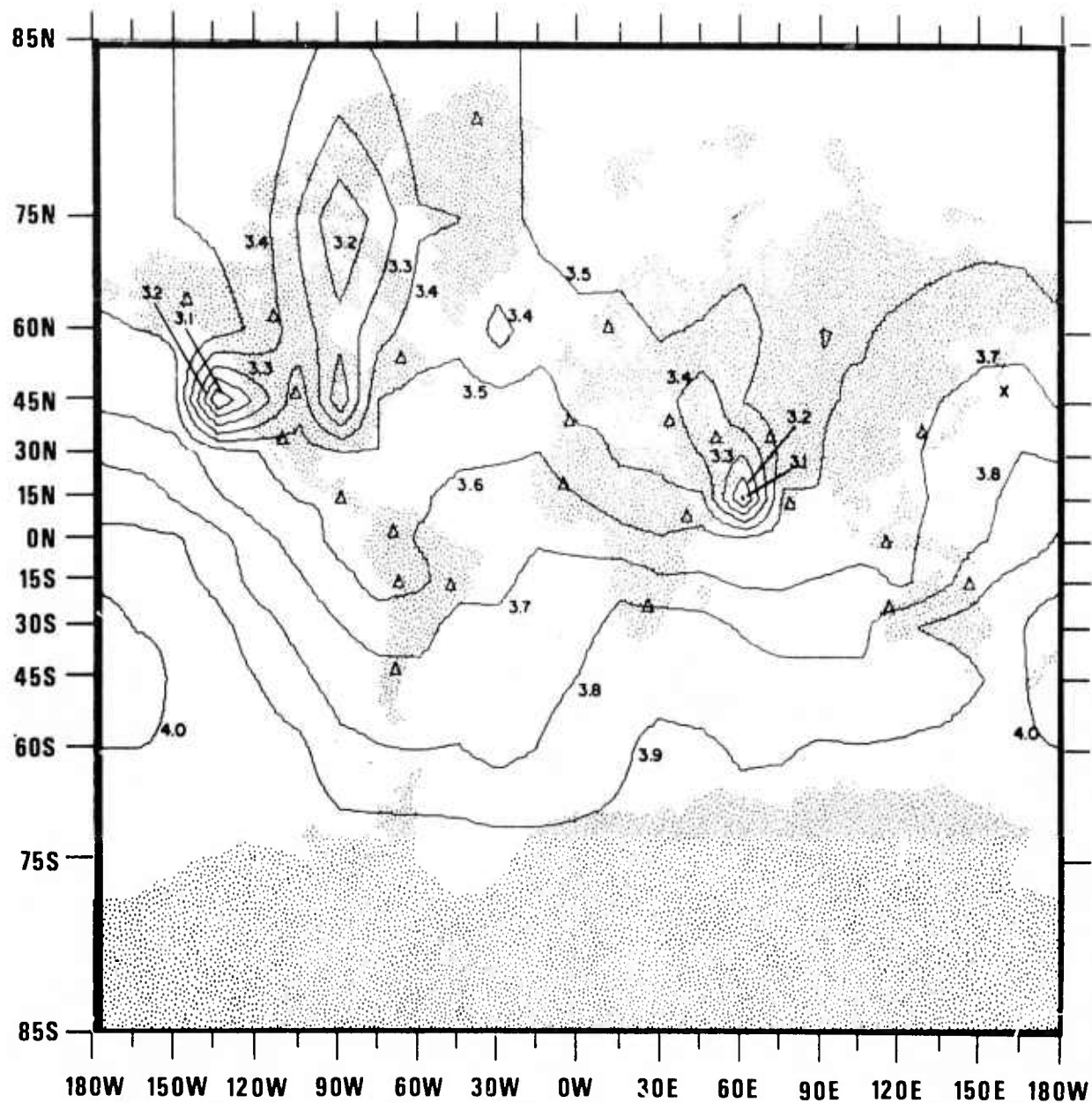as Figure 42.

Figure 48. Threshold magnitude for 90% probability of detection of S by
2 or more stations by a worldwide network of 25 stations with mean
zero-to-peak noise levels of 19 mμ except for 15 mμ for LASA, NORSAR, and
ALPA, a signal-to-noise ratio for detection of r=1.5, and a standard
deviation of signal and noise of 0.1 magnitude units. The star indicates
the epicenter assumed for the probability of detection versus M_s plots such
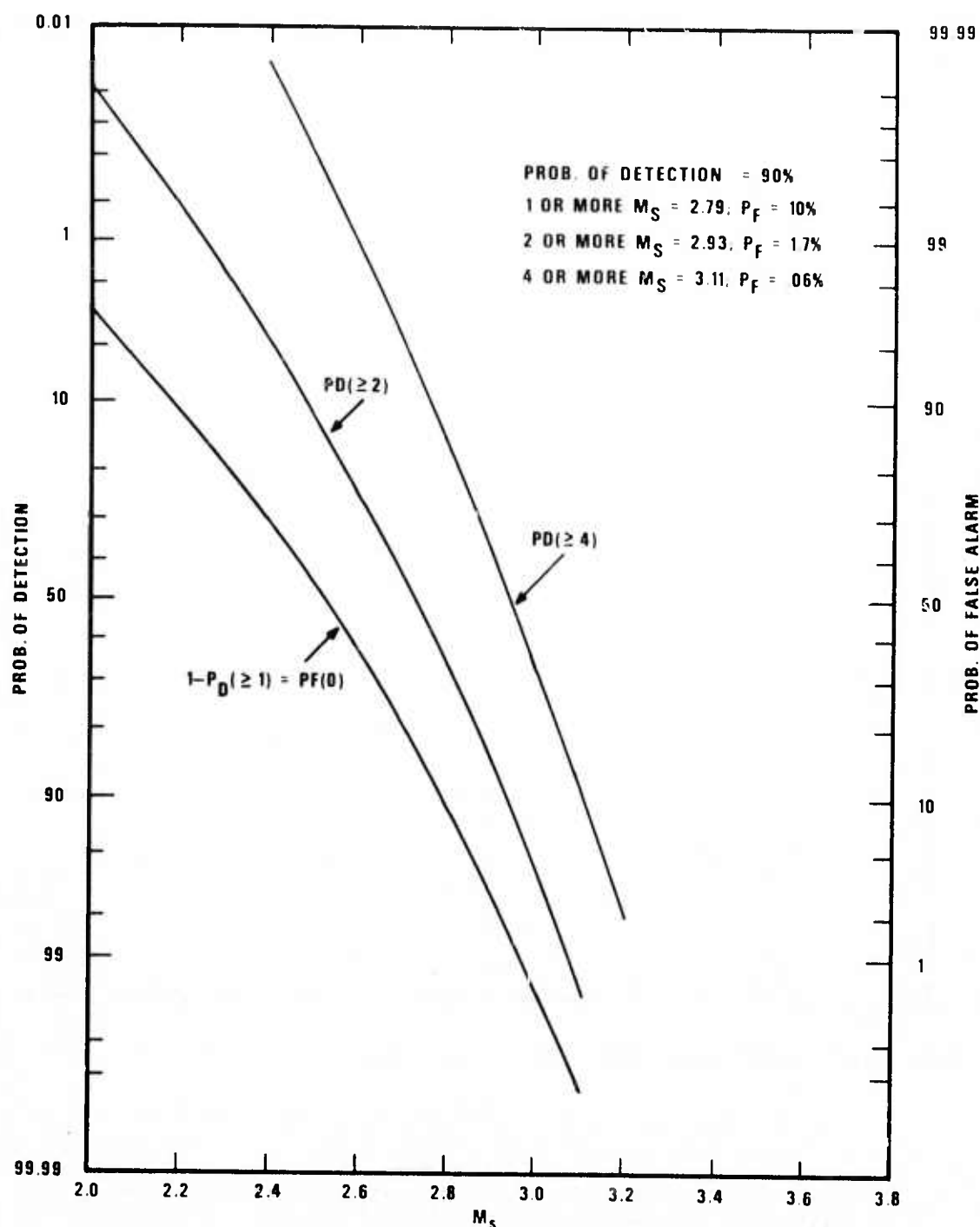as Figure 42.

Figure 49. Threshold magnitude for 90% probability of detection of S by 4 or more stations by a worldwide network of 25 stations with mean zero-to-peak noise levels of 19 mμ except for 15 mμ for LASA, NORSAR, and ALPA, a signal-to-noise ratio for detection of r=1.5, and a standard deviation of signal and noise of 0.1 magnitude units. The star indicates the epicenter assumed for the probability of detection versus M_s plots such as Figure 42.

Figure 50. Probability of detection of LR by $\geq$ 1, 2, or 4 stations out of 25 and probability of a false alarm (no detection resulting in a decision that an earthquake is an explosion by means of negative discrimination) as a function of M_s for a 25-station worldwide network after Romney (1971) for an epicenter in Kamchatka. Noise and signal standard deviation is 0.3 magnitude units.
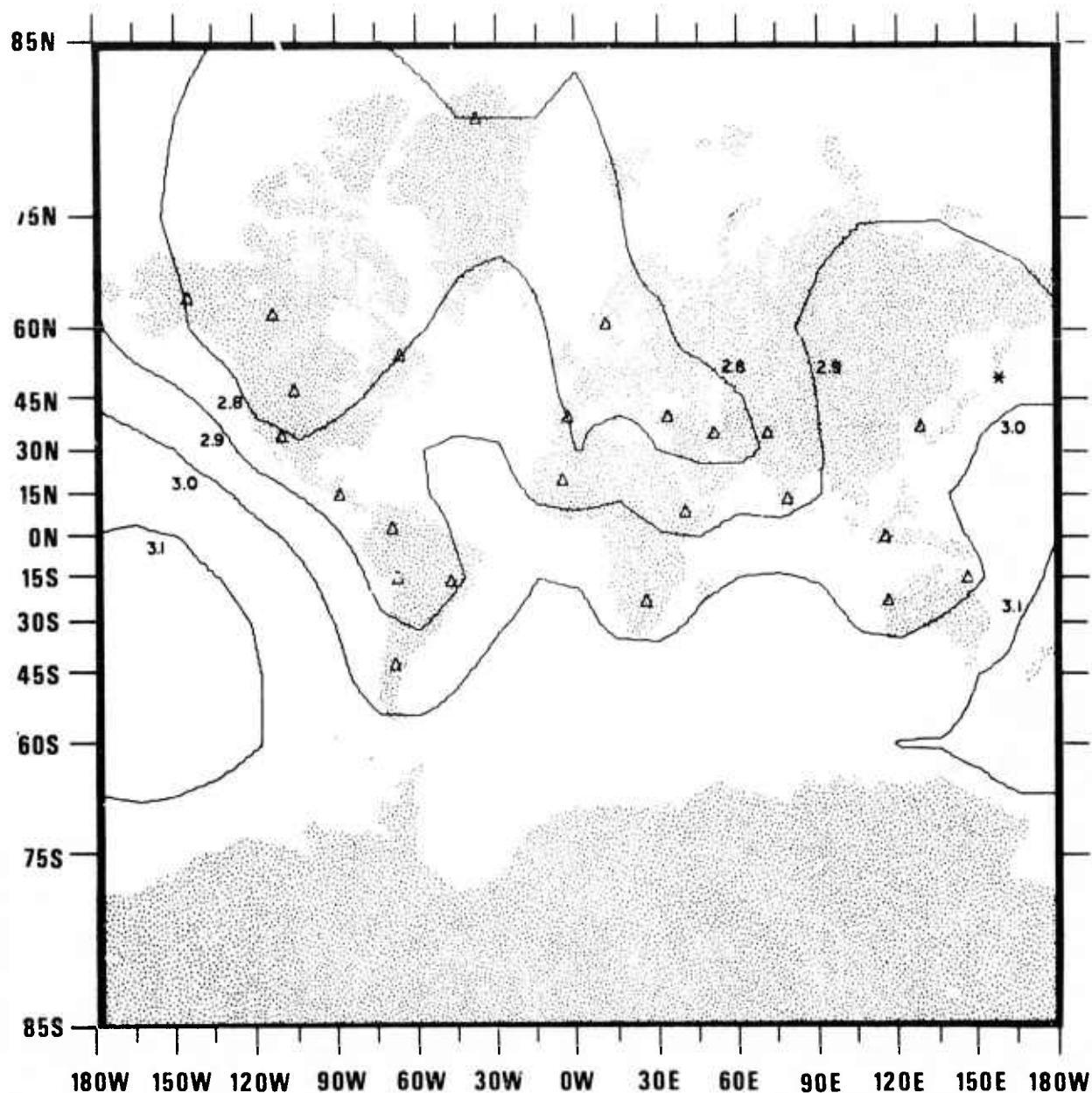
-102-

Figure 51. Threshold magnitude for 99% probability of detection of LR by 1 or more stations by a worldwide network of 25 stations with mean zero-to-peak noise levels of 19 mμ except for 15 mμ for LASA, NORSAR, and ALPA, a signal-to-noise ratio for detection of r=1.5, and a standard deviation of signal and noise of 0.3 magnitude units. The star indicates the epicenter assumed for the probability of detection versus M_s plots such as Figure 42.
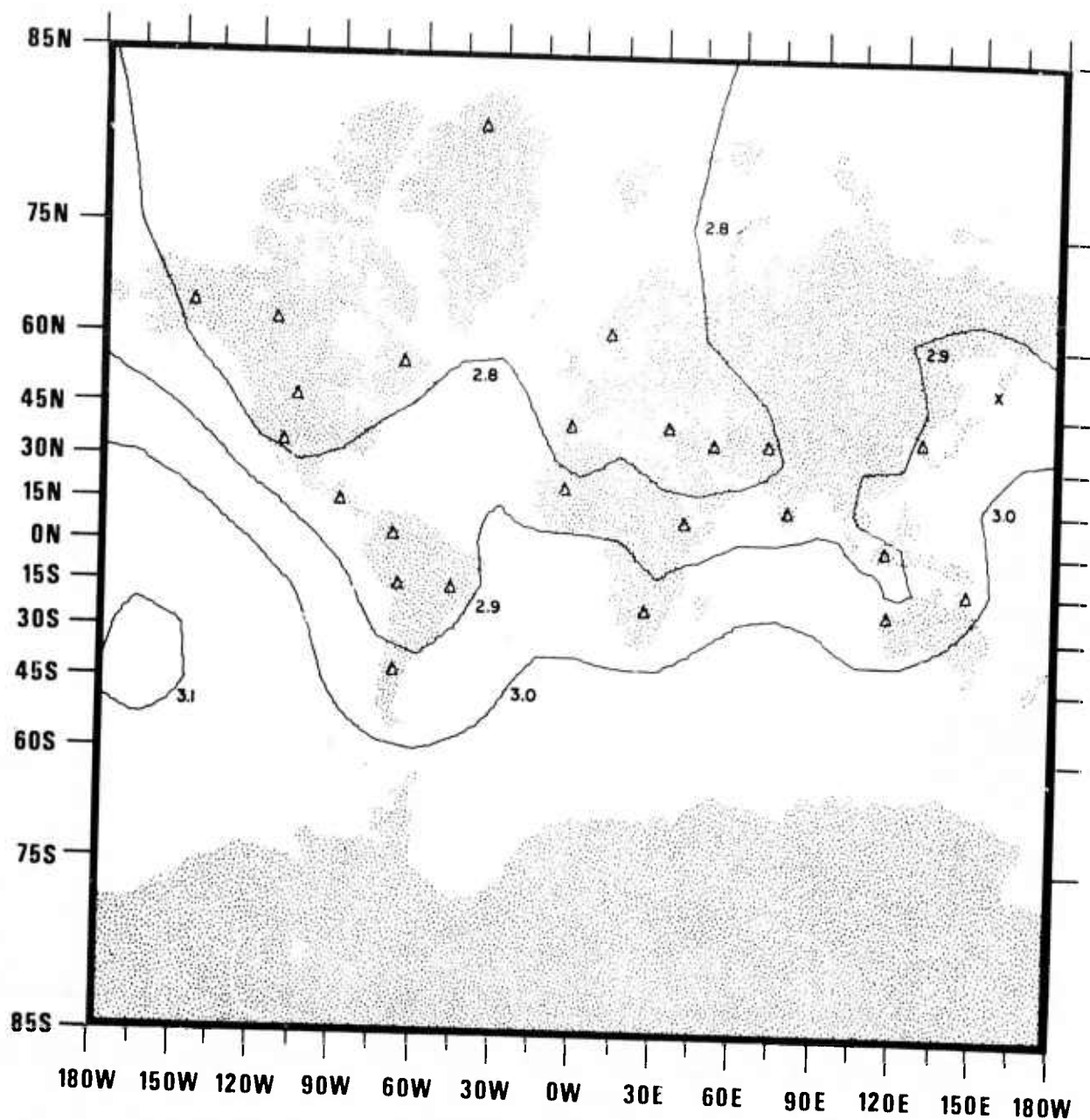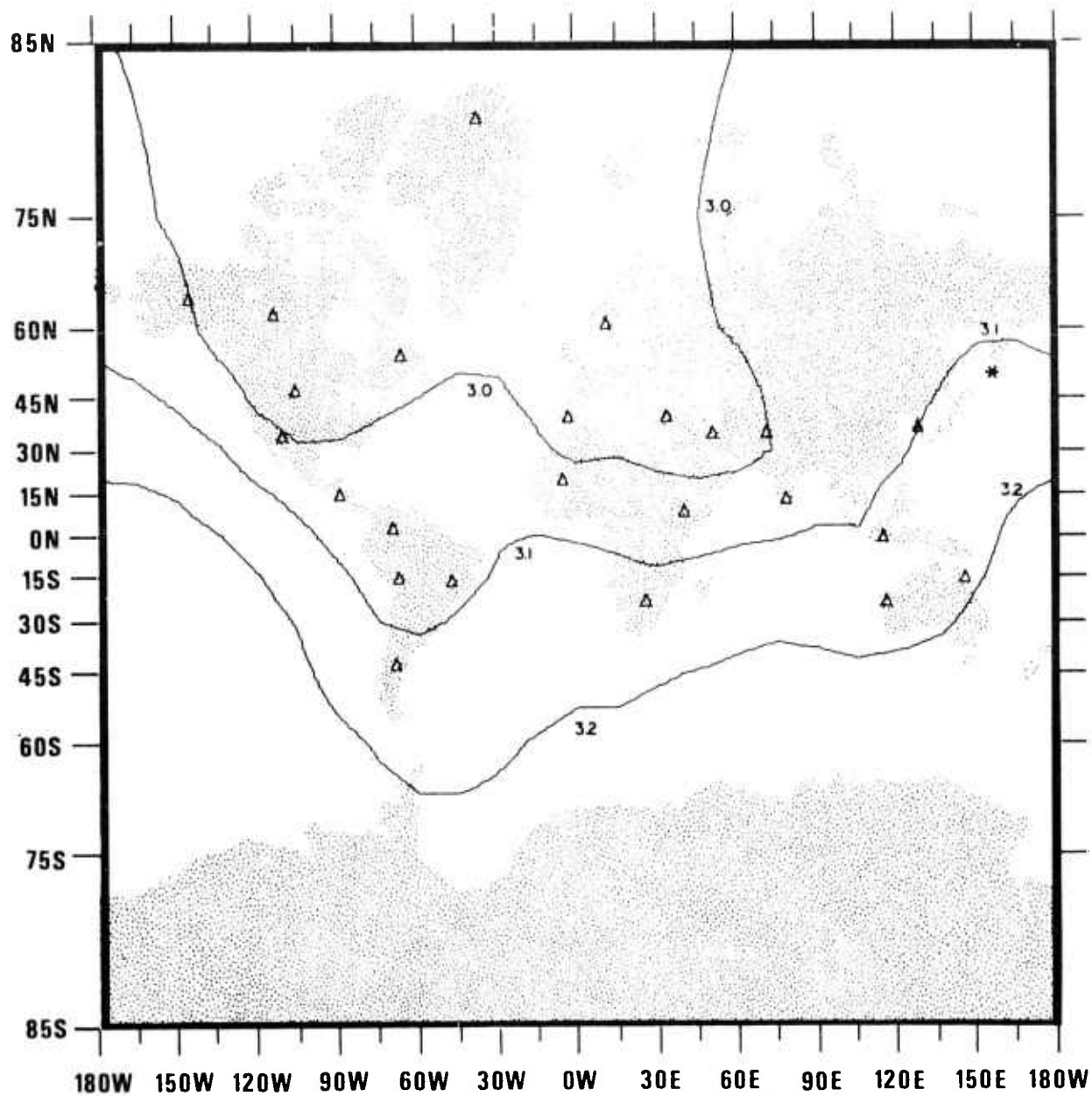
Figure 52. Threshold magnitude for 90% probability of detection of LR by 2 or more stations by a worldwide network of 25 stations with mean zero-to-peak noise levels of 19 mμ except for 15 mμ for LASA, NORSAR, and ALPA, a signal-to-noise ratio for detection of r=1.5, and a standard deviation of signal and noise of 0.3 magnitude units. The star indicates the epicenter assumed for the probability of detection versus M_s plots such as Figure 42.

Figure 53. Threshold magnitude for 90% probability of detection of LR by 4 or more stations by a worldwide network of 25 stations with mean zero-to-peak noise levels of 19 mμ except for 15 mμ for LASA, NORSAR, and ALPA, a signal-to-noise ratio for detection of r=1.5, and a standard deviation of signal and noise of 0.3 magnitude units. The star indicates the epicenter assumed for the probability of detection versus M_s plots such as Figure 42.
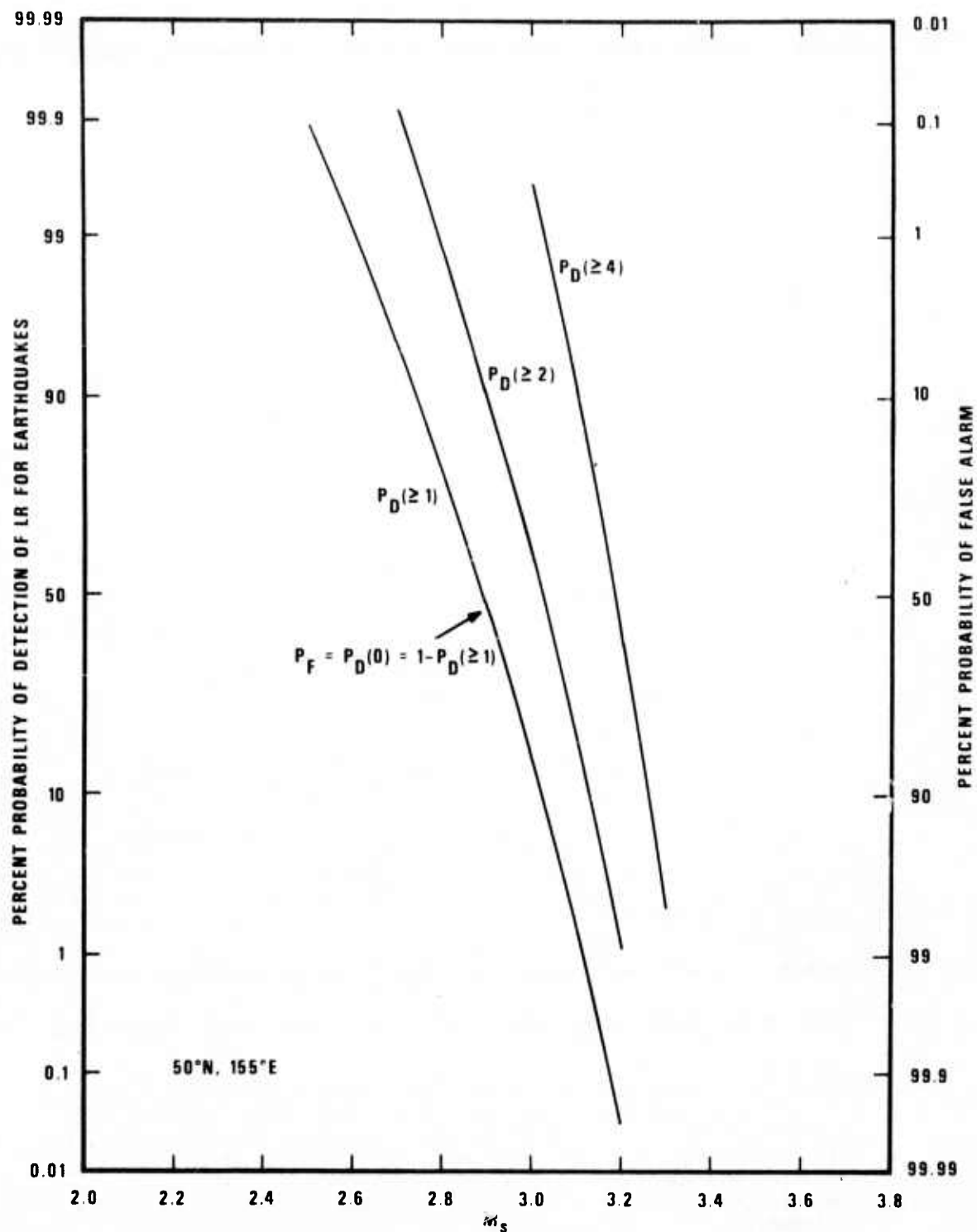
Figure 54. Probability of detection of LR by $\geq$ 1, 2, or 4 stations out of 25 and probability of a false alarm (no detection resulting in a decision that an earthquake is an explosion by means of negative discrimination) as a function of M_s for a 25-station worldwide network after Romney (1971) for an epicenter in Kamchatka. Noise and signal standard deviation is 0.1 magnitude units.
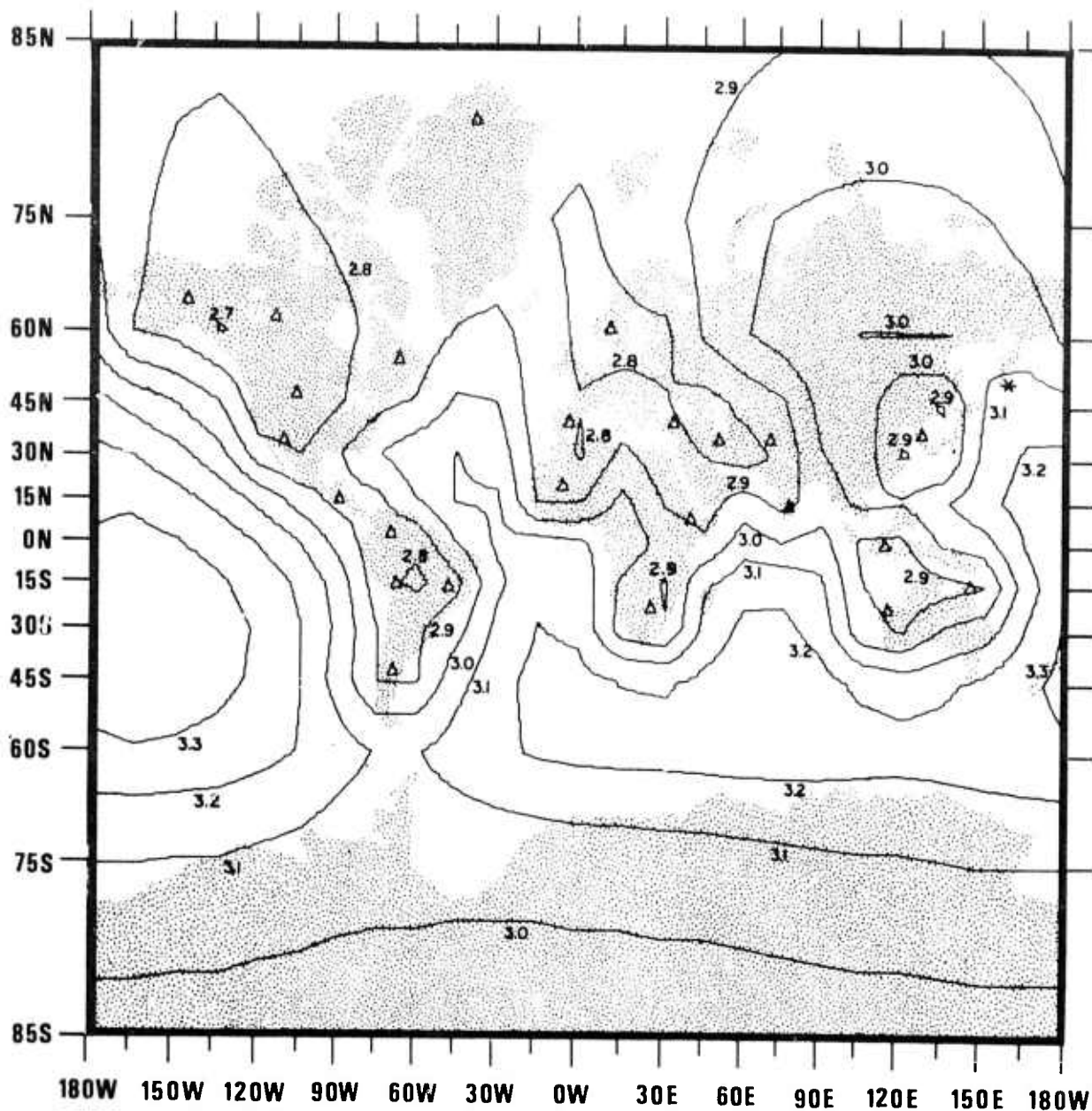
-106-

Figure 55. Threshold magnitude for 99% probability of detection of LR by 1 or more stations by a worldwide network of 25 stations with mean zero-to-peak noise levels of 19 mμ except for 15 mμ for LASA, NORSAR, and ALPA, a signal-to-noise ratio for detection of r=1.5, and a standard deviation of signal and noise of 0.1 magnitude units. The star indicates the epicenter assumed for the probability of detection versus M_s plots such as Figure 42.
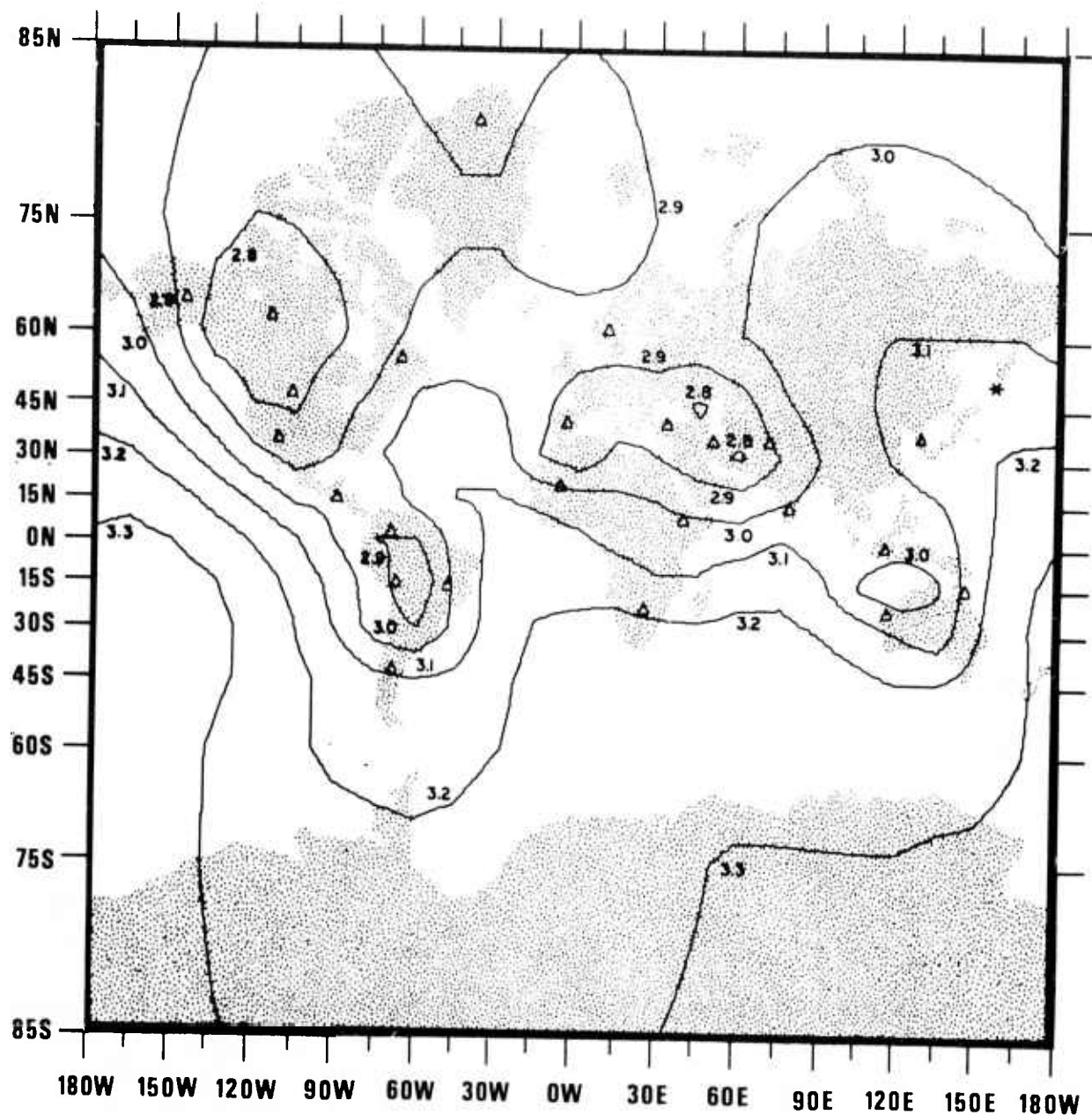
Figure 56. Threshold magnitude for 90% probability of detection of LR by
2 or more stations by a worldwide network of 25 stations with mean
zero-to-peak noise levels of 19 mμ except for 15 mμ for LASA, NORSAR, and
ALPA, a signal-to-noise ratio for detection of r=1.5, and a standard
deviation of signal and noise of 0.1 magnitude units. The star indicates
the epicenter assumed for the probability of detection versus M_s plots such
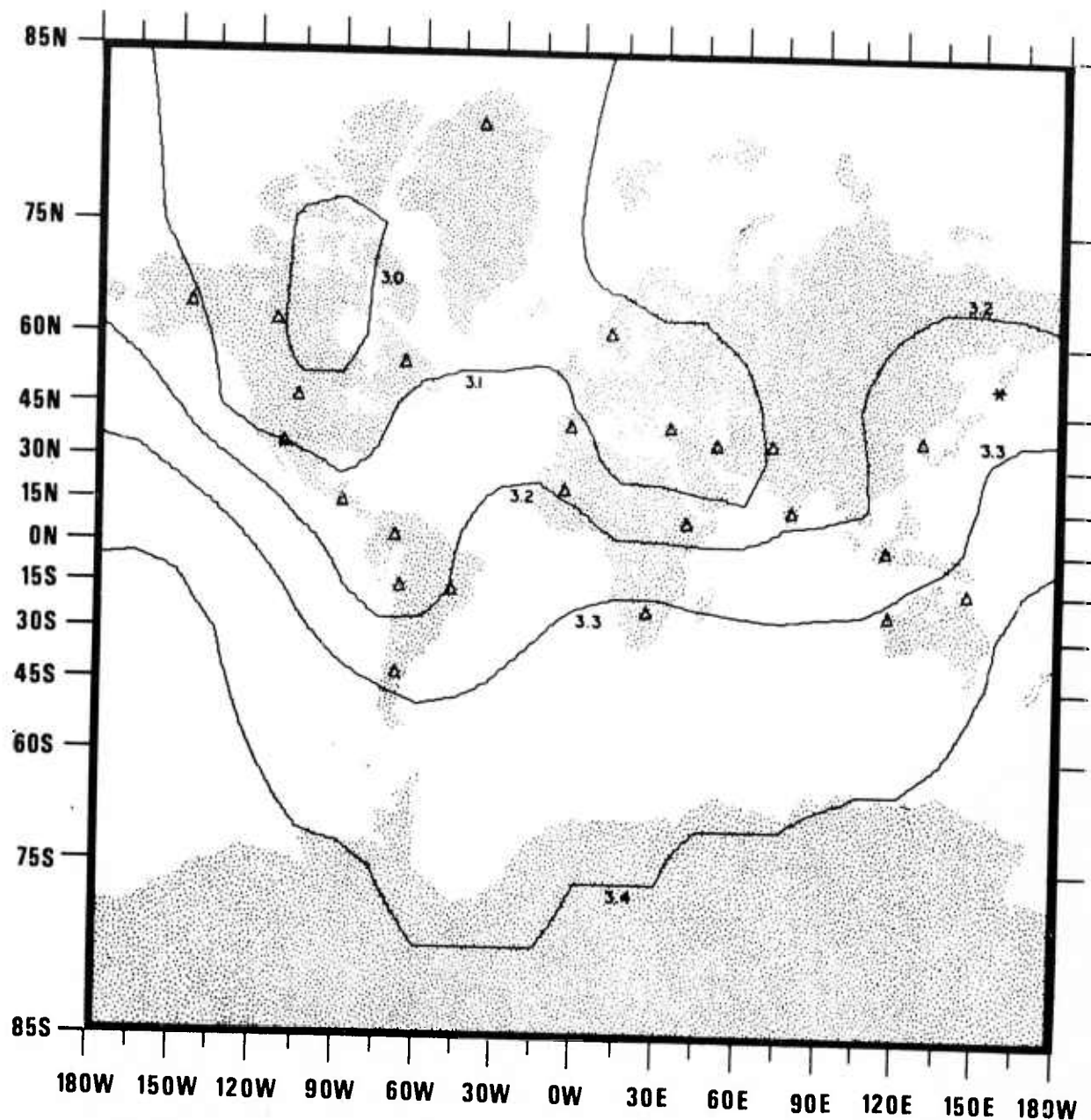as Figure 42.

Figure 57. Threshold magnitude for 90% probability of detection of LR by
4 or more stations by a worldwide network of 25 stations with mean
zero-to-peak noise levels of 19 mμ except for 15 mμ for LASA, NORSAR, and
ALPA, a signal-to-noise ratio for detection of r=1.5, and a standard
deviation of signal and noise of 0.1 magnitude units. The star indicates
the epicenter assumed for the probability of detection versus M_s plots such
as Figure 42.